AD-A050 973 TEXAS TECH UNIV LUBBOCK OPTICAL SYSTEMS LAB F/G 20/6
SPACE-VARIANT COHERENT OPTICAL PROCESSING.(U)
DEC 77 R J MARKS AFOSR-75-2855
UNCLASSIFIED SCIENTIFIC-1 AFOSR-TR-78-0212 NL

OF 3
AD
A050 973

Scientific Report
AFOSR-75-2855-1

SPACE-VARIANT COHERENT OPTICAL PROCESSING

by

Robert J. Marks II

December 1, 1977

OPTICAL SYSTEMS LABORATORY
DEPARTMENT OF ELECTRICAL ENGINEERING

TEXAS TECH UNIVERSITY

Lubbock, Texas 79409

410594

UNCLASSIFIED

SECURITY CLASSIFICATION OF THIS PAGE (When Data Entered)

REPORT DOCUMENTATION PAGE	READ INSTRUCTIONS BEFORE COMPLETING FORM
1. REPORT NUMBER: AFOSR-TR-78-0212	2. GOVT ACCESSION NO. / 3. RECIPIENT'S CATALOG NUMBER
4. TITLE (and Subtitle): SPACE-VARIANT COHERENT OPTICAL PROCESSING,	5. TYPE OF REPORT & PERIOD COVERED: Interim rept.,
	6. PERFORMING ORG. REPORT NUMBER: AFOSR-75-2855-1
7. AUTHOR(s): Robert J. Marks, II	8. CONTRACT OR GRANT NUMBER(s): AFOSR-75-2855
9. PERFORMING ORGANIZATION NAME AND ADDRESS: Texas Tech University, Department of Electrical Engineering, Lubbock, Texas 79409	10. PROGRAM ELEMENT, PROJECT, TASK AREA & WORK UNIT NUMBERS: 61102F; Project-Task 2305/B1
11. CONTROLLING OFFICE NAME AND ADDRESS: AFOSR/NE, Building 410, Bolling AFB, DC 20332	12. REPORT DATE: December 1, 1977 (1 Dec 77)
	13. NUMBER OF PAGES: 218 (212 p.)
14. MONITORING AGENCY NAME & ADDRESS (if different from Controlling Office): SCIENTIFIC-1	15. SECURITY CLASS. (of this report): UNCLASSIFIED
	15a. DECLASSIFICATION/DOWNGRADING SCHEDULE

16. DISTRIBUTION STATEMENT (of this Report)

Approved for Public Release; Distribution Unlimited

17. DISTRIBUTION STATEMENT (of the abstract entered in Block 20, if different from Report)

18. SUPPLEMENTARY NOTES

19. KEY WORDS (Continue on reverse side if necessary and identify by block number)

Space-Variant Optical Processing
Optical Computing
Hologram Optical Elements

20. ABSTRACT (Continue on reverse side if necessary and identify by block number)

This report describes various techniques for performing linear, space-variant operations with coherent optical processors. Both theoretical and experimental results are presented. Generalized one-dimensional space-variant processors capable of performing a broad class of superposition integral operations are presented. Applications including integral transform evaluation and ambiguity function display are presented. Two-dimensional space-variant processors are also discussed, with several approaches being discussed.

DD FORM 1 JAN 73 1473 EDITION OF 1 NOV 65 IS OBSOLETE

UNCLASSIFIED 410 594

SPACE-VARIANT COHERENT OPTICAL PROCESSING

BY

Robert J. Marks II

December 1, 1977

Scientific Report No. 1 on

Grant AFOSR 75-2855

"Space-Variant Optical Systems"

Principal Investigator: John F. Walkup, Assoc. Prof.

Co-Principal Investigator: Marion O. Hagler, Prof.

Optical Systems Laboratory

Department of Electrical Engineering

Texas Tech University

Lubbock, Texas 79409

ABSTRACT

This report describes various techniques for performing linear, space-variant operations with coherent optical processors. General linear systems theory is developed for application to processor design. Three analytical characterizations are separately examined based on (a) a continuum orthonormal basis set response; (b) a piecewise isoplanatic approximation and (c) modifications of the Whittaker-Shannon sampling theorem for space-variant systems. Advantages and disadvantages of each approach are considered. Generalized one-dimensional (1-D) space-variant coherent optical processors capable of performing a broad class of 1-D superposition integral operations are presented. Applications discussed include magnification, coordinate distortion, convolution, correlation, cross-power spectrum display, ambiguity function display, and evaluation of Laplace and inverse Abel transforms. A technique for lensless 1-D space-variant processing is also presented wherein a one-dimensional linear operation can be performed with an input, a processor mask, and a few centimeters of free space. Two dimensional space-variant processors are discussed from the frameworks of (a) a composite hologram scheme resulting from a direct application of a space-variant system sampling theorem and (b) angle-multiplexing of a number of holograms in a thick recording medium. An improvement on the volume hologram approach based on the use of phase-coding diffusers in the multiple reference beams is also discussed.

TABLE OF CONTENTS

LIST OF FIGURES

Chapter I

1. INTRODUCTION

Initial recognition of the ability to perform general mathematical operations with coherent light can be attributed to the members of the research team involved in the so called Project Michigan.[1-2] In initially classified research, they demonstrated the feasibility of utilizing coherent optical processors to handle vast quantities of data at the speed of light. Coherent processors can thus perform operations at a rate far in excess of that required by conventional digital computers. Being an analog computer, however, the coherent processor suffers from inflexibility and inexactitude when compared with the digital computer. The coherent processor, though, has a far greater capacity for information throughput.

There are two basic building blocks for any coherent processor. The first is the thin lens which, besides familiar imaging operations, is capable of performing a Fourier transformation on incident light field amplitudes. The second is the hologram on which complex field amplitude distributions can be represented. The most basic processor utilizing these components is shown in Figure 1-1. A two-dimensional transmittance, f, is illuminated from the left by a coherent plane wave. The Fourier transform of another

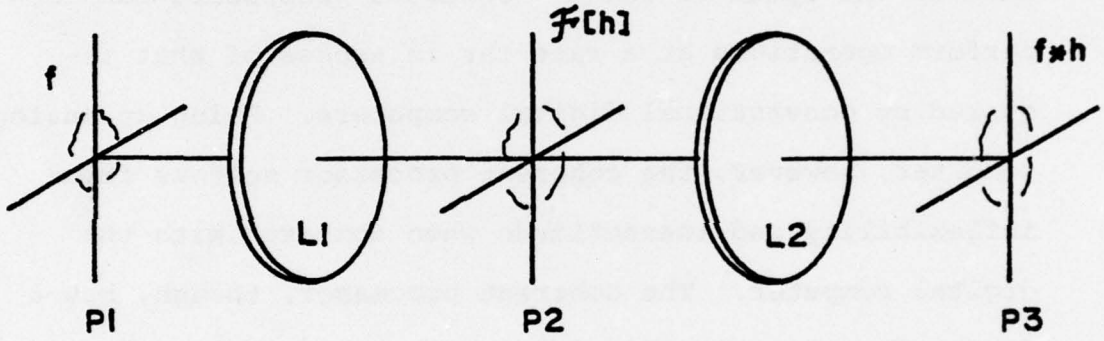

Figure 1.1 A basic coherent optical processor for performing space-invariant (isoplanatic, convolution) operations.

function, say h, is placed in plane P2. The convolution of h and f then appears on the processor output plane. The convolution operation performed here is also referred to as a linear space-invariant (or isoplanatic) operation. The space-invariant operation is a subclass of the more general class of linear operations. If a linear operation is not space-invariant, then it is said to be space-variant. A more rigorous treatment of these concepts is presented in Chapter II.

The use of the term "space-variant" in the report title is somewhat inexact and is used not because of the author's preference but rather due to precedence. Due to the wide spread use of the coherent processor in Figure 1-1 and the predominance of time-invariant systems in the sister electrical sciences, the term "space-(time-) variance" has been used to stress that a linear operation is "not space-invariant." There are also those to whom the term "linear" implies "invariant" although such is not rigorously the case. Following this unfortunate historical development, we herein also use the term "space-variant" although the term "linear" (space-variant and space-invariant) is rigorously more appropriate in most cases.

The class of space-invariant operations that can be performed by the coherent processor in Figure 1-1 is fun-

damentally limited only by the implementability of the so called transfer function mask on plane P2. More excitedly, any coherent processor which performs a two-dimensional space-invariant operation, irregardless of the number of components or complexity, can, in principle, be reduced to the elementary configuration in Figure 1-1.

Unfortunately, most coherent processors are, in fact, not space-invariant. Many, however, are linear in nature. As such, it would be a useful undertaking to develop a space-variant coherent processor displaying the simplicity of Figure 1-1 to which all linear coherent processors could be reduced. Investigation of this possibility is the main topic of this report.

There are of course, many specific coherent processors which perform space-variant operations. The thin lens Fourier transformer and non-unity magnification imaging systems are prime examples. In our investigations, however, we are more concerned with developing a general processor capable of performing a wide class of operations.

We begin treatment of processor design in Chapter II where several aspects of linear system theory are developed. System characterization by determination of the system response to all elements in a continuum orthonormal basis set is presented and leads to the well known line spread

function and frequency response characterizations as special cases. The continuum orthonormal basis set response characterization brings to light the possibility of alternate system descriptions which allow for the enrichment of linear systems theory beyond conventional impulse and frequency response characterization.[3-4] Furthermore, it is shown that due to the choice of our system response notation,[5] Fourier analysis, conventionally utilized only for space-invariant system description, can straightforwardly be generalized for description of the more general class of linear systems.

The remainder of Chapter II is concerned with system characterization wherein certain restrictive assumptions are placed on the system and/or input. The result of these constraints in all cases considered is the reduction of the required system responses needed for system characterization from an uncountable to countable number. The first scheme, titled the piecewise isoplanatic approximation (PIA)[6-7], requires that the shape of the system impulse response change slowly with respect to a small interval in the input space. Under this constraint, the system can be approximated by the superposition of a number of space-invariant systems.

The second constrained system characterization in Chapter II is termed the discrete orthonormal basis set

response characterization.[8] Here, the constraint is placed on the input which we restrict to be in that signal class spanned by a given orthonormal basis set. In this case, the system is completely characterized by knowledge of the system response to each element in the basis set.

Finally, in Chapter II, a number of sampling theorem characterizations are presented that correspond to various compact support and bandlimited constraints on the system input and/or line spread function.[9-10] For the most part, these characterizations depend on both the input and system.

Chapter III presents various schemes for performing one-dimensional space-variant operations utilizing astigmatic processors.[11] The processors here are as general for performing space-variant operations as that in Figure 1-1 is for performing space-invariant operations. We can, however, perform only one-dimensional operations here as opposed to the two-dimensional capability of the processor in Figure 1-1. The basic idea for the one-dimensional processor was initially proposed by Cutrona.[12] Generalizations and implementations of 1-D processors were simultaneously reported by Goodman et. al.[13] and Marks et. al.[14] An interesting serendipity is a processor for simultaneous display of the complete ambiguity function display first suggested by Said and Cooper[15] and later

reported by Marks et. al.[16-18]

Chapter IV discusses the present state-of-the-art in the effort to formulate a generalized coherent optical processor for performing two-dimensional space-variant operations. The first scheme (the composite hologram approach) is a straightforward implementation of a sampling theorem developed in Chapter II. It suffers, however, from a strict limitation on the class of allowable systems and inputs.

The second two-dimensional space-variant processor discussed utilizes the selective diffraction efficiency effects inherent in volume holography. This scheme was initially proposed by Burton et. al.[19] and was developed via the PIA by Marks[6] and via a sampling theorem by Deen et. al.[20-21] The volume hologram approach, however, suffers from the one-dimensional nature of the useful angular bandpass which prohibits a straightforward generalization of the scheme to two dimensions.

The final two-dimensional space-variant processing scheme utilizes phase coded reference beams. This approach, proposed by Krile et. al.,[22] smears unwanted crosstalk terms into diffuse background noise.

Chapter V contains some concluding remarks and suggests some possible areas of future investigation.

CHAPTER II

2. GENERAL LINEAR SYSTEMS CHARACTERIZATION THEORY

A system may be abstracted into three basic components: an input, a black box, and an output. For a given set of conditions on the black box, the output is simply the response of the black box to a given input. A system can be multidimensional and have associated with its input-output domain any number of physical quantities. An electronic circuit-type system, for example, has associated with its input-output domain temporal voltage and current waveforms. A coherent processor, on the other hand, has associated with its input-output domains two-dimensional spatial variations in electric field intensity (light). Input-output domains for a given system need not be the same. For example, television has both acoustical and optical output domains corresponding to a single temporal voltage input.

In a more mathematical sense, we can think of a system in terms of a mapping. An input is mapped to an output, according to a deterministic mapping rule dictated by the black box. If we denote our input by f(y) and our output by g(x), then[23]

$$g(x) = S[f(y)]. \qquad (2\text{-}1)$$

Here, S(·) corresponds to the mapping rule or system operator. That is, the output, g(x), corresponds to the input, f(y), being operated on by the system operator S(·). Again, the input and output can correspond to any physical quantity such as voltage or temperature, and the variables x and y can correspond to any variable domain (such as space or time) in any desired dimension. When applied to coherent optical processors, both g(·) and f(·) denote electric field amplitude, and both x and y correspond to two-dimensional spatial output and input planes respectively.

The general system characterization in Eq. 2-1 leaves little room for further development. In order to characterize this system completely, we would need to catalog the system output corresponding to every possible input under all possible system conditions. To avoid performing of this formidable task, further assumptions need to be made concerning out black box.

2.1. Classical Linear System Characterization

The most popular system assumption is that of linearity where two basic suppositions are made: 1) The response of the system to the sum of a number of inputs is equivalent to the sum of the system's response to each of the inputs individually and 2) amplification of the

input will result only in the equivalent amplification of the output. These system properties are known respectively as superposition and homogeneity and together constitute the definition of linearity. We write these conditions respectively as

$$S[f_1(y) + f_2(y)] = S[f_1(y)] + S[f_2(y)] \qquad (2\text{-}2)$$

and

$$S[af(y)] = aS[f(y)] \qquad (2\text{-}3)$$

where a is a constant independent of the y variable. These two conditions may be combined into a single necessary and sufficient condition for linearity:

$$S[af_1(y) + bf_2(y)] = aS[f_1(y)] + bS[f_2(y)]. \qquad (2\text{-}4)$$

While no physical system is exactly linear, the concept of linearity allows powerful mathematical treatment and in many instances excellent description of a system process.

Linear systems can be described by the superposition integral which we shall now derive. We begin with the sifting property of the Dirac delta function:[23]

$$f(y) = \int_{-\infty}^{\infty} f(\xi)\delta(y-\xi)d\xi. \qquad (2\text{-}5)$$

This relationship is substituted into the system characterization in Eq. 2-1. Since the system operator, $S(\cdot)$, is linear, we can make the following two observations: 1) Thinking of the integral as a continuum sum, we can take the operator inside the integral sign due to the superposition property of Eq. 2-2. 2) Since the system operator operates only on functions of y, the terms $f(\xi)$ and $d\xi$ may be factored out of the system operation due to the homogeneity property of Eq. 2-3. This leaves

$$g(x) = \int_{-\infty}^{\infty} f(\xi) S[\delta(y-\xi)] d\xi. \qquad (2\text{-}6)$$

The quantity $S[\delta(y-\xi)]$ is interpreted as the system response to an input Dirac delta function located at the input coordinate $y = \xi$. This response has various names, including the impulse response and the system Greens function. In optics, it is referred to as either the system line spread function or the system point spread function depending on whether analysis is being performed in one or two dimensions. Since our treatment to date has a one-dimensional flavor, we will refer to this response as the system line spread function and write it as

$$h(x - \xi; \xi) \triangleq S[\delta(y- \xi)]. \qquad (2\text{-}7)$$

Then, Eq. 2-6 becomes the superpositional integral:

$$g(x) = \int_{-\infty}^{\infty} f(\xi)h(x - \xi;\xi)d\xi, \qquad (2\text{-}8)$$

It should be noted that the use of the line spread function notation here is not that which is conventionally used.[23-24] There are, however, certain computational advantages of this notation[5,25-27] which will soon become clear.

Let us now physically interpret the superposition integral description of the linear system. In order to completely characterize a system in this manner, we must catalog the responses of our system to Dirac delta inputs at every point of our input space. The number of required responses is thus uncountably infinite.

For coherent optical systems, we make the following physical interpretation: A line source placed on our input plane at $y = \xi$, possibly by the focusing of an incident plane wave with a lens, gives rise to a field amplitude distribution on our output plane which is the system line spread function corresponding to the input coordinate $y = \xi$. As the input line source explores new positions on the input plane, the line spread function shifts and/or changes shape.

Suppose that the line spread function shifts directly with the input Dirac delta without changing shape. That is, if we move our input Dirac delta a distance d, then

our output also shifts a distance d and otherwise remains unchanged. The system is then said to be space-invariant and the line spread function takes on the form

$$h(x - \xi; \xi) \rightarrow h(x - \xi). \qquad (2\text{-}9)$$

In temporal systems, this property is referred to as time-invariance and in optics as spatial invariance or isoplanicity.

Actually, the properties of linearity and invariance are independent. That is, there are systems which are invariant and not linear. An invariant system is simply one in which the output shifts directly with the input for all inputs.

For linear invariant systems, the superposition integral becomes the convolution integral:

$$g(x) = \int_{-\infty}^{\infty} f(\xi)h(x - \xi)d\xi. \qquad (2\text{-}10)$$

One of the computational advantages of linear invariant systems is the applicability of Fourier analysis in their treatment. We define the Fourier transform of a signal s(x) as

$$\begin{aligned} S(f_x) &= F_x[s(x)] \\ &= \int_{-\infty}^{\infty} s(x)\exp(-j2\pi f_x x)dx. \end{aligned} \qquad (2\text{-}11)$$

Here $F_x(\cdot)$ refers to the Fourier transform operator with

respect to x, and f_x is the frequency variable corresponding to x. Here, and henceforth, a capital letters refers to the Fourier transform of the corresponding lower case letter. (e.g., $S(f_x)$ is the Fourier transform of $s(x)$).

Suppose, then, we apply the Fourier transform operator to both side of the convolution integral in Eq. 2-10. Since the Fourier operator is linear, we may bring it through the integral sign and past the input to operate only on the system line spread function. Utilizing the shift theorem[28] we write

$$\begin{aligned} G(f_x) &= F_x[g(x)] \\ &= \int_{-\infty}^{\infty} f(\xi) F_x[h(x)] \exp(-j2\pi f_x \xi) d\xi \\ &= F(f_x) H_x(f_x). \end{aligned} \tag{2-12}$$

This familiar relationship is the statement of the Fourier domain input-output statement of a linear invariant system. The Fourier transform of the line spread function, $H_x(f_x)$, is referred to as the system transfer function, or simply the system function. The relationship in Eq. 2-12 reduces the convolution integral to the more computationally attractive operation of multiplication.

The system discriptions presented to this point are relatively standard.[23-24,28-29] In the remainder of this chapter, various other methods of linear system characterization are presented. These include generalization of

the superposition integral concept to other response mappings of continuum orthonormal basis sets of which the Dirac delta set is a special case. Also presented are three schemes by which the required number of cataloged responses is reduced from a continuum to a countably infinite set. Each of these three methods requires assumptions on the system input and/or line spread function. As will be seen, the three schemes are highly complementary to each other. The overall purpose of this chapter is to establish a wealth of linear system theory to be later utilized in the development of coherent processors capable of performing a wide class of linear operations. The theory, however, is applicable to all linear systems.

2.2. Continuum Orthonormal Response Characterization

The conventional superposition integral can be viewed as a special case of system characterization through cataloging the system response to each element in a continuum basis set. A continuum set, $\{\psi_x(\xi)\}$, is said to be orthonormal if[30]

$$\int_{-\infty}^{\infty} \psi_x(\xi)\psi_y^*(\xi)d\xi = \delta(x-y), \qquad (2\text{-}13)$$

where "*" denotes complex conjugation. In our linear system treatment in the previous section, $\{\delta(y - \xi)\}$

obviously conforms to this definition.[29]

A system input, f(y), can be expressed in terms of a continuum basis set by

$$f(y) = \int_{-\infty}^{\infty} \alpha(\xi)\psi_y(\xi)d\xi \qquad (2\text{-}14)$$

where

$$\alpha(\xi) = \int_{-\infty}^{\infty} f(y)\psi_y^*(\xi)dy. \qquad (2\text{-}15)$$

We can prove the validity of this relationship as follows: Substitute Eq. 2-15 into Eq. 2-14 and interchange the order of integration. Utilizing the orthonormality condition of Eq. 2-13 and the sifting property of the Dirac delta function in Eq. 2-7 will then reduce the result to the identity f(y) = f(y).

To develop the input-output relationship of a linear system corresponding to an input f(y), we substitute Eq. 2-14 into our system operator in Eq. 2-1. As in the development of the superposition integral, we make the following two observations concerning our linear operator S(•): 1) Viewing the integral as a continuum sum, we can bring the system operator inside the integral due to the superposition property of Eq. 2-2. 2) Since the operator only operates on functions of y, we can factor out the input f(ξ) and the differential dξ due to the

homogeneity property of Eq. 2-3. The system operator thus only operates on the orthonormal basis set element:

$$g(x) = \int_{-\infty}^{\infty} \alpha(\xi) S[\psi_y(\xi)] d\xi. \qquad (2\text{-}16)$$

Together with Eq. 2-15, this is the general statement of the continuum orthonormal basis set response characterization of a linear system.

Let's interpret it. In our input space, we place our continuum basis set element $\psi_y(\xi)$. As we vary ξ in $\psi_y(\xi)$ the corresponding system output, $S[\psi_y(\xi)]$, is cataloged. With knowledge of the system response for all ξ, the system is completely defined. For an arbitrary input, $f(y)$, the functional coefficient $\alpha(\xi)$ is computed from Eq. 2-15 and substituted into Eq. 2-16 to determine the corresponding system output. Note that, in general, the set $\{S[\psi_y(\xi)]\}$ is not orthogonal.

2.2.1. Spatial Frequency Response

As was mentioned, the superposition integral in Eq. 2-8 is a special case of this relation. Here, $\psi_y(\xi) = \delta(y - \xi)$. By the sifting property of the Dirac delta in Eq. 2-5, it follows that $\alpha(\xi) = f(\xi)$ and, from Eq. 2-7, $S[\psi_y(\xi)] = h(x - \xi; \xi)$.

Another continuum basis set that is meaningful in engineering applications is the complex sinusoid:

$$\psi_y(\nu) = \exp(j2\pi y\nu). \qquad (2\text{-}17)$$

Here, ν is used instead of ξ due to the obvious frequency personality of the variable. From Eq. 2-15, our functional coefficient is seen to be the Fourier transform of the input:

$$\alpha(\nu) = \int_{-\infty}^{\infty} f(y)\exp(-j2\pi\nu y)dy \qquad (2\text{-}18)$$
$$= F(\nu).$$

Due to its extensive use later, we will distinguish the response to an input complex sinusoid with the name "frequency response" and denote it by

$$k(x - c\nu;\ \nu) \triangleq S[\exp(j2\pi\nu y)]. \qquad (2\text{-}19)$$

This particular notation is used due to certain computational advantages.[5] The constant c merely retains dimensional consistancy between x and ν which have reciprocal units.

Substituting Eqs. 2-18 and 2-19 into the general continuum orthonormal response characterization of Eq. 2-16 gives

$$g(x) = \int_{-\infty}^{\infty} F(\nu)k(x - c\nu;\ \nu)d\nu. \qquad (2\text{-}20)$$

Note the computational similarities between this frequency response characterization and the superposition integral repeated here:

$$g(x) = \int_{-\infty}^{\infty} f(\xi)h(x - \xi;\ \xi)d\xi. \quad (2\text{-}21)$$

From our definition of the frequency response in Eq. 2-19, we can use the superposition integral to write

$$k(x - c\nu;\ \nu) = \int_{-\infty}^{\infty} h(x - \xi;\ \xi)\exp(j2\pi\xi\nu)d\xi. \quad (2\text{-}22)$$

As such, the frequency response is simply the inverse Fourier transform of the line spread function. Inspection of Eqs. 2-20 and 2-21 also dictates this must be true if Parseval's theorem is to be satisfied.[28] That is, if $f(\xi)$ and $F(\nu)$ are Fourier transform pairs, then $h(x-\xi;\xi)$ and $k(x-c\nu;\nu)$ must also be Fourier transform pairs.

2.2.2. Output Frequency Mapping

For purposes of discussion, assume that both ξ and x are spatial variables. It follows then that ν and f_x respectively are the corresponding frequency variables. Thus, the superposition integral maps an input spatial domain to an output spatial domain and the frequency response characterization maps the input frequency domain to an output spatial domain. It is also possible to directly map to the output frequency domain. To do this, in accordance to our observations concerning the relation between spatial and frequency variables, the following two Fourier transform operators are defined on function $s(x,\xi)$:

$$F_x[s(x;\xi)] \triangleq \int_{-\infty}^{\infty} s(x;\xi)\exp(-j2\pi f_x x)\,dx \qquad (2\text{-}23)$$

and

$$F_\xi[s(x;\xi)] \triangleq \int_{-\infty}^{\infty} s(x;\xi)\exp(-j2\pi\nu\xi)\,d\xi. \qquad (2\text{-}24)$$

Application of the linear operator $F_x(\cdot)$ to both sides of the superposition integral of Eq. (2-8) gives

$$\begin{aligned} G(f_x) &= \int_{-\infty}^{\infty} f(\xi)F_x[h(x-\xi;\,\xi)]\,d\xi \\ &= \int_{-\infty}^{\infty} f(\xi)F_x[h(x;\,\xi)]\exp(-j2\pi f_x\xi)\,d\xi \\ &= F_\xi\, F_x[f(\xi)h(x;\,\xi)]\Big|_{\nu=f_x} \end{aligned} \qquad (2\text{-}25)$$

where, in the second step we have utilized the shift theorem of Fourier transform theory.[28] Here, we are directly mapping the input spatial domain to the output frequency domain. Before applying a similar procedure to the frequency response characterization, it is instructive to discuss the interpretation of Eq. 2-25.

First of all, note that we are still using the line spread function notation given in Eq. 2-7. The computational advantage of this particular notation choice is made clear in the development of Eq. 2-25. Mathematically, one makes the transition from $h(x-\xi;\,\xi)$ to $h(x;\,\xi)$ by simple variable manipulation. A straightforward procedure for doing this is to make the substitution $x = (x-\xi) + \xi$ for all x's appearing in $h(x-\xi;\,\xi)$. To form $h(x;\,\xi)$,

one then simply substitutes x's for all $(x - \xi)$'s.

In a more physical sense, the transition from $h(x-\xi;\xi)$ to $h(x; \xi)$ can probably be best interpreted by visualizing a temporal linear system. With reference to Fig. 2.1a, we first excite the system with a Dirac delta at input time $\xi = 0$. The system responds in this example with the triangular response shown. We wait a bit, and again excite the system at a later time $\xi > 0$. The system response is now a triangle of shorter duration. Note that the system shown here is causal in that we can have no system response prior to application of an input. As such, the system impulse response (line spread function) must be identically zero for $x - \xi < 0$. Thus the line $x - \xi = 0$ is a reference line of sorts for our response. In the more general (non-causal) case, the line $x = \xi$ is a reference or a common system axis for comparison of the relation of the location of the input Dirac delta to the corresponding system line spread function. As is shown in Fig. 2.1b, the transition from $h(x - \xi; \xi)$ to $h(x; \xi)$ is thus a shift of this reference axis to the origin for all possible ξ.

In a cruder sense, we can envision the transition from $h(x - \xi; \xi)$ to $h(x; \xi)$ as follows. For the invariant case, $h(x - \xi)$ varies directly as $\delta(y - \xi)$. That is, as $\delta(y - \xi)$ moves up the input plane, $h(x - \xi)$ moves up the

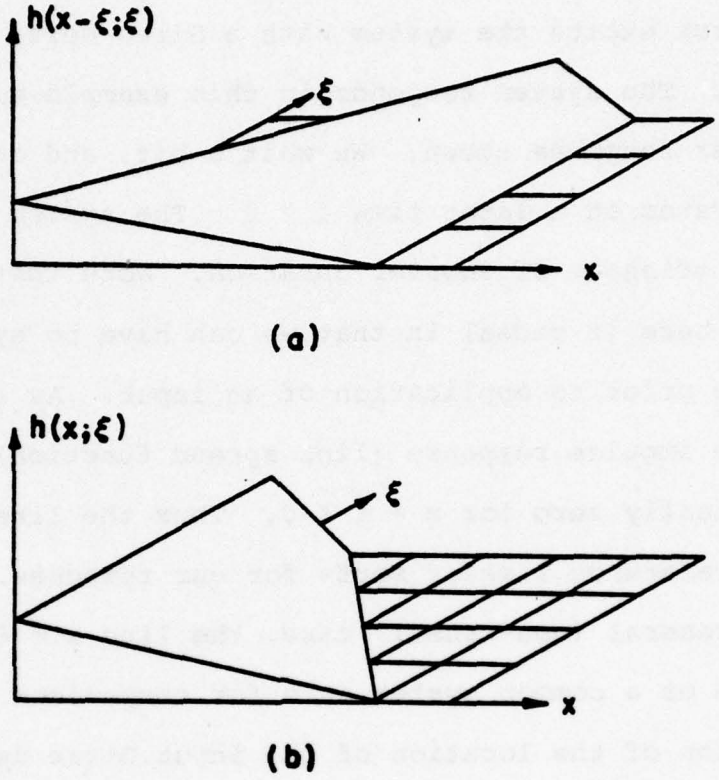

Figure 2.1 An example of a space-variant system's line spread function on the (x,ξ) plane in two different forms.

output plane without changing shape. In the linear variant case we can also envision $h(x - \xi; \xi)$ moving up the plane, but changing shape as it does so. Returning to the invariant case, make the transition from $h(x - \xi)$ to $h(x)$ as in Fig. 2.2. As the input Dirac delta moves up the plane, $h(x)$ remains unchanged in position and shape. Similarly, $h(x; \xi)$ may be thought of as remaining unchanging in its position. That is, it does not shift as before, but, as the input Dirac delta moves, $h(x; \xi)$ changes shape. Again, this view of $h(x - \xi; \xi)$ vs $h(x; \xi)$ is crude, but does provide for a somewhat intuitive feeling of physical interpretation.

Returning now to the output frequency mapping relation in Eq. 2-25, we can generalize the idea of the system transfer function to a general linear system. We define the system transfer function as

$$H_x(f_x; \xi) \triangleq F_x[h(x; \xi)]. \qquad (2\text{-}26)$$

Our output frequency mapping in Eq. 2-25 can then be written

$$G(f_x) = F_\xi[f(\xi)H_x(f_x; \xi)]\Big|_{\nu = f_x}. \qquad (2\text{-}27)$$

Note that the generalized transfer function is sensitive to input location, ξ. Note also that, for the invariant case, $H_x(f_x; \xi) \rightarrow H_x(f_x)$ and Eq. 2-27 takes on the famil-

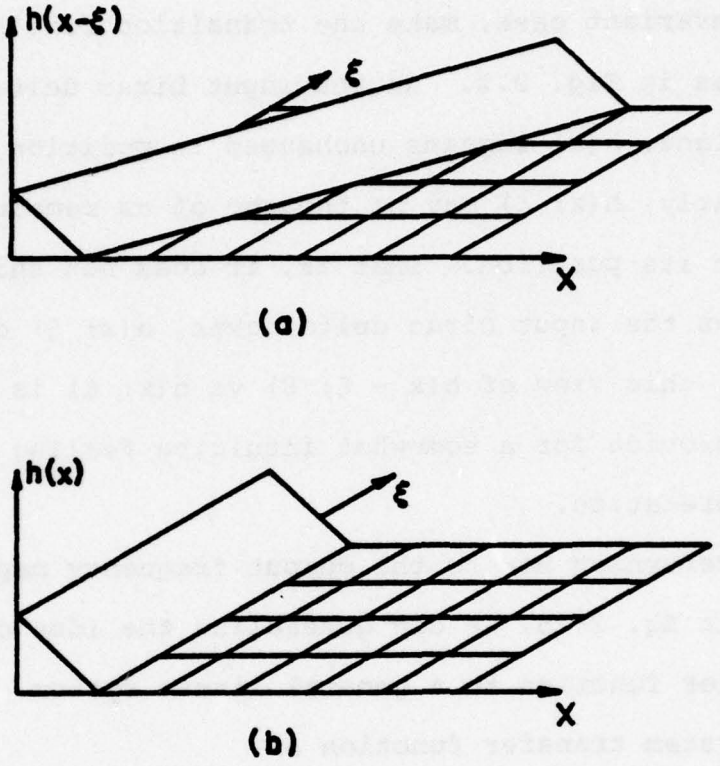

Figure 2.2 An example of a space-invariant system's line spread function on the (x,ξ) plane in two different forms.

iar product form given in Eq. 2-12.

Equation 2-25 gives an input spatial to output frequency mapping. An input frequency to output frequency mapping can be developed by applying similar steps to the frequency response characterization in Eq. 2-20:

$$\begin{aligned} G(f_x) &= \int_{-\infty}^{\infty} F(\nu)\ F_x[k(x - c\nu;\ \nu)]d\nu \\ &= \int_{-\infty}^{\infty} F(\nu)\ F_x[k(x;\ \nu)]\exp(-j2\pi c\nu f_x)d\nu \\ &= F_\xi^{-1}F_x[F(\nu)k(x;\ \nu)]\Big|_{\xi\ =\ -cf_x} \end{aligned} \tag{2-28}$$

where the inverse Fourier transform operator with respect to ξ is given by

$$F_\xi^{-1}[S(x,\nu)] = \int_{-\infty}^{\infty} S(x;\ \nu)\exp(j2\pi\nu\xi)d\nu. \tag{2-29}$$

From Eqs. 2-20, 2-21, 2-25, and 2-28, we have expressions covering all possible frequency/spatial-input/output mappings. A summary is given in Table 2.1. These relationships, which have roots in the generalized continuum orthonormal basis set response characterization of linear systems, lend a flexibility to linear system representation which will later be utilized in linear coherent processor implementation schemes.

2.3. The Piecewise Isoplanatic Approximation (PIA)

In the previous section, we require a continuum

DOMAIN input → output		EQUATION	Eq. in TEXT
spatial	spatial	$g(x) = \int_{-\infty}^{\infty} f(\xi)\, h(x-\xi;\xi)\, d\xi$	2-8
frequency	spatial	$g(x) = \int_{-\infty}^{\infty} F(\nu)\, k(x-c\nu;\nu)\, d\nu$	2-20
spatial	frequency	$G(f_x) = \mathcal{F}_\xi \mathcal{F}_x \left[f(\xi)\, h(x;\xi) \right] \Big\|_{\nu=f_x}$	2-25
frequency	frequency	$G(f_x) = \mathcal{F}_\xi^{-1} \mathcal{F}_x \left[F(\nu)\, k(x;\nu) \right] \Big\|_{\xi=-cf_x}$	2-28

Table 2.1 Summary of all possible input to output mappings from space and/or frequency domain to space and/or frequency domain.

cataloging of system responses in order to completely characterize our linear system. By making certain assumptions or approximations concerning the system and/or input class, it is possible to reduce this to a countably infinite number of required input-output relationships. We will discuss three such linear system characterizations the first of which is the piecewise isoplanatic approximation (PIA).[7]

In optics nomenclature, the terms space-invariant and isoplanatic are equivalent. Thus, an isoplanatic system's input-output relationship is given by the convolution integral. A class of systems which lie between the isoplanatic and space-variant classification consists of those systems which are piecewise isoplanatic.[26] The input spaces of such systems consist of a number of adjoined isoplanatic patches.[31-32] For this class of linear systems, as an input Dirac delta explores a given isoplanatic patch, the corresponding line spread function shifts directly without changing shape. That is, within a single isoplanatic patch, the system is space-invariant. When the input Dirac delta moves from one patch to the next, the line spread function immediately changes shape. While the input Dirac delta explores this second isoplanatic patch, however, the corresponding output response will again shift accordingly. Thus, we may interpret the piecewise isoplanatic system as a number of space-invariant systems.

A given input, $f(\xi)$, is divided into isoplanatic regions. Each isoplanatic input region serves as an input to a space-invariant system defined by the impulse response assigned to the isoplanatic patch. The outputs of each of these component systems are summed to give the output of the overall piecewise isoplanatic system.

The power of the piecewise isoplanatic system concept lies in its use for approximating space-variant systems. If the line spread function of a space-variant system does not change shape drastically corresponding to small input region, then we may approximate the system as isoplanatic over this region. The result of making this approximation over a large number of disjoint regions is appropriately termed a piecewise isoplanatic approximation or PIA.[7] An illustration of a possible PIA as applied to an example line spread function is pictured in Fig. 2.3.

We now will proceed with a brief overview of the mathematics of the PIA. Let the n^{th} input isoplanatic patch in our one-dimensional treatment extend from $\xi=\ell_n$ to $\xi=u_n$. The midpoint of this patch is

$$m_n = \frac{u_n + \ell_n}{2} \qquad (2\text{-}30)$$

and the patch's width is

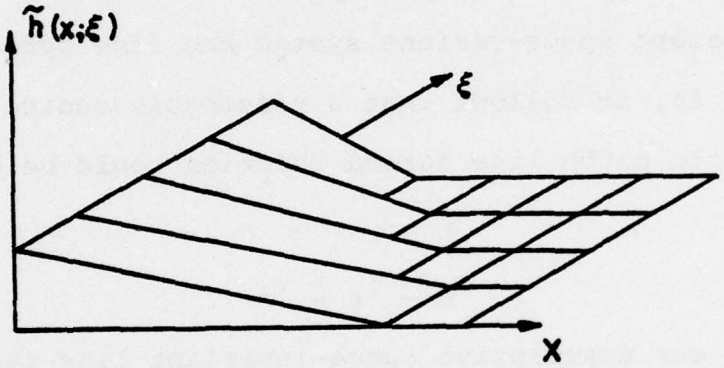

Figure 2.3 A possible piecewise isoplanatic approximation (PIA) of the space-variant system line spread function in Figure 2.1.

$$w_n = u_n - \ell_n. \tag{2-31}$$

We assume adjacent patches are adjoined so that the upper point on the n^{th} patch is equivalent to the lower point of the $(n + 1)^{st}$ patch. That is

$$u_n = \ell_{n+1}. \tag{2-32}$$

For each isoplanatically modeled patch, we must somehow choose a single space-invariant line spread function. If our parent space-variant system has line spread function $h(x - \xi; \xi)$, it follows that a reasonable choice of the isoplanatic patch line spread function would be $h(x-\xi_n;\xi_n)$ where

$$\ell_n \leq \xi_n \leq \nu_n. \tag{2-33}$$

This is, our descriptive space-invariant line spread function should correspond to the system response to an input Dirac delta function placed somewhere within the isoplanatic patch.

Suppose then, we have knowledge of

$$h(x - \xi_n; \xi_n) = S[\delta(y - \xi_n)] \tag{2-34}$$

for each isoplanatic patch. We must now divide our input, $f(\xi)$, into isoplanatic patches. Thus, let

$$f(\xi) = \sum_n f_n(\xi - \xi_n) \tag{2-35}$$

where

$$f_n(\xi-\xi_n) \triangleq f(\xi)\,\mathrm{rect}\left(\frac{\xi-m_n}{w_n}\right). \qquad (2\text{-}36)$$

The output of our piecewise isoplanatically modeled system can now be determined by operating on the input with our linear system operator in Eq. 2-1. We can extract the summation sign due to the homogeneity property of Eq. 2.2 to give

$$\tilde{g}(x) = \sum_n S[f_n(y - \xi_n)]. \qquad (2\text{-}37)$$

We place the "~" over g to denote that our computed output is a PIA of the true output. Over each segment of the input lying within an isoplanatic patch, the system operator is space-invariant and can thus be expressed via the convolution integral in Eq. 2-10. Our desired line spread function is given by Eq. 2-34. Thus:

$$S[f_n(\xi - \xi_n)] = \int_{-\infty}^{\infty} f_n(\xi - \xi_n)h(x - \xi;\ \xi_n)d\xi$$

$$= f_n(x - \xi_n) * h(x;\ \xi_n) \qquad (2\text{-}38)$$

where "*" denotes *convolution*. Substituting this result into Eq. 2-37 gives

$$\tilde{g}(x) = \sum_n f_n(x - \xi_n) * h(x;\ \xi_n). \qquad (2\text{-}39)$$

Using the shift theorem and the linearity of the Fourier

operator,[28] we can write the Fourier transform of the PIA as

$$\tilde{G}(f_x) = \sum_n F_n(f_x)\exp(-j2\pi f_x \xi_n) H_x(f_x;\xi_n). \tag{2-40}$$

We now inverse transform, this time grouping the complex exponential with the system transfer function. Doing this changes the shift from the input to the line spread function:

$$\tilde{g}(x) = \sum_n f_n(x) * h_n(x - \xi_n;\xi_n). \tag{2-41}$$

This is the desired final form of the PIA. Note that we have here approximated our superposition integral as a summation of convolutions. Equivalently, we can interpret the PIA as a number of outputs of isoplanatic systems which, when superimposed, give an approximate output to the parent space-variant system.

To further compare the PIA output to the true output, we substitute Eq. 2-36 into Eq. 2-41 and express our convolutional operation in integral form. The result is

$$\tilde{g}(x) = \sum_n \int_{\ell_n}^{u_n} f(\xi)h(x - \xi;\ \xi_n)d\xi. \tag{2-42}$$

Consider then, the system output given by the superposition integral in Eq. 2-21. We can break up our range of

integration from $-\infty$ to ∞ into those regions we have modeled as isoplanatic and write:

$$g(x) = \sum_n \int_{\ell_n}^{u_n} f(\xi)h(x - \xi; \xi)d\xi. \qquad (2\text{-}43)$$

One sees that as each isoplanatic patch width narrows around ξ_n (matched by a corresponding increase in patch density), the PIA in Eq. 2-42 approaches the true output given by the superposition integral in Eq. 2-43.

Let us now discuss some of the properties of the PIA. First of all, as promised, the number of required system responses has been reduced from the continuum number required by the superposition integral to a countable number. That is, for the PIA, we need only one defining system relationship per isoplanatic patch. For inputs with finite support (space limited inputs), the PIA will require only a finite number of defining relationships. The price we pay lies in the work "approximation." How good an approximation is the PIA? For the general case, this is a difficult question to answer. The development and use of the PIA is simply intuitively pleasing. For some specific example systems, the reader is referred to the work of Marks and Krile[7] who have shown that the PIA gives "good" results when applied to the magnifier and Fourier transformer. It should be noted also that when applied to invariant systems, the PIA and true outputs are identical

since invariant systems can be thought of as a special class of piecewise isoplanatic systems.

An important aspect of the PIA scheme is its characteristic of being essentially input independent. That is, the manner in which our line spread function changes shape as an input Dirac delta shifts is determined solely by the system. If the line spread function changes shape only slightly corresponding to an input interval, then we can model that interval as an isoplanatic patch. The act of input plane patch calibration is therefore independent of the input we choose.

As a final note in this section, we should note that the PIA can also be applied to the input frequency domain using the system frequency response instead of the line spread function. Although the concept of a "piecewise frequency-invariant*" system requires a different physical interpretation, the mathematical development is identical to that of the PIA. One merely divides up the input spectrum into frequency-invariant (instead of isoplanatic) patches and utilizes a sample frequency response (instead of line spread function) from somewhere within each patch.

*Frequency-invariant systems are defined rigourously in Appendix A.

2.4. Discrete Orthonormal Basis Set Response (DBR) Characterization

2.4.1. General

The piecewise isoplanatic approximation is a method by which the required number of defining input-output relationships of a system can be reduced to a countable set. Another method of performing such a reduction uses a method somewhat similar to the previously discussed continuum orthonormal basis set response characterization. The only difference is that the orthonormal basis set is now discrete. Whereas the PIA is primarily system dependent, the discrete orthonormal basis set response characterization[8] (DBR for short) will be seen to be primarily dependent on the system input.

In order to reduce our required number of defining input-output relations to a countable set, it is always necessary to make a restrictive assumption. In the PIA, we assumed the space-variant system was piecewise isoplanatic. For the DBR characterization, our restrictive assumption is that the class of allowable inputs can be expressed in terms of a specified orthonormal basis set. As we will see, the system can then be completely characterized by knowledge of the system response to each element in the given discrete orthonormal basis set.

Before developing the DBR characterization of a linear system, it is instructive to review the concepts of the discrete orthonormal basis set. A set of functions, $\{\psi_n(y)\}$, is said to be orthonormal in the discrete sense, if

$$\int_{-\infty}^{\infty} \psi_n(y)\psi_m^*(y)dy = \delta_{nm} \tag{2-44}$$

where δ_{nm} is the Kronecker delta:

$$\delta_{nm} = \begin{cases} 1 & ; \quad n = m \\ 0 & ; \quad n \neq m. \end{cases} \tag{2-45}$$

A discrete orthonormal basis set is said to be complete[30] if

$$\sum_n \psi_n^*(\xi)\psi_n(\eta) = \delta(\xi - \eta). \tag{2-46}$$

A signal, f(y), can be expressed in terms of a complete discrete orthonormal basis set by the expansion

$$f(y) = \sum_n \alpha_n \psi_n(y) \tag{2-47}$$

where the coefficients, α_n, are found from the inner product

$$\alpha_n = \int_{-\infty}^{\infty} f(y)\psi_n^*(y)dy. \tag{2-48}$$

We can prove the validity of this expansion as follows. First, substitute Eq. 2-48 into Eq. 2-47 and exchange orders of summation and integration. Utilizing the completeness property in Eq. 2-46 and the sifting

property of the Dirac delta in Eq. 2-5 then reduces the relationship to the identity $f(y) = f(y)$.

The DBR characterization of a linear system is found by substituting the orthonormal expansion in Eq. 2-47 into the linear system operator of Eq. 2-1. We can extract the summation sign from the system operator due to the superposition property in Eq. 2-2. The coefficients may be factored out by using the homogeneity property of Eq. 2-3. The result is

$$g(x) = \sum_n \alpha_n S[\psi_n(y)]. \tag{2-48}$$

Thus, we can express the output to the linear system with knowledge of the system's response to each element in the discrete orthonormal basis set. Let us denote this response by

$$\phi_n(x) = S[\psi_n(y)]. \tag{2-49}$$

Thus, our expansion for the system output in Eq. 2-48 becomes

$$g(x) = \sum_n \alpha_n \phi_n(x). \tag{2-50}$$

We can relate the response set elements in terms of the system line spread function by

$$\phi_n(x) = \int_{-\infty}^{\infty} \psi_n(\xi) h(x - \xi; \xi) d\xi. \tag{2-51}$$

Note that the DBR set, $\{\phi_n(x)\}$, is in general not orthogonal.

2.4.2. The Sinc and Rect Response Characterizations

With the general concept of the DBR characterization of linear systems established, we now specifically address two classes of inputs commonly encountered in signal processing. The first is the bandlimited signal[33] whose expansion coefficients are simply the signal's sampled values for an appropriately chosen basis set. The second class are those inputs with finite support which can be expressed in the familiar Fourier series expansion.

A bandlimited signal is, by definition, a signal whose Fourier transform has finite support. We will here specifically consider that class of low-pass signals, $f(\xi)$, whose Fourier transform is identically zero outside the interval $|\nu| \leq W$. As such, we can write

$$F(\nu) = F(\nu)\,\mathrm{rect}\left(\frac{\nu}{2W}\right). \qquad (2\text{-}52)$$

Such signals can be expressed via the Whittaker[34] - Shannon[35] sampling theorem[23]:

$$f(\xi) = \sum_n f(\xi_n)\,\mathrm{sinc}\ 2W(\xi - \xi_n) \qquad (2\text{-}53)$$

where

$$\xi_n = \frac{n}{2W} \qquad (2\text{-}54)$$

and

$$\text{sinc } x \triangleq \frac{\sin \pi x}{\pi x} . \tag{2-55}$$

The uniformly converging[36] sampling theorem expansion in Eq. 2-54 can be considered as a special case of a discrete orthonormal expansion. Here, our basis set elements are

$$\psi_n(y) = \sqrt{2W} \text{ sinc } 2W(y - \xi_n). \tag{2-56}$$

The expansion coefficients are simply the signal's sample values:

$$\alpha_n = \sqrt{2W} \int_{-\infty}^{\infty} f(\xi) \text{sinc } 2W(\xi - \xi_n) d\xi. \tag{2-57}$$

Utilizing Parseval's theorem gives

$$\begin{aligned} \alpha_n &= \frac{1}{\sqrt{2W}} \int_{-\infty}^{\infty} F(\nu) \exp(j2\pi\nu\xi_n) \text{rect}(\tfrac{\nu}{2W}) d\nu \\ &= \frac{1}{\sqrt{2W}} \int_{-\infty}^{\infty} F(\nu) \exp(j2\pi\nu\xi_n) d\nu \qquad (2\text{-}58) \\ &= \frac{1}{\sqrt{2W}} f(\xi_n). \end{aligned}$$

To characterize a linear system for the class of bandlimited inputs, we need knowledge of the system response to all elements in the sinc basis set of Eq. 2-56. In accordance with Eqs. 2-50 and 2-58, our system output can be written as

$$g(x) = \sum_n f(\xi_n)\ S[\text{sinc } 2W(y - \xi_n)]. \quad (2\text{-}59)$$

This "sinc-response" characterization has quite nice implementation properties as far as coherent processing is concerned. First of all, the sinc function is one that can be generated by quite straightforward optical means. We will dwell on this facet further in Chapter IV. Secondly, the expansion coefficients are simply the sample values of the signal. As such, no inner product computation, such as in Eq. 2-48, is required. Again the sinc response linear system characterization is valid only for the class of bandlimited inputs.

A second input class consists of those inputs of finite support. This class may be considered the Fourier dual of the bandlimited signal whose Fourier transform has finite support. In the bandlimited case, sampling is performed in the spatial domain. For the class to now be considered, sampling will be performed in the frequency domain.

We here consider only those inputs that are identically zero outside the interval $|\xi| \leq T$. That is

$$f(\xi) = f(\xi)\,\text{rect}(\tfrac{\xi}{2T}). \quad (2\text{-}60)$$

Such signals can be expressed in a Fourier series[24] expansion:

$$f(\xi) = \frac{1}{2T} \sum_n F(f_n)\exp(j2\pi f_n \xi)\,\mathrm{rect}(\tfrac{\xi}{2T}) \qquad (2\text{-}61)$$

where $f_n = n/2T$. The rect term merely retains the zeroth order term of the periodic expansion which is our input. The Fourier series is also a special case of a discrete orthonormal expansion. The n^{th} orthonormal basis function for the Fourier series is

$$\psi_n(y) = \frac{1}{\sqrt{2T}}\, e^{j2\pi f_n y}\ \mathrm{rect}(\tfrac{y}{2T}). \qquad (2\text{-}62)$$

The expansion coefficients are thus sample values of the input's Fourier transform:

$$\alpha_n = \frac{1}{\sqrt{2T}} \int_{-\infty}^{\infty} f(\xi)\exp(-j2\pi f_n \xi)\,d\xi$$

$$= \frac{1}{\sqrt{2T}}\, F(f_n). \qquad (2\text{-}63)$$

In this computation, we have included the finite support of the input by virtue of Eq. 2-60.

To characterize a linear system for the specified class of finite support (or space-limited) inputs, we require knowledge of the system response to all elements of the form of Eq. 2-62. With reference to Eqs. 2-50 and 2-63, our system output is

$$g(x) = \frac{1}{2T} \sum_n F(f_n)\ S[\exp(j2\pi f_n y)\,\mathrm{rect}(\tfrac{y}{2T})]. \qquad (2\text{-}64)$$

As with the sinc-response characterization, this "rect-response" characterization has quite nice implementation properties when applied to coherent processing. The required orthonormal basis set elements can be generated straightforwardly and the expansion coefficients are simply the sample values of the input's Fourier transform.

The sinc and rect responses are only two examples of orthonormal basis sets that can be applied to the characterization of a linear system. They do, however, utilize elements that, as we shall see, are easily generated by coherent optical techniques. Note also that, in general, DBR characterizations of linear systems places restriction only on the permissable class of inputs and is thus system independent.

2.5. Sampling Theorem Representations

In the previous section, we have seen that the class of bandlimited signals can be expressed via the Whittaker-Shannon sampling theorem. For certain systems, the sampling theorem can also be applied to the line spread function. We will here look at two cases. The first is when the line spread function, $h(x; \xi)$, is bandlimited in x. In this case, we can express the system output an expansion utilizing samples of the line spread function of the form $h(x_n; \xi)$. This scheme is essentially input independent

and thus can be grouped with the PIA in this regard. The second case where the sampling theorem is applicable to system characterization is when the line spread function, $h(x; \xi)$, is bandlimited in ξ. In order to apply the sampling theorem to this class of systems, the system input must also be bandlimited. Thus, unlike any other method thus far discussed, this scheme is both input and system dependent.

The class of linear systems to which the two sampling theorems are applicable can be enlarged by considering the system frequency response instead of the line spread function. For example, if $h(x; \xi)$ is not bandlimited in x or ξ, it might be possible that the corresponding $k(x - c\nu; \nu)$ might be bandlimited with respect to one of its variable.

For both of the sampling theorems considered, the system output is shown to be bandlimited and, as such, can be expressed by a conventional Whittaker-Shannon sampling theorem expansion. The required sample values of the output are shown to be the product of infinite matrices the components of which are the sample values of the system line spread function and input. A great simplification occurs for those systems falling into both classes for which the sampling theorems are applicable, that is, for line spread functions, $h(x; \xi)$, that are bandlimited in both x and ξ.

2.5.1. Line Spread Function Bandlimited in x

When we say a line spread function, $h(x; \xi)$, is bandlimited in x, we simply mean that the generalized transfer function, $H_x(f_x; \xi)$ as defined in Eq. 2-26, has finite support in f_x for all ξ. Let us consider only the low pass case where $H_x(f_x; \xi)$ is identically zero for all $|f_x| > W_x$. That is

$$H_x(f_x; \xi) = H_x(f_x; \xi)\,\mathrm{rect}\left[\frac{f_x}{2W_x}\right]. \quad (2\text{-}65)$$

This relation is satisfied if our output line spread function is bandlimited irrespective of the location of our input Dirac delta. We would thus expect that, regardless of our input, our output would be bandlimited. We can show this by substituting Eq. 2-65 into the output frequency relationship in Eq. 2-27:

$$G(f_x) = \mathcal{F}_\xi[f(\xi)H_x(f_x; \xi)]\Big|_{\nu = f_x}\,\mathrm{rect}\left(\frac{f_x}{2W_x}\right). \quad (2\text{-}66)$$

Thus, irrespective of our input, the corresponding spectrum (Fourier transform) of the output will be identically zero for all $|f_x| > W_x$. As such, we can express the system output by the following sampling theorem expansion:

$$g(x) = \sum_n g(x_n)\,\mathrm{sinc}\ 2W_x\ (x - x_n). \quad (2\text{-}67)$$

The output sample coefficients of this expansion are given by

$$g(x_n) = \int_{-\infty}^{\infty} f(\xi)h(x_n - \xi;\ \xi)d\xi. \quad (2\text{-}68)$$

We will later give alternate more computationally prone expressions of the sample output. The system line spread function can also be expressed in sampling theorem form:[25]

$$h(x;\ \xi) = \sum_n h(x_n;\ \xi)\,\mathrm{sinc}\ 2W_x(x - x_n). \quad (2\text{-}69)$$

Substituting this result into the output frequency relationship in Eq. 2-25 gives

$$G(f_x) = F_\xi F_x[f(\xi) \sum_n h(x_n;\ \xi)\,\mathrm{sinc}\ 2W_x(x - x_n)]\Big|_{\nu = f_x}$$

$$= \frac{1}{2W_x} \sum_n F_\xi[f(\xi)h(x_n;\ \xi)]\Big|_{\nu = f_x} \exp(-j2\pi x f_x)\,\mathrm{rect}\left(\frac{f_x}{2W_x}\right) \quad (2\text{-}70)$$

where, in the second step, we have recognized that

$$F_x[\mathrm{sinc}\ 2W_x(x-x_n)] = \frac{1}{2W_x} \exp(-j2\pi f_x x_n)\,\mathrm{rect}\left(\frac{f_x}{2W_x}\right). \quad (2\text{-}71)$$

Utilizing the similarity in definition between $F_x(\cdot)$ and $F_\xi(\cdot)$ as given in Eqs. 2-23 and 2-24, we can rewrite Eq. 2-70 as

$$G(f_x) = \frac{1}{2W_x} \sum_n F_x[f(x)h(x_n;\ x)]\ \exp(-j2\pi x_n f_x). \quad (2\text{-}72)$$

Inverse Fourier transformation then gives

$$g(x) = \sum_n [f(x)h(x_n; x)]*\text{sinc } 2W_x(x - x_n) \tag{2-73}$$

where, again, "*" denotes convolution. Note that in this expression we have expressed the system output as a summation of convolutions. Thus, in effect, the space-variant system is represented by a number of isoplanatic systems each with an input-output relationship dictated by a convolution operation.

In our sampling theorem expression in Eq. 2-73 we are using sample line spread functions of the form $h(x_n;\xi)$ as exemplified in Figure 2-4. We physically measure these sample functions by placing on our output plane an array of detectors spaced as $x_n = n/2W_x$. These detectors measure the system output for an input $\delta(y)$. As the input Dirac delta moves to $\delta(y - \xi)$, our corresponding output is $h(x - \xi; \xi)$. In order for the n^{th} detector to measure $h(x_n; \xi)$, we must also shift our entire output array to be centered at $x = \xi$. The output measured by the n^{th} detector as a function of ξ is the desired $h(x_n; \xi)$.

It is also possible, however, to measure our sample line spread function using an array that does not shift in accordance with the location of our input Dirac delta. This follows from the observation that if $h(x; \xi)$ is bandlimited in x, then so is $h(x - \xi; \xi)$. That is from the shift theorem [28]

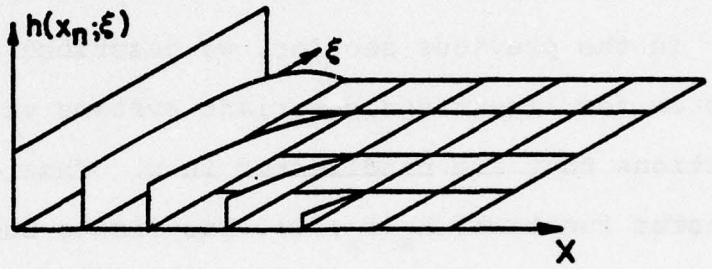

Figure 2.4 A result of sampling the line spread function in Figure 2.1b in x.

$$F_x[h(x - \xi; \xi)] = F_x[h(x; \xi)]\exp(-j2\pi\xi f_x). \quad (2\text{-}74)$$

Our measurement scheme here utilizes the same detector array as before but with no shifting of the detectors. As the input Dirac delta is positioned at different values of ξ, the n^{th} output detector will measure $h(x_n - \xi; \xi)$. Note that through use of this sampling scheme, we cannot regain the functional form $h(x_n; \xi)$.

2.5.2. Line Spread Function Bandlimited in ξ

In the previous section, we described a sampling theorem for linear space-variant systems with line spread functions that are bandlimited in x. That is, the system transfer function, $H_x(f_x; \xi)$, has finite support in f_x for all ξ. An alternate sampling theorem exists when the line spread function $h(x; \xi)$, is bandlimited in ξ for all x.[9] To facilitate definition of the corresponding bandwidth, we define the system "variation spectrum" as

$$H_\xi(x; \nu) = F_\xi[h(x; \xi)]. \quad (2\text{-}74)$$

Note the similarity between the definitions of the system variation spectrum and the system transfer function repeated here from Eq. 2-26:

$$H_x(f_x; \xi) = F_x[h(x; \xi)]. \quad (2\text{-}75)$$

The function, $H_\xi(x;\nu)$, is called the variation spectrum because its support is a measure of how the system line spread function changes shape when ξ is varied. The system is said to be variation limited if $H_\xi(x;\ \nu)$ has finite support in ν for all x. We will here consider the low pass case where

$$H_\xi(x;\ \nu) = H_\xi(x;\ \nu)\,\mathrm{rect}\left(\frac{\nu}{2W_\nu}\right). \qquad (2\text{-}76)$$

The quantity $2W_\nu$ is appropriately called the variation bandwidth.

To illustrate the application of the variation bandwidth to measure the spatial variance of a system, consider the case where the system is isoplanatic. That is $h(x;\ \xi) \rightarrow h(x)$. In this case, the corresponding variation spectrum is $H_\xi(x;\ \nu) = h(x)\delta(\nu)$. The corresponding variation bandwidth is zero. Thus, we can conclude, as expected, that an isoplanatic system is indeed space-invariant.

Returning now to the sampling theorem derivation, we inspect the computational form of the output frequency relationship in Eq. 2-25 which is repeated here:

$$G(f_x) = F_\xi F_x[f(\xi)h(x;\ \xi)]\Big|_{\nu=\ f_x}. \qquad (2\text{-}77)$$

A sufficient condition for the product $f(\xi)h(x;\ \xi)$ to be

bandlimited in ξ is that our input, $f(\xi)$, be bandlimited and that our system be variation limited with a variation bandwidth of, say, $2W_\nu$. Let the bandwidth of our input be $2W_f$ where

$$\begin{aligned} F(\nu) &= \mathcal{F}_\xi[f(\xi)] \\ &= F(\nu)\ \text{rect}\ (\frac{\nu}{2W_f}). \end{aligned} \tag{2-78}$$

Multiplication in the spatial (ξ) domain corresponds to convolution in the frequency (ν) domain. If two functions have finite support, then the support of the convolution of the two functions is upper bounded by the sum of the supports of the component functions. Thus, we conclude that the upper bound for the bandwidth of the product $f(\xi)h(x;\xi)$ in ξ is given by the sum of the component bandwidths. That is

$$\mathcal{F}_\xi[f(\xi)h(x;\ \xi)] = \mathcal{F}_\xi[f(\xi)h(x;\ \xi)]\text{rect}(\frac{\nu}{2W_s}) \tag{2-79}$$

where the bandwidth sum, $2W_s$, is given by

$$2W_s = 2W_f + 2W_\nu . \tag{2-80}$$

We can immediately express the product $f(\xi)h(x;\xi)$ in a sampling theorem expansion:

$$f(\xi)h(x;\ \xi) = \sum_n f(\xi_n)h(x;\ \xi_n)\text{sinc}\ 2W_s(\xi - \xi_n) \tag{2-81}$$

where

$$\xi_n = \frac{n}{2W_s} . \tag{2-82}$$

Substituting Eq. 2-81 into Eq. 2-77 and utilizing the Fourier transform relationship in Eq. 2-71 gives

$$G(f_x) = \sum_n f(\xi_n) F_x[h(x; \xi_n)] F_\xi[\text{sinc } 2W_s(\xi - \xi_n)] \Big|_{\nu = f_x}$$

$$= \frac{1}{2W_s} \sum_n f(\xi_n) H_x(f_x; \xi_n) \exp(-j2\pi f_x \xi_n) \text{rect}\left(\frac{f_x}{2W_s}\right). \tag{2-83}$$

Here, we have used the system transfer function notation in Eq. 2-26. Inverse Fourier transformation gives the final result:

$$g(x) = \sum_n f(\xi_n) h(x - \xi_n; \xi_n) * \text{sinc } 2W_s x. \tag{2-84}$$

As with the case where $h(x; \xi)$ was bandlimited in x, we have here reduced our system characterization to a summation of convolutions or, equivalently, the output of our space-variant system is given by the superposition of the outputs of a number of isoplanatic systems. In Eq. 2-84, however, the input as well as the line spread function is sampled in contrast to the previous scheme of Eq. 2-72 where only the line spread function is sampled. Thus, this scheme is both input and system dependent. In a sense we have oversampled in the expression in Eq. 2-84. That is, the minimum allowable sampling rate for

our input is $2W_f$ and the line spread function requires a sampling rate of only $2W_\nu$. But we have sampled both the input and line spread function at a rate of $2W_s = 2W_f + 2W_\nu$. As is shown in Appendix B, however, sampling at the minimum allowable rates results in an expression that is highly unattractive in a computational sense when compared to the intuitively pleasing form of Eq. 2-84.

The physical interpretation of sampling $h(x; \xi)$ in ξ is much different than sampling it in x. In the latter case, we have seen that an array of output detectors is required which records the system line spread function as the input $\delta(y-\xi)$ explores the continuum values of ξ. When sampling $h(x; \xi)$ in ξ, however, it is necessary to record the entire output field. An input $\delta(y-\xi_n)$ appears at the output as $h(x - \xi_n; \xi_n)$ which is a sample line spread function. The Dirac delta is then translated by a sampling interval corresponding to the next value of n and the process is repeated. An example of a line spread function sampled in this manner is in Fig. 2.5. It is important to note that the condition that $h(x; \xi)$ is bandlimited in ξ does not necessarily imply that $h(x-\xi;\xi)$ is bandlimited in ξ. This point will be discussed shortly.

Consider, next, the implementation of Eq. 2-84. Again, our space-variant system is represented as the sum of a number of isoplanatic systems. The n^{th} component isopla-

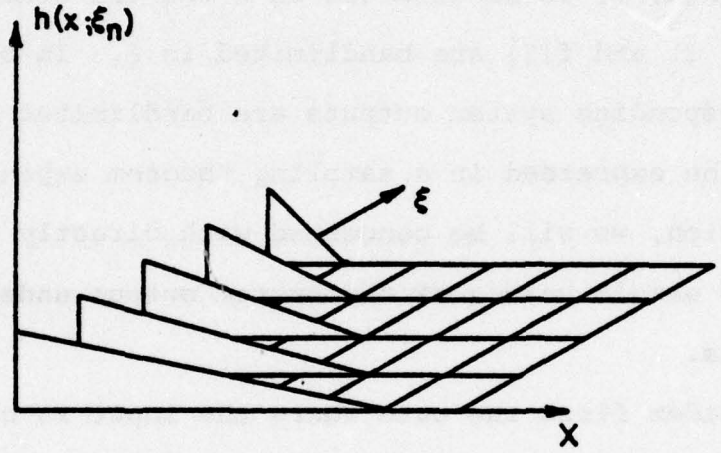

Figure 2.5 A result of sampling the line spread function in Figure 2.1b in ξ.

natic system has a line spread function $h(x - \xi_n; \xi_n)$ and is fed a sample value of the input of the form $f(\xi_n)\delta(y-\xi_n)$. The outputs from the component systems are added and then passed through a low pass filter of bandwidth $2W_s$ which supplies the required convolution sinc in Eq. 2-84.

2.5.3. Discrete (Matrix) Representations

We have discussed two space-variant sampling theorems; one when $h(x; \xi)$ is bandlimited in x and the other when both $h(x; \xi)$ and $f(\xi)$ are bandlimited in ξ. In both cases, the corresponding system outputs are bandlimited and thus can also be expressed in a sampling theorem expansion. In this section, we will be concerned with directly determining these sample values of the system output under various conditions.

Consider first the case where the input is bandlimited and $h(x; \xi)$ is bandlimited in ξ. From the rect term in Eq. 2-83, we conclude the system output is bandlimited with bandwidth $2W_s$. As such, we can express the output in the following sampling theorem expansion:

$$g(x) = \sum_m g(x_m)\,\mathrm{sinc}\; 2W_s(x - x_m) \qquad (2\text{-}85)$$

where here

$$x_m = \frac{m}{2W_s}.$$

We now define the low-pass line spread function

$$\hat{h}(x - \xi_n;\xi_n) \triangleq 2W_s h(x - \xi_n;\xi_n) * \text{sinc } 2W_s x. \qquad (2\text{-}86)$$

The coefficient $2W_s$ is used to assure that both $\hat{h}(\cdot,\cdot)$ and $h(\cdot,\cdot)$ have identical units. Using the low-pass line spread function, the sampling theorem expression in Eq. 2-84 can be written

$$g(x) = \frac{1}{2W_s} \sum_n f(\xi_n)\hat{h}(x - \xi_n;\ \xi_n). \qquad (2\text{-}87)$$

The expression for our output sample values follows immediately as

$$g(x_m) = \frac{1}{2W_s} \sum_n f(\xi_n)\hat{h}(x_m - \xi_n;\ \xi_n). \qquad (2\text{-}88)$$

This relationship can be viewed as a discrete version of the superposition integral in Eq. 2-8. The computational form is that of an infinite matrix. That is, an infinite vector composed of the sample input values multiplies an infinite matrix of the sample line spread function values to give an infinite vector composed of the corresponding output sample values.

Let's now investigate the corresponding case when the system line spread function is bandlimited in x. From the rect term in Eq. 2-71, the system output is bandlimited in x with bandwidth $2W_x$ and can thus be expressed in the sampling theorem expansion in Eq. 2-85. But it is necessary to redefine x_m in this relationship as

$$x_m = \frac{m}{2W_x}. \tag{2-89}$$

In order to determine the output sample values in this case, we rewrite Eq. 2-72 in integral form:

$$g(x) = \sum_n \int_{-\infty}^{\infty} f(\xi)h(x_n;\ \xi)\,\mathrm{sinc}\ 2W_x(x - \xi - x_n)d\xi. \tag{2-90}$$

It follows that

$$g(x_m) = \sum_n \int_{-\infty}^{\infty} f(\xi)h(x_n;\ \xi)\,\mathrm{sinc}\ 2W_x(x_m - x_n - \xi)d\xi$$

$$= \sum_n [f(x)h(x_n;\ x)]*\mathrm{sinc}\ 2W_x x\Big|_{x = x_m - x_n}. \tag{2-91}$$

As can be seen, the discrete treatment for this case does not in general result in the computational attractive matrix form encountered in Eq. 2-88.

Computational simplifications occur in the discrete treatment for systems in which 1) the input is bandlimited and 2) the line spread function is bandlimited in both x and ξ. Consider first the spectrum of the convolution term in Eq. 2-91:

$$\mathcal{F}_x[f(x)h(x_n;x)*\mathrm{sinc}\ 2W_x x]$$

$$= \frac{1}{2W_x}\,\mathcal{F}_x[f(x)h(x_n;x)]\,\mathrm{rect}\left(\frac{f_x}{2W_x}\right).$$

Consider then the case where, from Eq. 2-79, $h(x;\xi)$ and

$f(\xi)$ are also bandlimited in ξ:

$$F_x[f(x)h(x_n;x)] = F_x[f(x)h(x_n;x)]\,\mathrm{rect}\left(\frac{f_x}{2W_x}\right). \tag{2-92}$$

If $W_s < W_x$, then the $\mathrm{rect}(f_x/2W_x)$ term in Eq. 2-92 serves no purpose. That is, the term does not chop off higher frequencies simply because there are no frequencies greater than $W_s < W_x$. For this condition, we conclude that

$$f(x)h(x_n;x) * \mathrm{sinc}\ 2W_x x = \frac{1}{2W_x} f(x)h(x_n;x);\ W_s < W_x. \tag{2-93}$$

Thus, our sampling theorem expression in Eq. 2-91 becomes

$$g(x_m) = \frac{1}{2W_x} \sum_n f(x_m - x_n)h(x_n;\ x_m - x_n);\ W_s < W_x. \tag{2-94}$$

Making the index change $\hat{n} = m - n$ gives the final desired relationship for this case:

$$g(x_m) = \frac{1}{2W_x} \sum_{\hat{n}} f(x_{\hat{n}})h(x_m - x_{\hat{n}};x_{\hat{n}})\ ;\ W_s < W_x. \tag{2-95}$$

We have again arrived at an infinite matrix relationship. Note that we are again oversampling but in a different manner. Before sampling was performed at a rate of $2W_s$ in the ξ direction. In Eq. 2-95, sampling is performed at a rate $W_x > W_s$ in the ξ direction so that sampling indexes will match.

Let us now apply a similar approach to the expansion in Eq. 2-88 in which the input is bandlimited and $h(x;\xi)$

is bandlimited in ξ. Consider the low-pass line spread function as defined in Eq. 2-86 for the case where $W_x < W_s$. Employing arguments identical to those just used, we conclude that

$$\hat{h}(x - x_n; x_n) = h(x - x_n; x_n) \; ; \; W_s > W_x \quad (2\text{-}96)$$

in which case, Eq. 2-88 becomes

$$g(x_m) = \frac{1}{2W_s} \sum_n f(x_n) h(x_m - x_n; x_n) \; ; \; W_s > W_x . \quad (2\text{-}97)$$

When $f(\xi)$ and $h(x;\xi)$ are bandlimited in both x and ξ, either the expression in Eq. 2-95 or in Eq. 2-97 applies depending on which bandwidth, W_s or W_x, is larger. We can combine these two relations into a single expression by writing

$$g(x_m) = \frac{1}{2W} \sum_n f(\xi_n) h(x_m - \xi_n; \xi_n) \quad (2\text{-}98)$$

where

$$x_m = \xi_m = m/2W \quad (2\text{-}99)$$

and

$$W = \max[W_x, W_s]. \quad (2\text{-}100)$$

In all cases of Eq. 2-98, we are oversampling. Suppose that we wished to sample at the minimum allowable rate. That is, sample $f(\xi)$ at a rate of $2W_f$ and sample

$h(x; \xi)$ at a rate of $2W_x$ in x and $2W_\nu$ in ξ. As is shown in Appendix B, the sample value of the output is given in this case by

$$g(x_m) = \sum_r \sum_p \sum_q f(\frac{p}{2W_f})\ h(\frac{r}{2W_x}; \frac{q}{2W_\nu}) I_{pqr}(\frac{m}{2W}) \qquad (2\text{-}101)$$

where

$$I_{pqr}(x) = [\text{sinc}(2W_f x - p)\ \text{sinc}(2W_\nu x - q)] * \text{sinc}\ (2W_x x - r), \qquad (2\text{-}102)$$

Clearly, the discrete superposition in Eq. 2-98 is computationally much simpler than the above triple sum of continuous convolutions. The price we pay for this reduction in complexity, however, is the increased sampling rate.

2.5.4. Alternate Sampling Theorems

We have developed two basic sampling theorems applicable to two classes of linear systems. The first is applicable to systems in which $h(x; \xi)$ (and thus $h(x-\xi;\xi)$) is bandlimited in x. The second is for variation limited systems with a bandlimited input. Clearly, these two linear system classes form only two small subsets of the set of all linear systems.

It is possible, however, to widen this class by utilization of various forms of the system line spread function which might be bandlimited in one or more variables. For example, if $h(x - \xi; \xi)$ has finite support

in ξ for all x, it follows that its Fourier transform with respect to ξ will be bandlimited in ν for all x. The Fourier transform of the line spread function, as is given in Eq. 2-22, is simply the system frequency response. Thus we can utilize the frequency response characterization in Eq. 2-20 and develop a corresponding sampling theorem. For another system, $h(x - \xi; \xi)$ might be bandlimited in ξ. Note that, from Fig. 2.1, the condition of $h(x; \xi)$ being bandlimited in ξ does not necessarily assure that $h(x - \xi; \xi)$ is bandlimited in ξ. At any rate this is a condition not yet discussed for which a sampling theorem can be easily derived.

In this section, we will present a brief rundown of these and other possible input/system conditions where the sampling theorem is applicable. The list is in no way meant to be exhaustive. There are forms of the line spread function that we here have not even considered yet.[25] The expressions to be listed are rather meant to illustrate the relative ease in application of sampling theorem concepts to the system process. For the purpose of completeness, the two sampling theorems previously discussed are included. In stating these sampling theorems, we use various forms of the system line spread function such as the frequency response, transfer function, variation spectrum, etc. Throughout, we use the notation

$F(\nu) = F_{\xi}[f(\xi)]$. All of these sampling theorems are special cases of the superposition integral:

$$g(x) = \int_{-\infty}^{\infty} f(\xi)h(x - \xi;\ \xi)d\xi. \qquad (2\text{-}103)$$

1) For the case where $h(x;\ \xi)$ is bandlimited in x, we rewrite from Eq. 2-65:

$$H_x(f_x;\ \xi) = H_x(f_x;\ \xi)\,\mathrm{rect}\left(\frac{f_x}{2W_x}\right). \qquad (2\text{-}104)$$

This relation is a sufficient condition for the sampling theorem expansion in Eq. 2-73 repeated here:

$$g(x) = \sum_n [f(x)h(x_n;\ x)]*\mathrm{sinc}\ 2W_x(x - x_n) \qquad (2\text{-}105)$$

where $x_n = n/2W_x$.

2) The Fourier dual of the above occurs when

$$K_x(f_x;\ \nu) \triangleq F_x[k(x;\ \nu)]$$

$$= K_x(f_x;\ \nu)\,\mathrm{rect}\left(\frac{f_x}{2W_x}\right). \qquad (2\text{-}106)$$

Note that this condition is equivalent to that in Eq. 2-104. That is, if $h(x;\ \xi)$ has bandwidth $2W_x$ in x, then so does $k(x;\ \xi)$. Under the condition of Eq. 2-106, our sampling theorem expansion is simply the Fourier dual of Eq. 2-105:

$$g(x) = \frac{1}{c}\sum_n \left[F\left(\frac{x}{c}\right)k\left(x_n;\frac{x}{c}\right)\right]*\mathrm{sinc}\ 2W_x(x - x_n) \qquad (2\text{-}107)$$

where, again, $x_n = n/2W_x$.

3) For the case where both $f(\xi)$ and $h(x; \xi)$ are band-limited in ξ, our conditions are

$$H_\xi(x; \nu) = H_\xi(x; \nu)\text{rect}(\frac{\nu}{2W}) \tag{2-108}$$

and

$$F(\nu) = F(\nu)\text{rect}(\frac{\nu}{2W_f}), \tag{2-109}$$

From Eq. 2-84, our corresponding sampling theorem expression is

$$g(x) = \sum_n f(\xi_n)h(x - \xi_n; \xi_n)*\text{sinc } 2W_s x \tag{2-110}$$

where $W_s = W_\nu + W_f$ and $\xi_n = n/2W_s$.

4) The conditions for the Fourier dual of the above sampling theorem expansion are

$$K_\nu(x; \xi) \triangleq \int_{-\infty}^{\infty} k(x; \nu)e^{-j2\pi\nu\xi}d\nu$$

$$= K_\nu(x; \xi)\text{rect}(\frac{\xi}{2T_\nu}) \tag{2-111}$$

and

$$f(\xi) = f(\xi)\text{rect}(\frac{\xi}{2T_f}). \tag{2-112}$$

It follows that the Fourier dual of Eq. 2-110 is then

$$g(x) = \frac{1}{c} \sum_n F(\nu_n)k(x - c\nu_n; \nu_n)*\text{sinc } (2T_s x/c) \tag{2-113}$$

where $T_s = T_\nu + T_f$ and $\nu_n = n/2T_s$.

5) We here consider the case where $h(x - \xi; \xi)$ is bandlimited in ξ. Since the frequency response is the Fourier transform of $h(x - \xi; \xi)$, it follows that this condition is satisfied when

$$k(x - c\nu; \nu) = k(x - c\nu; \nu)\,\mathrm{rect}\left(\frac{\nu}{2W_h}\right). \quad (2\text{-}114)$$

We must also restrict the input to be bandlimited:

$$F(\nu) = F(\nu)\,\mathrm{rect}(\nu/2W_h). \quad (2\text{-}115)$$

It then follows from previous arguments that the product $f(\xi)h(x - \xi; \xi)$ has bandwidth $2W_t = 2W_h + 2W_f$. Thus, we can write:

$$f(\xi)h(x-\xi;\xi) = \sum_n f(\xi_n)h(x-\xi_n;\xi_n)\,sinc\ 2W_t(\xi-\xi_n) \quad (2\text{-}116)$$

where $\xi_n = n/2W_t$. Integrating over all ξ yields

$$\begin{aligned} g(x) &= \int_{-\infty}^{\infty} f(\xi)h(x-\xi;\xi)\,d\xi \\ &= \sum_n f(\xi_n)h(x-\xi_n;\xi_n)\int_{-\infty}^{\infty} sinc\ 2W_t(\xi-\xi_n) \\ &= \frac{1}{2W_t}\sum_n f(\xi_n)h(x-\xi_n;\xi_n). \end{aligned} \quad (2\text{-}117)$$

This is the desired sampling theorem expansion for the conditions in Eqs. 2-114 and 2-115.

6) The conditions for the Fourier dual of the above sampling theorem expansion are

$$h(x-\xi;\xi) = h(x-\xi;\xi)\,\mathrm{rect}\left(\frac{\xi}{2T_h}\right) \tag{2-118}$$

and

$$f(\xi) = f(\xi)\,\mathrm{rect}\left(\frac{\xi}{2T_f}\right). \tag{2-119}$$

The Fourier dual of Eq. 2-117 follows immediately as

$$g(x) = \frac{1}{2T_t} \sum_n F(\nu_n)\,k(x - c\nu_n;\ \nu_n) \tag{2-120}$$

where $T_t = T_h + T_f$ and $\nu_n = n/2T_t$.

2.6. Characterization Comparisons

In this chapter, we have explored various methods by which a linear system can be characterized. In all cases, this characterization is performed by probing the system with various inputs and observing the corresponding system response. Under certain system and/or input class constraints, the set of sufficient conditions required to completely characterize the system performance varies.

For the general linear system with no restriction on the input class, cataloging the system response to all elements in a continuum orthonormal basis set sufficies for complete system characterization. Special cases of this scheme include use of the Dirac delta orthonormal basis set in which case the system is characterized by the superposition integral. The system response to each element in the Dirac delta class is termed the system line spread

function. Another orthonormal basis set consists of the complex exponential whose input into the system results in the system frequency response. By appropriate manipulations of the frequency response and line spread function characterizations with Fourier transform operations, it was shown that the output spectrum in each case could be directly expressed. The ease in performing these manipulations was due primarily to our particular choice of line spread function and frequency response notation.

Three characterization schemes in which restrictions were placed on the system and/or input were also discussed in this chapter. These consisted of the discrete orthonormal basis set response (DBR) characterization, the piecewise isoplanatic approximation (PIA), and the sampling theorem characterizations. In each case, the continuum number of system responses required in the general case was reduced to a countable number. In certain instances, the system characterization reduced to the superposition of a number of invariant systems. Each of the three schemes is characterized by distinct properties that we shall now review and contrast.

The DBR characterization scheme places a restriction on the class of allowable system inputs. That is, system inputs are restricted to those signals which can be expressed in an orthonormal series expansion for a given

orthonormal basis set. The scheme is thus only input dependent and can be utilized for any linear system. The system is completely characterized with knowledge of the system response due to each element in the discrete orthonormal basis set.

The PIA is a scheme that is input independent. That is, the restrictive assumption concerns only the system. The system line spread function is assumed to have sufficiently negligible variation with respect to its second variable over an input patch. The system can be then approximated as piecewise isoplanatic. In order to completely characterize a piecewise isoplanatic system, we need knowledge of the system line spread functions corresponding to an input Dirac delta placed within each of the input isoplanatic patches. The resulting system characterization consists of a countable number of invariant systems whose outputs are summed to give the approximated output of the parent linear variant system.

The final method discussed for characterizing linear variant systems utilized application of the sampling theorem. One sampling theorem requires a bandlimiting assumption on the system line spread function and is thus input independent. The second sampling theorem requires that the system is variation limited and that the system input be bandlimited. This latter scheme is thus

both input and system dependent.

All of the system characterizations discussed will be applied in one degree or another, to the design of coherent optical processors for performing general space-variant operations although they can be applied to any linear system. The continuum orthonormal basis set response characterization will be utilized in the next chapter for design of one-dimensional space-variant processors. The PIA, DBR, and sampling theorem characterization are used in Chapter IV to extend generalized space-variant processing to two dimensions.

We note finally that the derivations of the system characterizations here were formal. That is, they lack mathematical rigor. Such treatment was used for reasons of continuity and clarity of presentation. The manipulations used however, are relatively standard[2,23,24,28,40,64,66] and can be shown to be valid under certain physical realizability criteria which, as witnessed by the experimental results in Chapter III, are characteristic of coherent optical processors.

CHAPTER III

3. ONE-DIMENSIONAL SPACE-VARIANT PROCESSORS

In this chapter we shall utilize the continuum orthonormal basis set response characterizations of linear systems to develop coherent optical processors capable of performing a wide class of one-dimensional (1-D) space-variant operations. Recognition of the capability of coherent processors to perform general linear integral type of operations can probably be credited to Cutrona et.al.[1,12] More recent schemes in one-dimensional processing include those of Rhodes et.al.,[37-38] whose work primarily was concerned with frequency-variant processing. The bulk of the one-dimensional processing schemes in this chapter are due to the work of Marks et.al.[14] and also follow closely the independent work of Goodman et.al.[13]

We begin this chapter with a presentation of two basic coherent processing schemes capable of performing a wide class of 1-D space-variant operations. The first, called the direct output display method, performs a one-dimensional space-variant operation and displays the system output along a line in the output plane of the coherent processor. The second scheme, termed the output spectrum display method does essentially the same thing, except the Fourier transform (or spectrum) of the system output is displayed.

Both schemes utilize a line spread function mask on which the system line spread function is recorded. Thin lenses are utilized to perform appropriate Fourier transformation and imaging operations. Numerous examples and experimental results are presented for various forms of these processors.

Due to the limited dynamic range of photographic transparencies, the line spread function masks corresponding to certain linear operations might possibly not be implementable. It might be possible, however, to record the corresponding frequency response of the operation may be able to be recorded on a mask. Thus, it is instructive to consider the Fourier duals of the previous two processors thereby increasing the class of space-variant systems to which the processor techniques are applicable.

3.1. Direct Output Display (DOD) Method

The direct output display (DOD) method for space-variant processing directly evaluates the superposition integral which we repeat here from Eq. 2-8:

$$g(x) = \int_{-\infty}^{\infty} f(\xi) h(x - \xi; \xi) d\xi. \quad (3\text{-}1)$$

A coherent processor capable of evaluating the superposition integral is shown in Figure 3-1. The one-dimensional

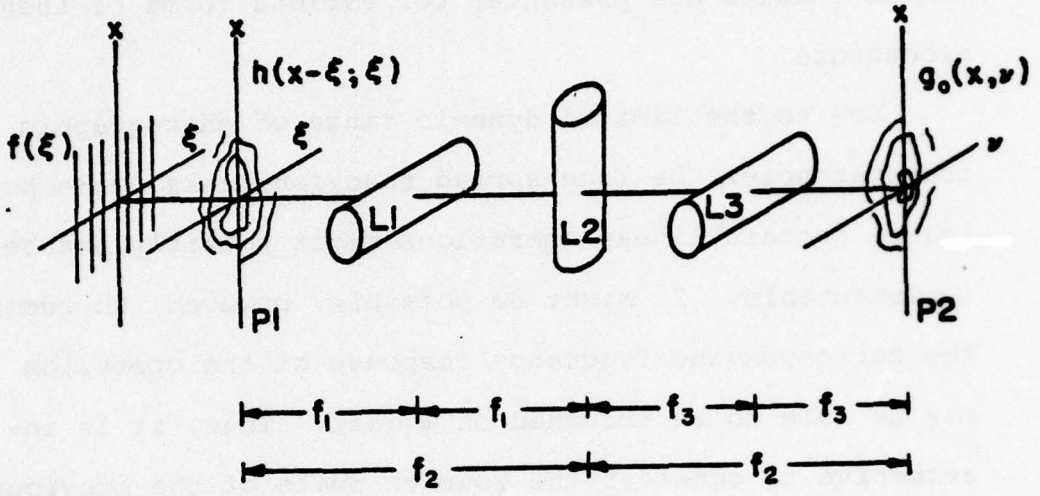

Figure 3.1 A coherent optical processor for performing 1-D space-variant operations. The desired processor output lies along the x axis on plane P_2.

input $f(\xi)$ is placed in plane P_1 directly adjacent to a mask on which the system line spread function $h(x - \xi; \xi)$ is recorded. Note that $f(\xi)$ covers the entire (x, ξ) plane with no variation in the x direction. Cylindrical lenses L_1, L_2 and L_3 have respective focal lengths of

$$2f_1 = f_2 = 2f_3. \tag{3-2}$$

Thus, when plane P_1 is illuminated from the left with a coherent plane wave, Fourier transformation is performed in the ξ direction, and imaging is performed in the x direction.[11] The field amplitude $g_o(x, \nu)$ on the output plane P_2 is then given by*

$$g_o(x; \nu) = \int_{-\infty}^{\infty} f(\xi)h(x - \xi; \xi)\exp(-j2\pi\nu\xi)d\xi \tag{3-3}$$

where the spatial frequency ν is related to the actual horizontal distance x_2 on plane P_2 by

$$\nu = x_2/\lambda f_2. \tag{3-4}$$

Here, λ is the wavelength of the spatially coherent illumination.

*Here and henceforth, constant multiplicative factors associated with field amplitude relations will be omitted since it is the functional interelations we are actually interested in.

Comparing the superposition integral in Eq. 3-1 with the processor output [Eq. 3-3], we find that

$$g(x) = g_o(x,0), \tag{3-5}$$

That is, the 1-D output, corresponding to the input and line spread function mask, appears in the processor output plane along the x axis. The desired space-variant operation has thus been performed. For later reference, this processing scheme, or modifications thereof, will be referred to as the direct output display or DOD method.

An alternate and somewhat simpler scheme for performing 1-D Fourier transformation is pictured in Fig. 3-2. As shown, spherical and cylindrical lenses, placed back to back, replace the three cylindrical lenses in Fig. 3-1. If we assign a focal length of f to both the spherical and cylindrical lens, this processor's output <u>intensity</u> distribution is the same as in Fig. 3-1 with $\nu = x_2/\lambda f$.[11]

The primary limitation of this processor is the allowable dynamic range of our line spread function mask. If a holographic mask is used then we must require that the values of $h(x - \xi;\xi)$ lie within the unit circle on the complex plane.[23] As we shall see in our first example, however, this limitation can sometimes be overcome by clever design.

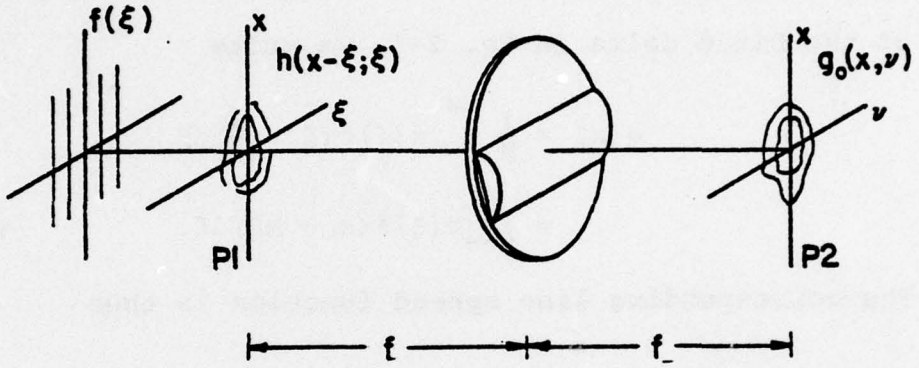

Figure 3.2 Another coherent processor for performing 1-D space-variant operations. The intensity distribution on P_2 is identical to that in Figure 1.

3.1.1. One-Dimensional Magnification

As our first example for specific application of the DOD processor, we consider the ideal magnifier which is characterized by the input-output relationship

$$g(x) = \frac{1}{M} f(x/M) \tag{3-6}$$

where M is the magnification. From the sifting property of the Dirac delta in Eq. 2-5, we write

$$\begin{aligned} g(x) &= \frac{1}{M} \int_{-\infty}^{\infty} f(\xi)\delta(\xi - \frac{x}{M})d\xi \\ &= \int_{-\infty}^{\infty} f(\xi)\delta(x - M\xi)d\xi. \end{aligned} \tag{3-7}$$

The corresponding line spread function is thus

$$h(x - \xi; \xi) = \delta(x - M\xi). \tag{3-8}$$

On the (x, ξ) plane, we interpret this relation as a Dirac delta sheet along the line $x = M\xi$. The magnification is simply the line's slope.

We may implement the DOD magnifier as shown in Fig. 3-3. The Dirac delta sheet is formed by focusing a plane wave with a cylindrical lens mounted on a rotatable assembly. We can change the slope of this sheet, and thus the resulting magnification, by simply rotating the lens. Note here, that by appropriate design, we have generated our line spread function without the use of a mask and thus have avoided the fundamental limitation of a

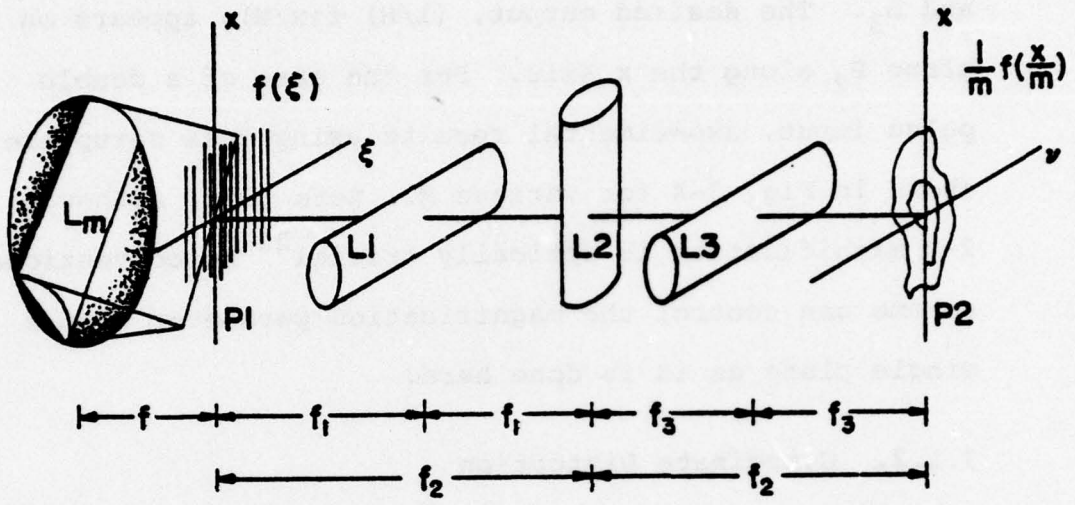

Figure 3.3 DOD processor for performing 1-D magnification. The magnification is equal to the slope of lens L_m which is mounted on a rotatable assembly.

mask's dynamic range in which a Dirac delta obviously does not fall.

In Fig. 3-3, at the lens' back focal plane, we place the input $f(\xi)$. As before, Fourier transformation is performed in the ξ direction by cylindrical lenses L_1, L_2, and L_3. The desired output, $(1/M)\ f(x/M)$, appears on plane P_2 along the x axis. For the case of a double pulse input, experimental results using this setup are shown in Fig. 3-4 for various M. Note that, although 2-D magnification is optically trivial[23] no conventional scheme can control the magnification parameter from a single plane as it is done here.

3.1.2. Coordinate Distortion

The magnifier scheme may be generalized to linear systems with input-output relationships of the form

$$g(x) = f[D(x)] \tag{3-9}$$

where we shall refer to $D(x)$ as the distortion function. From the sifting property of the Dirac delta, we can write

$$g(x) = \int_{-\infty}^{\infty} f(\xi)\delta[\xi - D(x)]d\xi. \tag{3-10}$$

The line spread function associated with Eq. 3-9 is thus

Figure 3.4 The output of the DOD processor in Fig. 3 to a double square pulse input. The magnifications are (a) M = 1/2, (b) M = 1, (c) M = 3.

$$h(x - \xi; \xi) = \delta[\xi - D(x)]. \qquad (3\text{-}11)$$

Our Dirac delta sheet is now bent along the locus $\xi = D(x)$ on the (x, ξ) plane. Such a bent Dirac delta may be crudely generated by an appropriately bent glass rod which acts as a curved cylindrical lens. Experimental results, using a glass rod with a single bend, are shown in Fig. 3-5. The resulting lens slopes, as shown in Fig. 3-6(a), constitute different magnifications for $\xi > 0$ and $\xi < 0$. The DOD processor output for the input pulse configuration in Fig. 3-6(b) is shown in Fig. 3-5.

An alternate form of distortion, used by Rhodes,[37] employs the line spread function

$$h(x - \xi; \xi) = \exp[-j2\pi\xi D(x)]. \qquad (3\text{-}12)$$

Here, the system output is a distorted version of the input's spectrum

$$\begin{aligned} g(x) &= \int_{-\infty}^{\infty} f(\xi)\exp[-j2\pi\xi D(x)]d\xi \\ &= F[D(x)] \end{aligned} \qquad (3\text{-}13)$$

where $F(\nu)$ is the Fourier transform of the input

$$F(\nu) = \int_{-\infty}^{\infty} f(\xi)\exp(-j2\pi\nu\xi)d\xi. \qquad (3\text{-}14)$$

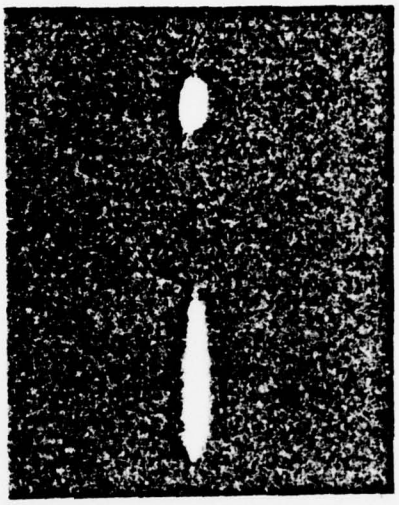

Figure 3.5 Output of a piecewise magnifier distortion processor corresponding to the inputs pictured in Fig. 3.6. The larger pulse is roughly three times the length of the smaller.

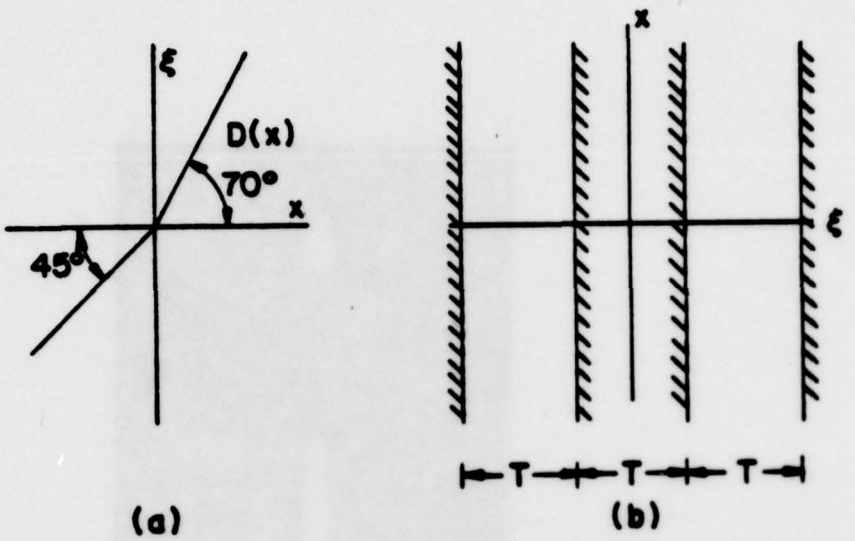

Figure 3.6 Inputs for piecewise magnification coordinate distortion DOD processor: (a) The distortion function D(x). For $\xi > 0$, we have magnification of $\tan 70° \approx 3$. For $\xi < 0$, $\tan 45° = 1$. (b) Double square pulse input.

Rhodes[37] uses such a system for generating a log-frequency display of the input by utilizing a distortion function proportional to ln(x).

3.1.3. Convolution and Correlation

The convolution operation is a special case of the superposition integral that arises when the linear system is space-invariant (or isoplanatic). From Eq. 2-10, the one-dimensional convolution integral is

$$g(x) = \int_{-\infty}^{\infty} f(\xi)h(x - \xi)d\xi$$
$$= f(x)*h(x). \qquad (3\text{-}15)$$

The capability of conventional coherent processors to perform two-dimensional convolution is well known.[23] All of these schemes, however, either necessitate that the Fourier transform of the line spread function (system transfer function) be recorded on an amplitude transmittance or require motion. These requirements inhibit real time application. As we will show, 1-D convolution can be performed with a variation of the DOD processor with no requirement of motion or Fourier encoding.

Before presenting the DOD processors capable of performing convolution and correlation, we digress briefly for a discussion of the geometrical interpretations of the spatial shift encountered in Eq. 3-15. Consider the

1-D function $r(\xi)$ in the (x, ξ) plane as pictured in Fig. 3-7(a). If we rotate this transparency about the origin through an angle of θ in the clockwise sense [Fig. 3-7(b)], the resulting 2-D function is described by

$$r[\xi\cos\theta - x \sin\theta]. \qquad (3\text{-}16)$$

For the case of a 45° rotation, we obtain $r[(\xi - x)/\sqrt{2}]$. To eliminate the $\sqrt{2}$ factor, scaling can be trivially accomplished by a conventional (2-D) imaging system with magnification $M = 1/\sqrt{2}$. Consider next physically rotating the transparency in Fig. 3-7(b) 180° about both its x and ξ axes. This constitutes coordinate reversal. For the case of $\theta = 45°$, the result would be the transmittance $r[(x - \xi)/\sqrt{2}]$, which is the scaled shift required by the convolution integral. Various other rotations could of course be employed to obtain a number of such shifts and scalings.

Consider, then, the DOD convolution processor as pictured in Fig. 3-8. In plane P_1, we place the transparency representing $h(\xi)$ with the 45° rotation shown. This function, $h[(\xi - x)/\sqrt{2}]$ is scaled and inverted by lenses L_a and L_b which have respective focal lengths of

$$f_a = \sqrt{2}\ f_b. \qquad (3\text{-}17)$$

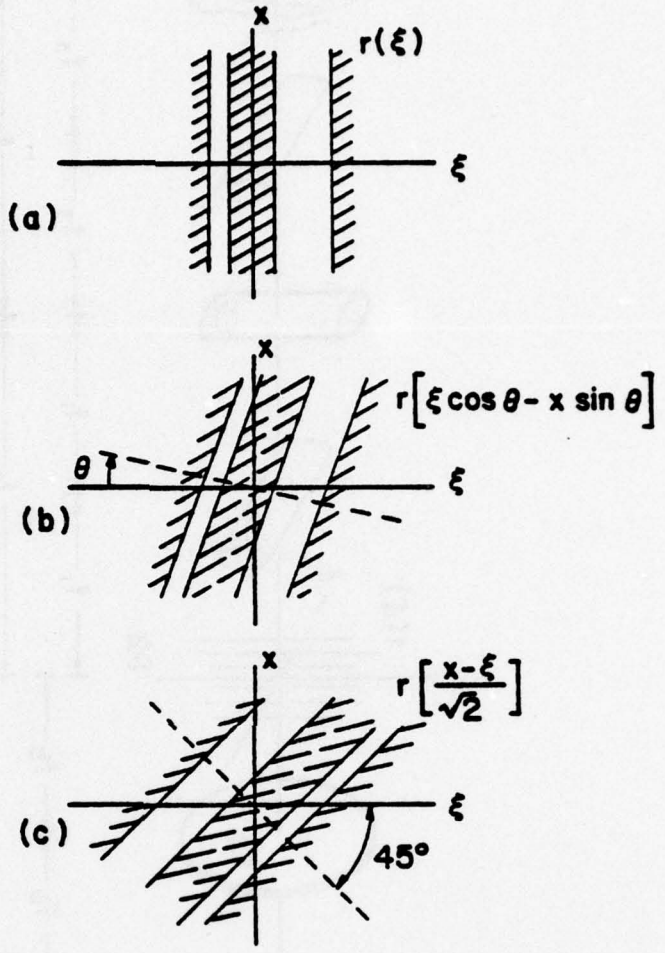

Figure 3.7 (a) A 1-D function $r(\xi)$ on the (x,ξ) plane. (b) The transmittance in (a) rotated clockwise about the origin and angle of θ. (c) The transmittance in (b) for $\theta = 45°$ with a coordinate reversal formed by physically rotating (b) about its ξ and x axes.

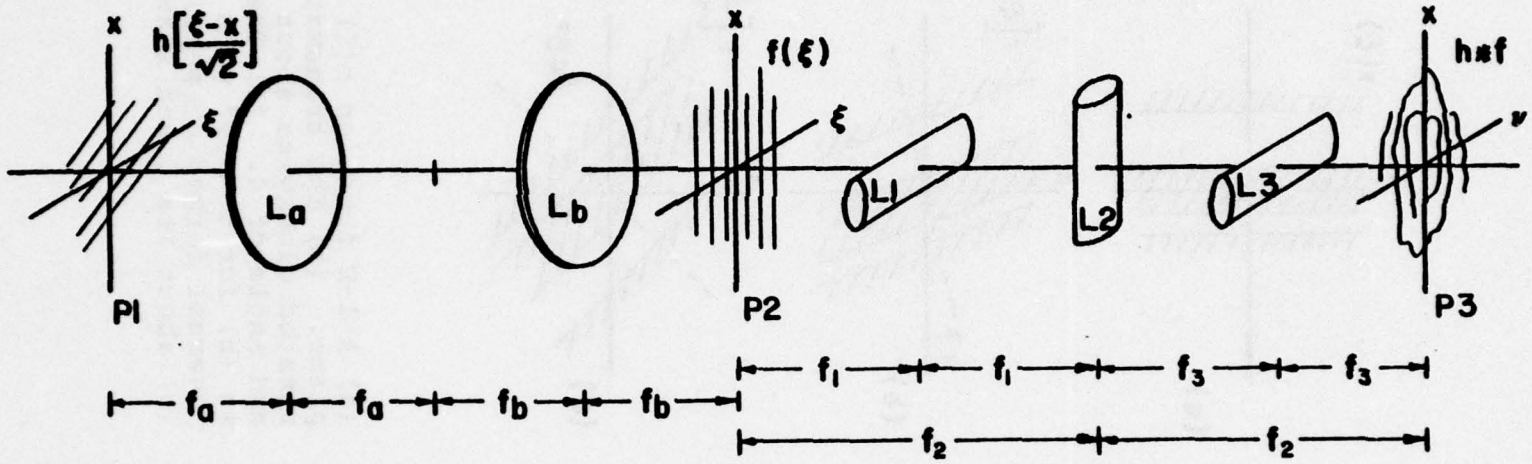

Figure 3.8 DOD processor for performing convolution. Lenses L_a and L_b have focal lengths related by $f_a = (2)^{1/2} f_b$ to perform scaling on the rotated transmittance on P_1.

Incident on plane P_2 is the desired $h(x - \xi)$ which multiplies the input transmittance $f(\xi)$. The product is then processed as before by the three cylindrical lenses. The output $(f * h)$ appears along the x axis in plane P_3.

A primary drawback to this processing scheme is finding two lenses which have a focal length ratio of $\sqrt{2}$. An alternate DOD processor exists, however, that does not require the use of these scaling lenses. We will illustrate such a processor that performs the correlation operation*:

$$g(x) = \int_{-\infty}^{\infty} f(\xi)h(\xi - x)d\xi$$
$$= f(x) \star h(x) \qquad (3\text{-}18)$$

where "$\star$" denotes correlation. Comparison with Eq. 3-15 reveals similar computational forms for convolution and correlation.

Consider, then, placing the 1-D transmittances, $f(\xi)$ and $h(\xi)$, in plane P_1 of the DOD processor in Fig. 3-1 each rotated 45° in such a manner as to form the product

$$f\left[\frac{\xi+x}{\sqrt{2}}\right] h \left[\frac{\xi-x}{\sqrt{2}}\right]. \qquad (3\text{-}19)$$

The field amplitude in plane P_2, after the 1-D Fourier transformation [Eq. 3-3], is

*For complex signals, $h(\cdot)$ is complex conjugated in this integral relation.

$$g_o(x;\ \nu) = \int_{-\infty}^{\infty} f(\frac{\xi+x}{\sqrt{2}})\, h(\frac{\xi-x}{\sqrt{2}}) \exp(-j2\pi\nu\xi)$$

$$= \sqrt{2}\, \exp(j2\pi\nu x) \int_{-\infty}^{\infty} f(\xi')$$

$$h[\xi' - \sqrt{2}x]\exp[-j2\pi(\sqrt{2}\nu)\xi']d\xi' \qquad (3\text{-}20)$$

where we have made the variable substitution $\xi' = (\xi+x)/\sqrt{2}$. Along the x axis, we obtain the output

$$g(x) = g_o(x;\ 0)$$

$$= \sqrt{2} \int_{-\infty}^{\infty} f(\xi')h(\xi - \sqrt{2}x)d\xi'. \qquad (3\text{-}21)$$

This relationship is recognized as a scaled version of the correlation integral and is thus the desired result. Convolution can of course be performed in a similar manner by choosing appropriate orientations of the 1-D input transparencies.

3.2. Entire Output Plane Utilization

The purpose of the DOD processor is to compute one-dimensional linear integral operations. The solution appears along a line in the processor output plane. There do exist some computational manipulations, however, in which the entire output plane can be utilized. These cases are serendipities of the DOD processor scheme. We briefly consider here two cases: Laplace transform and ambiguity function display.

AD-A050 973 TEXAS TECH UNIV LUBBOCK OPTICAL SYSTEMS LAB F/G 20/6
SPACE-VARIANT COHERENT OPTICAL PROCESSING.(U)
DEC 77 R J MARKS AFOSR-75-2855
UNCLASSIFIED SCIENTIFIC-1 AFOSR-TR-78-0212 NL

2 OF 3
AD
A050973

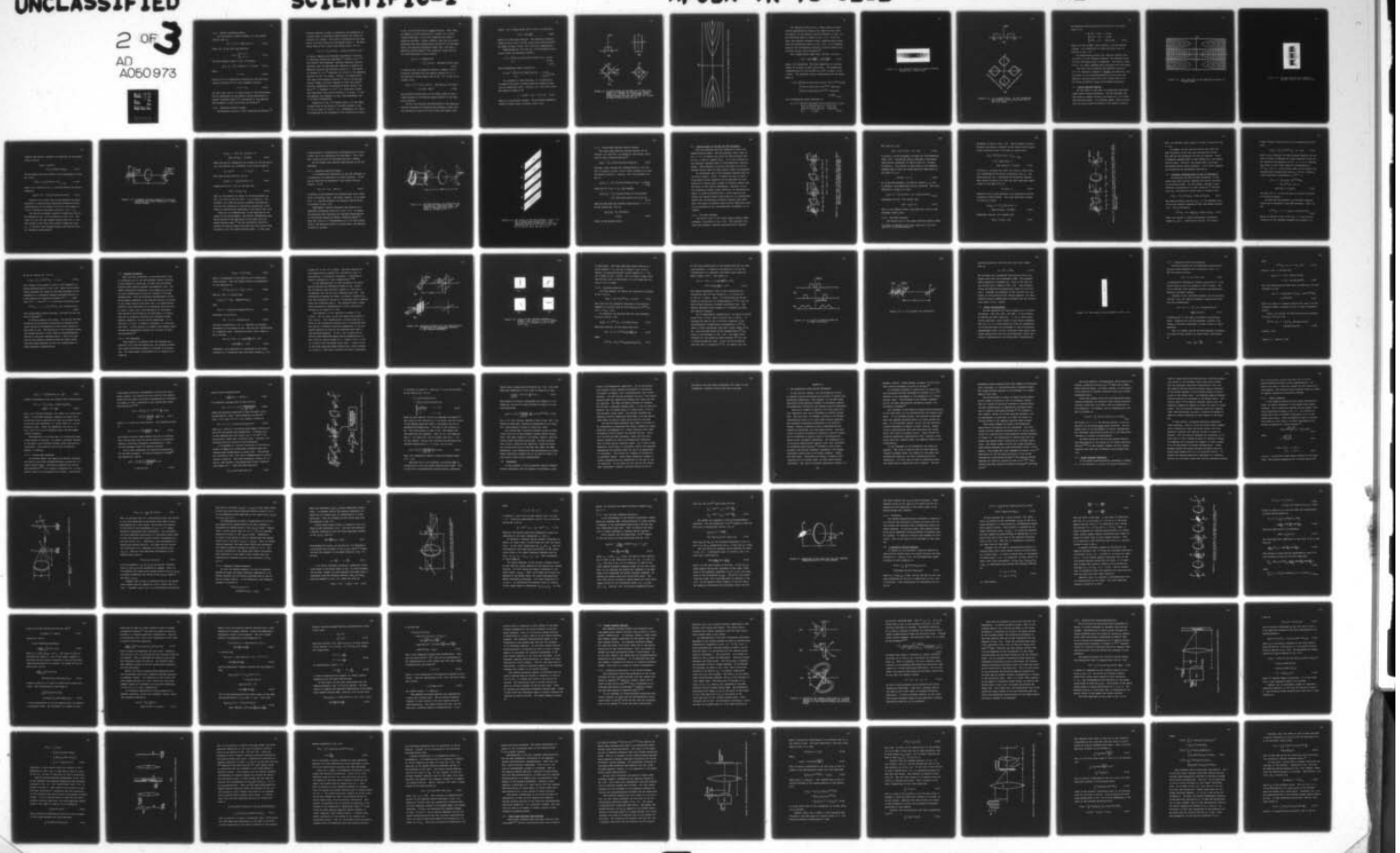

3.2.1. Laplace Transform Display

For the Laplace transform scheme, our line spread function mask is

$$h(\alpha - \xi; \xi) = \exp(-\alpha\xi)\mu(\xi) \tag{3-22}$$

where $\mu(\xi)$ is the unit step function:

$$\mu(\xi) = \begin{cases} 1 \;; \xi \geq 0 \\ 0 \;; \xi < 0 \end{cases} \tag{3-23}$$

The DOD processor output in Eq. 3-3 becomes

$$g_o(\alpha, \beta) = \int_o^\infty f(\xi)\exp[-(\alpha + j\beta)\xi]d\xi \tag{3-24}$$

where

$$\beta = 2\pi\nu. \tag{3-25}$$

Equation 3-23 is immediately recognized as the one-sided Laplace transform of $f(\xi)$ with frequency variable

$$s = \alpha + j\beta. \tag{3-26}$$

For this case, the (α, β) output plane of the DOD processor may be interpreted as the complex s plane encountered in Laplace transform theory.[28] A discussion of this specific DOD processor is given by Mueller and Carlson.[39]

3.2.2. Ambiguity Function Display

The ambiguity function, first introduced by Woodward,[40]

has been applied in radar in predicting the capability of a given signal to determine simultaneously the range and velocity of a target. The range is determined by the time delay x and the velocity by the Doppler shift ν. The ambiguity function for a given real-valued signal f(x) is

$$\chi(\nu; x) = \int_{-\infty}^{\infty} f(\xi)f(\xi - x)\exp(-j2\pi\nu\xi)d\xi. \quad (3\text{-}27)$$

In optics, Papoulis has employed the ambiguity function in analyzing diffraction phenomena.[41] Cutrona et.al.[1,12] and Preston[2] have proposed a coherent ambiguity function processor that utilizes multiple channels to display the ambiguity function for discrete values of x. The scheme of Casasent et. al.[42] generates 1-D slices of the ambiguity function in the (ν,x) plane. Similar 1-D displays have also been electronically produced.[43] Use of the DOD processing scheme, initially reported by Said and Cooper[15] and also independently discovered by Marks, Walkup, and Krile,[16] 1) displays $|\chi(\nu,x)|^2$ in a continuous (rather than quantized) form over the entire (ν,x) plane, 2) has the capacity for extension to real time processing, and 3) is easily implemented.

Inspection of Eq. 3-27 reveals that it is the computational form of the output of the DOD processor in Eq. 3-3 for an input of $f(\xi)f(\xi - x)$. Furthermore, the input is recognized as the integrand of the correlation integral

in Eq. 3-18 for the case of autocorrelation. Thus, when we compute an autocorrelation of a signal $f(\xi)$ as previously described, we are also computing the signal's ambiguity function. Recall, however, when the two transmittances were both appropriately rotated 45° in the input plane, the resulting processor output [Eq. 3-20] has a spatially varying phase.[11] For identical inputs the output field amplitude is then given by

$$g_o(x;\ \nu) = \sqrt{2}\exp(j2\pi\nu x) \times \int_{-\infty}^{\infty} f(\xi) f(\xi - \sqrt{2}x)\exp[-j2\pi(\sqrt{2}\nu)\xi]d\xi. \tag{3-27}$$

In dealing with the ambiguity function, however, one is primarily concerned with the modulus squared of $\chi(\cdot,\cdot)$. The spatially varying phase term in Eq. 3-27 is thus of no concern since

$$|g_o(x;\ \nu)|^2 = 2\left|\int_{-\infty}^{\infty} f(\xi) f(\xi - \sqrt{2}x)\exp[-j2\pi(\sqrt{2}\nu)\xi]d\xi\right|^2 = 2|\chi(\sqrt{2}\nu;\ \sqrt{2}x)|^2. \tag{3-28}$$

The intensity distribution on the output plane is thus a scaled version of the desired square modulus of the ambiguity function.

We will now evaluate the performance of the ambiguity function processor by comparing the processor output with the theoretical results for both single and double pulse

inputs. For a single pulse [Fig. 3-9(a)], we may write

$$f(\xi) = \text{rect}\left(\frac{\xi}{2T}\right) \tag{3-29}$$

where 2T is the pulse duration. The geometric interpretation of $f(\xi)$, $f[(\xi + x)/\sqrt{2}]$, and $f[(\xi+x)/\sqrt{2}]f[(\xi-x)/\sqrt{2}]$ are shown in Figs. 3-9(b), 9(c), and 9(d) respectively.

Substituting Eq. 3-29 into Eq. 3-27 followed by evaluation yields the ambiguity function

$$\chi(\nu;x) = \begin{cases} (2T-|x|)\,\text{sinc}\nu(2T-|x|)\exp(-j\pi\nu x); & |x| \leq 2T \\ 0 & ; \ |x|>2T. \end{cases} \tag{3-30}$$

The corresponding output intensity is

$$|\chi(\nu;x)|^2 = \begin{cases} (2T-|x|)^2\,\text{sinc}^2\nu(2T-|x|) & ; \ |x| \leq 2T \\ 0 & ; \ |x|<2T. \end{cases} \tag{3-31}$$

For purposes of identification, it is instructive to examine the locus of points where the ambiguity function is identically zero. From Eq. 3-31, this zero locus may easily be shown to be

$$\nu = n/(2T - |x|) \ ; \ |x| \leq 2T \tag{3-32}$$

where n is any nonzero integer. The piecewise hyperbolic nature of these curves is shown in Fig. 3-10.

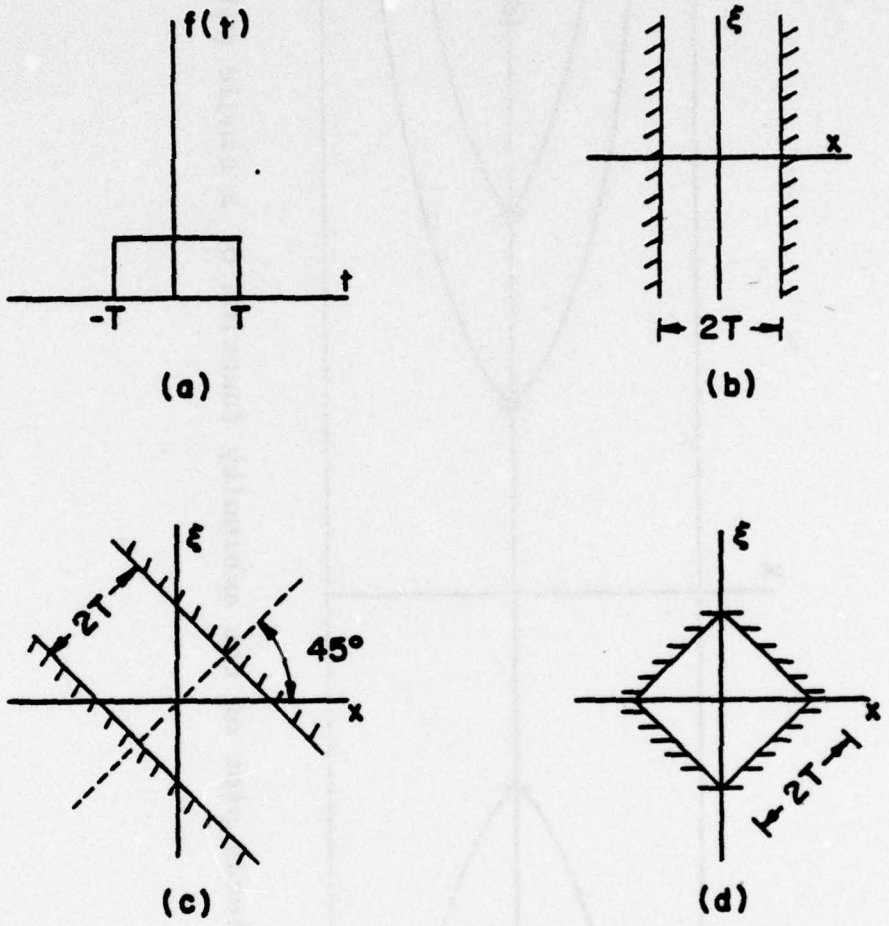

Figure 3.9 A single pulse (a) in time, (b) in the (x,ξ) plane, (c) rotated 45° on the (x,ξ) plane to form $f[(x + \xi)/\sqrt{2}]$, (d) the product of two pulses rotated 45° and -45° on the $(x;\xi)$ plane to form $f[(\xi+x)/\sqrt{2}]f[(\xi-x)/\sqrt{2}]$.

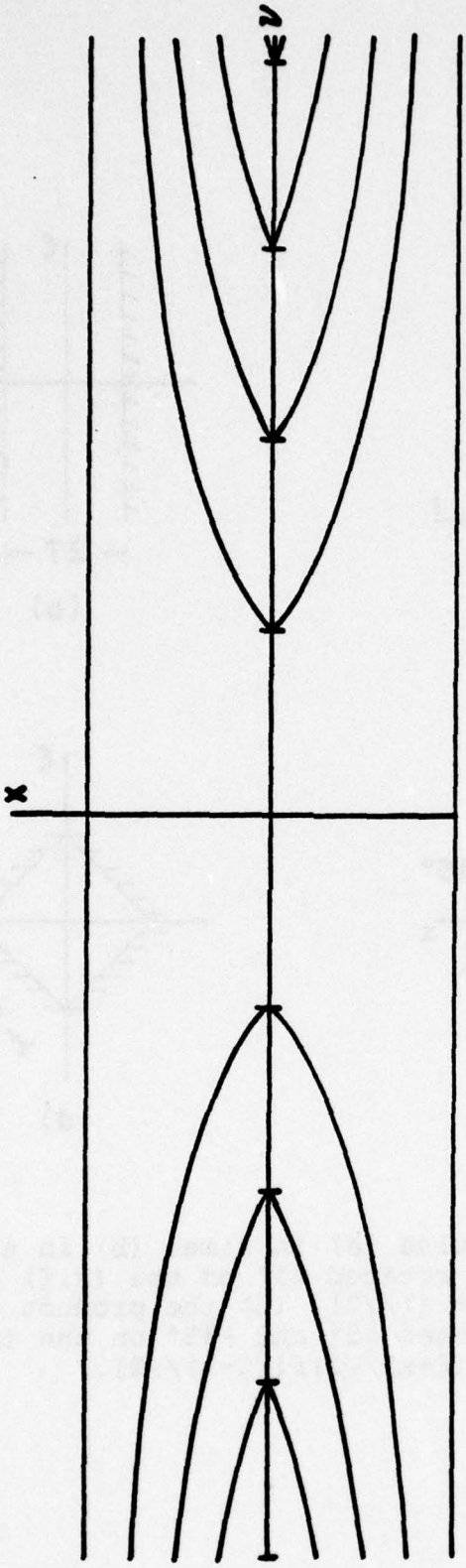

Figure 3.10 Zero locus plot of the ambiguity function of a single pulse.

The ambiguity function for a single pulse is generated by appropriately rotating two identical thin slits in plane P_1 of the coherent optical processor of Fig. 3-1. The resulting output is shown in Fig. 3-11. As can be seen, the coherent processor output compares quite nicely with the theoretical result in Fig. 3-10. A 3-D computer graph of the corresponding ambiguity function modulus can be found in Fig. 6-6 of Rihaczek.[44]

For a double pulse input [Fig. 3-12(a)], we write

$$f(\xi) = \text{rect}\left[\frac{\xi+2T}{2T}\right] + \text{rect}\left[\frac{\xi-2T}{2T}\right] \qquad (3\text{-}33)$$

where, for convenience, the pulse separation 2T has been chosen to be equal to each pulse width. The geometrical interpretation of $f[(\xi+x)/\sqrt{2}]f[(\xi-x)/\sqrt{2}]$ is shown in Fig. 3-12(b). The ambiguity function associated with the double pulse is

$$\chi(\nu,x) = \begin{cases} 2(2T-|x|)\,\text{sinc}\nu(2T-|x|)\cos(4\pi T\nu)e^{-j\pi x\nu}; & |x|\leq 2T \\ -(2T-|x|)\,\text{sinc}\nu(2T-|x|)e^{-j\pi x\nu}; & 2T\leq|x|\leq 4T \\ (6T-|x|)\,\text{sinc}\nu(6T-|x|)e^{-j\pi x\nu}; & 4T\leq|x|\leq 6T \\ & ; |x|\geq 6T. \end{cases} \qquad (3\text{-}34)$$

The corresponding output intensity is

$$|\chi(\nu,x)|^2 = \begin{cases} 4(2T-|x|)^2\text{sinc}^2\nu(2T-|x|)\cos^2(4\pi T\nu); & |x|\leq 2T \\ (2T-|x|)^2\text{sinc}^2\nu(2T-|x|) ; & 2T\leq|x|\leq 4T \\ (6T-|x|)^2\text{sinc}^2\nu(6T-|x|) ; & 4T\leq|x|\leq 6T \\ 0 ; & |x|\geq 6T. \end{cases} \qquad (3\text{-}35)$$

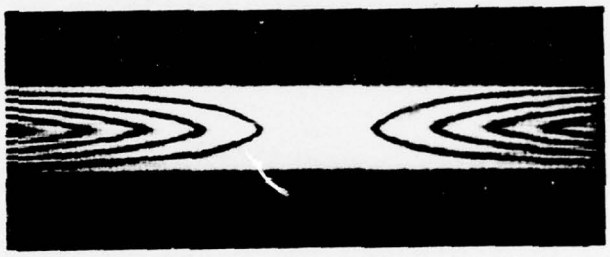

Figure 3.11 The ambiguity function (modulus squared) display for a single pulse.

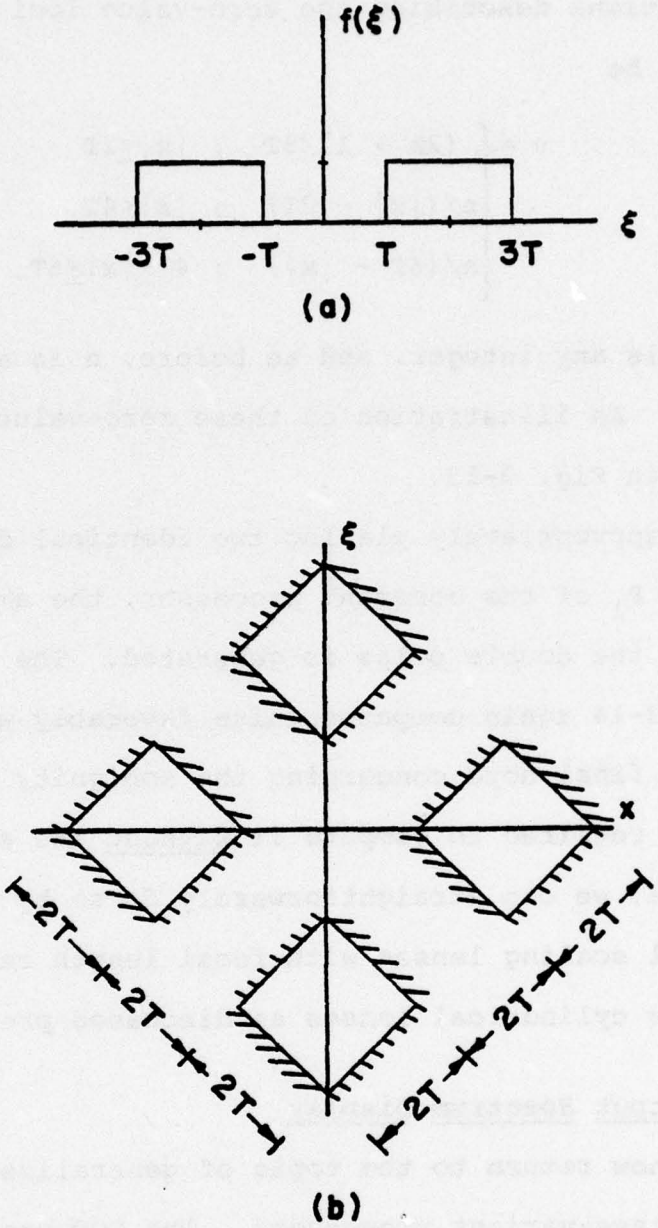

Figure 3.12 (a) A double pulse. (b) The corresponding function $f[(x+\xi)/\sqrt{2}]f[(x-\xi)/\sqrt{2}]$ in the (x,ξ) plane.

The equations describing the zero-value loci are easily shown to be

$$\nu = \begin{cases} (2m + 1)/8T & ; \ |x| \leq 2T \\ n/(|x| - 2T) & ; \ |x| \leq 4T \\ n/(6T - |x|) & ; \ 4T \leq |x| \leq 6T. \end{cases} \qquad (3\text{-}36)$$

where m is any integer, and as before, n is any nonzero integer. An illustration of these zero-value loci is offered in Fig. 3-13.

By appropriately placing two identical double slits in plane P_1 of the coherent processor, the ambiguity function for the double pulse is generated. The result, shown in Fig. 3-14 again compares quite favorably with the theory.

One final note concerning the ambiguity function. If it is required to compute it <u>without</u> the spatially varying phase, we can straightforwardly do so by using the spherical scaling lenses with focal length ratio of $\sqrt{2}$ and three cylindrical lenses as discussed previously.

3.3. Output Spectrum Display

We now return to the topic of generalized one-dimensional space-variant processors. The DOD processor has been shown to compute directly the output of a 1-D linear space-variant system. An alternate scheme, which we shall call the output spectrum display or DOD method, directly

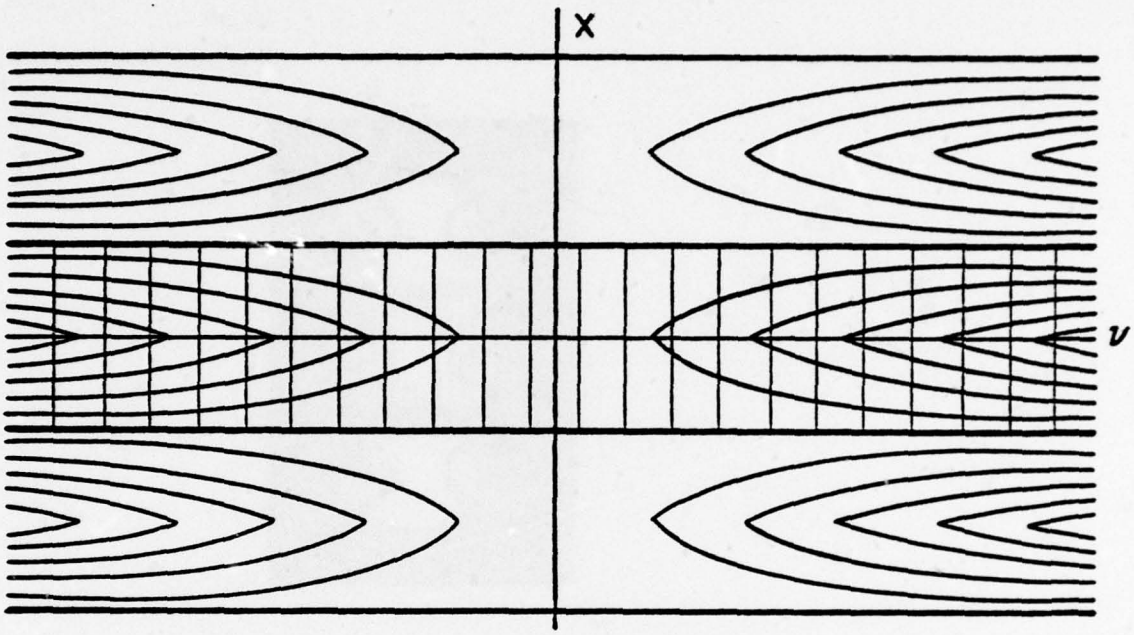

Figure 3.13 Zero locus plot of the ambiguity function of a double pulse.

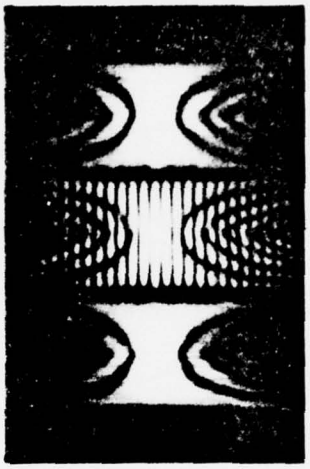

Figure 3.14 The ambiguity function (modulus squared) display for a double pulse

computes the Fourier transform (or spectrum) of the system output given by

$$G(f_x) = F_x[g(x)]$$
$$= \int_{-\infty}^{\infty} g(x)\exp(-j2\pi f_x x). \qquad (3\text{-}37)$$

We have shown that this relation can be expressed as [from Eq. 2-25]:

$$G(f_x) = F_\xi F_x[f(\xi)h(x;\ \xi)]\Big|_{\nu = f_x} \qquad (3\text{-}38)$$

where, for a function $p(x;\ \xi)$, we have defined the Fourier operation:

$$F_\xi[p(x;\ \xi)] = \int_{-\infty}^{\infty} p(x;\xi)\exp(-j2\pi\nu\xi)d\xi. \qquad (3\text{-}39)$$

Equation 3-38 states that we may generate the output spectrum of a space-variant system by successive Fourier transformation of the product $f(\xi)h(x;\xi)$ with respect to ξ and x followed by evaluation along the line $\nu = f_x$.

The coherent processor capable of generating the output spectrum in Eq. 3-38 is pictured in Fig. 3-15. The input $f(\xi)$ and the line spread function mask $h(x;\ \xi)$ are both placed in the front focal plane of spherical lens L_1. In the back focal plane we obtain the familiar Fourier transform relationship[23]

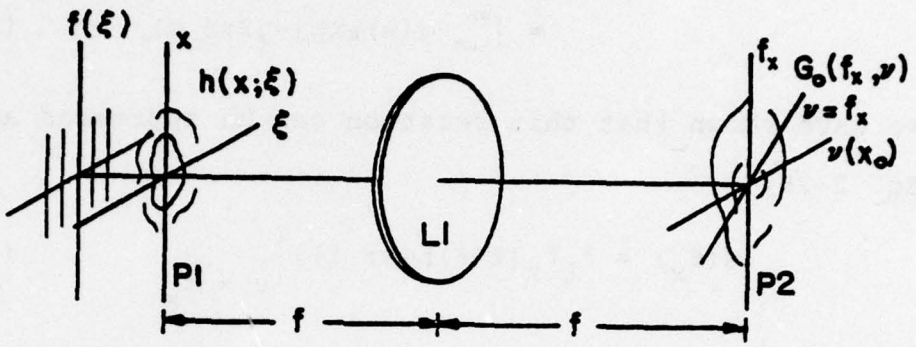

Figure 3.15 A coherent optical processor for directly displaying the output spectrum of a space-variant system.

$$G_o(f_x;\ \nu) = \int_{-\infty}^{\infty}\int_{-\infty}^{\infty} [f(\xi)h(x;\ \xi)]$$
$$\exp[-j2\pi(f_x x + \nu\xi)]dxd\xi \qquad (3\text{-}40)$$

where the spatial frequencies are related to the horizontal (x_o) and vertical (y_o) distances in the output plane by

$$f_x = y_o/\lambda f \qquad \nu = x_o/\lambda f . \qquad (3\text{-}41)$$

Note that we may write Eq. 3-40 as

$$G_o(f_x;\ \nu) = F_\xi F_x[f(\xi)h(x;\ \xi)]. \qquad (3\text{-}42)$$

Comparing with Eq. 3-38, we conclude that

$$G(f_x) = G_o(f_x,\ f_x). \qquad (3\text{-}43)$$

That is, the desired 1-D output of the OSD processor in Fig. 3-15 lies on the 45° line $\nu = f_x$ in plane P_2. Remarkably, this familiar Fourier transform configuration thus has the capability of potentially performing a wide number of space-variant operations of the form of Eq. 3-38.

When one is interested only in the magnitude of the output of the OSD processor, the Fourier transforming lens may be placed in the same plane as the input and line spread function mask.[23] One may furthermore completely discard the lens by simply including the lens' phase transmittance in the line spread function mask. In this case,

we may perform 1-D space-variant processing with an input, a mask, and a few centimeters of free space. Also, note that vignetting would be eliminated by such a scheme.

We now present some specific applications of the OSD processor.

3.3.1. Magnifier Spectrum Display

A straightforward application of the OSD processor is in displaying the spectrum of an ideal magnifier. We begin by rewriting the magnifier's line spread function from Eq. 3-8 as

$$h(x; \xi) = \delta[x - (M-1)\xi]. \qquad (3\text{-}44)$$

As before, we may generate the required Dirac delta sheet with a cylindrical lens. The slope, however, is now equal to M - 1. The OSD processor for spectrum magnification is pictured in Fig. 3-16.

Experimental results displaying the spectrum of a magnified rectangular pulse are in Fig. 3-17. As shown, the resulting sinc functions are inversely magnified due to the scaling theorem of Fourier transform theory.[28] Note that, for M = 0 (corresponding to a -45° delta sheet input), the magnified pulse is a Dirac delta, the spectrum of which is uniform.

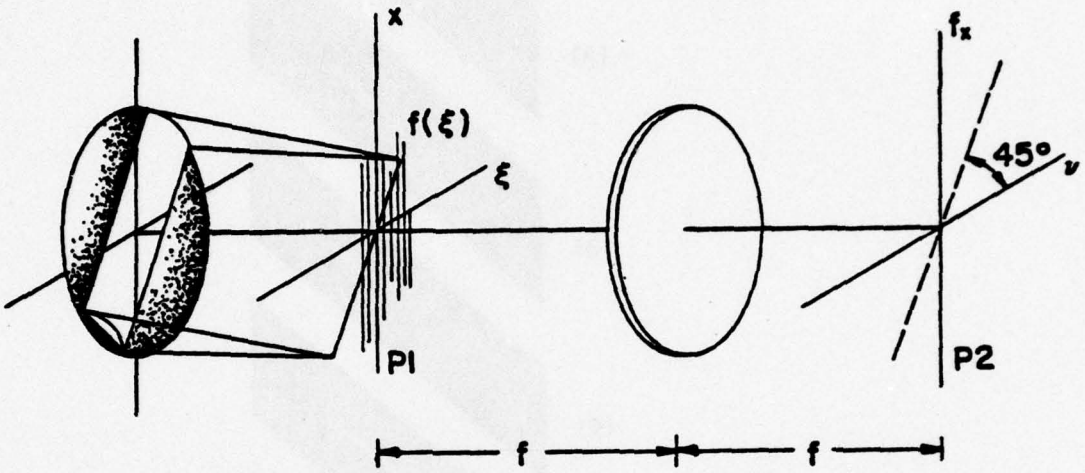

Figure 3.16 The OSD processor for displaying the spectrum of a magnified input. The slope of the Dirac delta sheet on plane P_1 is equal to M - 1.

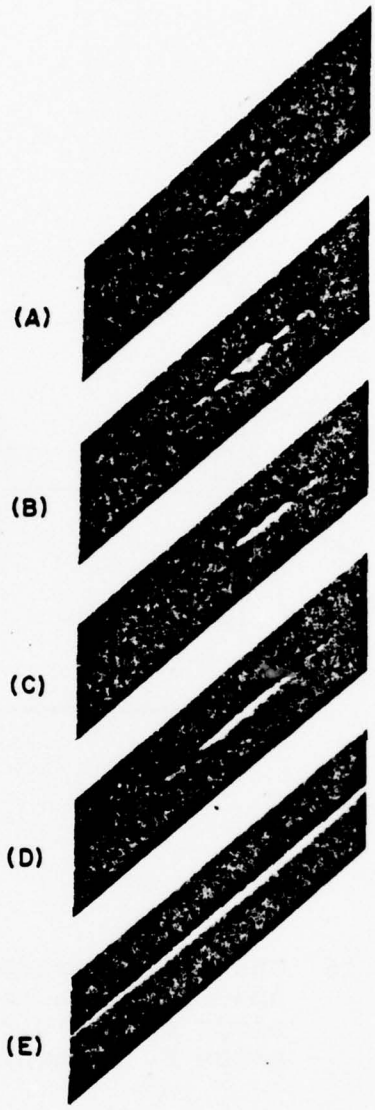

Figure 3.17 The output of the OSD processor in Fig. 3.15 for a single square pulse input. The spectrum displays correspond to pulse magnification of (a) M = 2, (b) M = 3/2, (c) M = 1, (d) M = 2/3, and (e) M = 0.

3.3.2. Cross Power Spectral Density Display

The cross power spectral density function of two signals, f(x) and h(x), is defined as the Fourier transform of their cross-correlation:[29]

$$S(f_x) = \int_{-\infty}^{\infty} [f(x) * h(x)] \exp(-j2\pi f_x x)\,dx. \qquad (3\text{-}45)$$

Consider, then, placing two transparencies of f(x) and s(x) in plane P_1 of Fig. 3-15 in such a manner as to form the product $f(x)h(\xi)$. From Eq. 3-40, the processor output is

$$G_o(f_x;\ \nu) = \int_{-\infty}^{\infty} \int_{-\infty}^{\infty} f(x)h(\xi)\exp[-j2\pi(f_x x + \nu\xi)]\,dx\,d\xi. \qquad (3\text{-}46)$$

Along the 45° line $\nu = f_x$, this becomes

$$\begin{aligned} G_o(f_x, f_x) &= \int_{-\infty}^{\infty} \int_{-\infty}^{\infty} f(x)h(\xi)\exp[-j2\pi(x+\xi)f_x]\,dx\,d\xi \\ &= \int_{-\infty}^{\infty} \int_{-\infty}^{\infty} f(x)h(\xi'-x)\exp(-j2\pi\xi' f_x)\,d\xi'\,dx \end{aligned} \qquad (3\text{-}47)$$

where we have made the variable substitution $\xi' = \xi + x$. We may rewrite Eq. 2-47 as

$$\begin{aligned} G_o(f_x, f_x) &= \mathcal{F}_{\xi}[f(\xi) * h(\xi)] \\ &= S(f_x) \end{aligned} \qquad (3\text{-}48)$$

which is the desired result.

3.4. Fourier Duals of the DOD and OSD Processors

The two processors thus far presented utilize line spread function masks. The DOD processor uses a mask of $h(x - \xi; \xi)$ to compute $g(x)$ while the OSD processor uses an $h(x; \xi)$ mask to compute $G(f_x)$. It is also possible to use frequency response masks in one-dimensional processor design. The processors utilizing such masks can be considered Fourier duals of their spatial domain counterparts.

We investigate use of the frequency response mask for two basic reasons. First, it widens the ways in which a given space-variant operation can be performed and thus allows us to choose from a number of possible schemes that one which is most easily implemented. Secondly, due to the fundamental dynamic range limitation of photosensitive media, it might be possible that a given space-variant system line spread function mask might not be implementable whereas the corresponding frequency response mask might. Thus, the number of possible space-variant operations which can be performed by the one-dimensional processors is increased.

3.4.1. The FDOD Processor

The Fourier dual of the direct output display (FDOD) processor is pictured in Fig. 3-18. This processor computes the frequency response characterization repeated

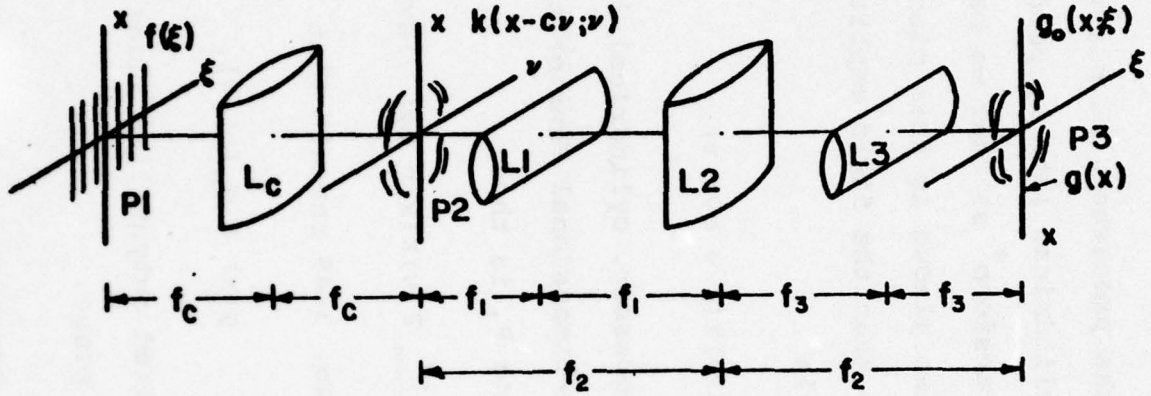

Figure 3.18 The Fourier dual of the direct output display (FDOD) processor. Here, the frequency response mask is used instead of the line spread function mask.

here from Eq. 2-20:

$$g(x) = \int_{-\infty}^{\infty} F(\nu)k(x - c\nu;\ \nu)d\nu. \qquad (3\text{-}49)$$

On plane P_1 of the processor, we place our one-dimensional input, $f(\xi)$. Cylindrical lens L_c performs a one-dimensional Fourier transform* so that we have $F(\nu)$ incident on plane P_2. Also placed in this plane is the frequency response mask so that the field amplitude immediately to the right of P_2 is

$$F(\nu)k(x - c\nu;\ \nu), \qquad (3\text{-}50)$$

As in the DOD processor, cylindrical lenses L_1, L_2 and L_3 perform a one-dimensional Fourier transform. The field amplitude on plane P_3 is thus

$$g_o(x;\ \xi) = \int_{-\infty}^{\infty} F(\nu)k(x - c\nu;\ \nu)\exp(-j2\pi\nu\xi)d\nu. \qquad (3\text{-}51)$$

Comparison with Eq. 3-49 reveals that

$$g(x) = g_o(x;\ 0). \qquad (3\text{-}52)$$

That is, our desired output lies along the x axis in the processor output plane.

3.4.2. The FOSD Processor

The Fourier dual to the output spectrum display (FOSD)

*A single cylindrical lens can be used due to the fact that $f(\xi)$ is one-dimensional.[11]

processor is shown in Fig. 3-19. This processor directly displays the Fourier transform of the space-variant system output according to Eq. 2-28 which we repeat here:

$$G(f_x) = F_\xi^{-1} F_x[F(\nu)k(x;\ \nu)]\Big|_{\xi = -cf_x}$$

$$= \int_{-\infty}^{\infty} \int_{-\infty}^{\infty} F(\nu)k(x;\ \nu)$$

$$\exp[-j2\pi f_x(x + c\nu)]dxd\nu. \qquad (3\text{-}53)$$

On plane P_1, we place our input $f(\xi)$ which is again Fourier transformed by the single cylindrical lens L_c. The input spectrum, $F(\nu)$, multiplies the frequency response mask placed in plane P_2 so that the field amplitude immediately to the right of P_2 is

$$F(\nu)k(x;\ \nu). \qquad (3\text{-}54)$$

Spherical lens L_s then performs a two-dimensional Fourier transform on this product. The field amplitude incident on plane P_3 is thus

$$G_o(f_x;\ \xi) = \int_{-\infty}^{\infty} \int_{-\infty}^{\infty} F(\nu)k(x;\ \nu)$$

$$\exp[-j2\pi(f_x x + \nu\xi)]dxd\nu. \qquad (3\text{-}55)$$

Comparison with Eq. 3-53 reveals that

$$G(f_x) = G_o(f_x;\ cf_x). \qquad (3\text{-}56)$$

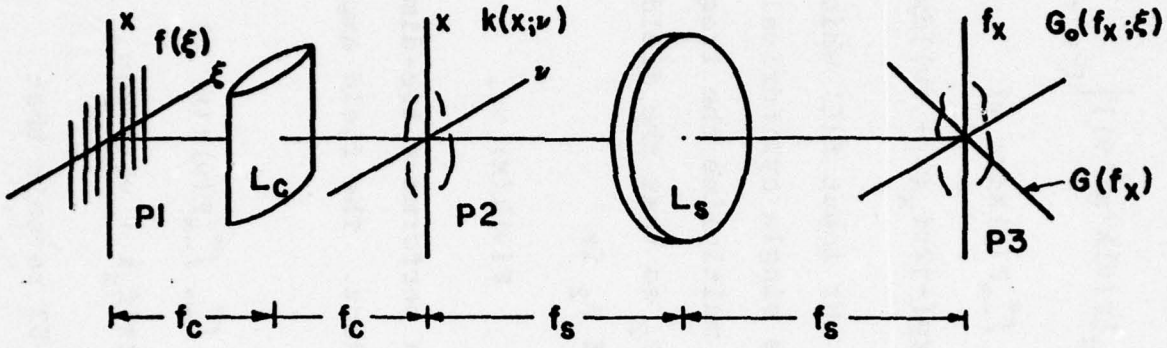

Figure 3.19 The Fourier dual of the output spectrum display (FOSD) processor. Again, a frequency response mask is used instead of a line spread function mask.

Thus, our desired output appears in plane P_3 along the line $\xi = cf_x$.

In summary, we see that the Fourier dual FDOD and FOSD processors differ from the corresponding Fourier dual DOD and OSD processors in only two respects. First, a frequency response mask is used instead of a line spread function mask. Secondly, the system input is Fourier transformed before being processed. In all other respects, the processors are implemented identically.

3.5. Alternate Interpretations of the 1-D Processors

In presenting the OSD and FOSD processors, it was stated that they directly computed the Fourier transform of the system output. We can however, ascribe a quite different interpretation to their operation.[45] Consider first Eq. 3-38 which we rewrite here in integral form:

$$G(f_x) = \int_{-\infty}^{\infty} f(\xi) H_x(f_x; \xi) \exp(-j2\pi\xi f_x) d\xi. \qquad (3\text{-}57)$$

The system transfer function, $H_x(\cdot,\cdot)$, was defined in Eq. 2-26 as the Fourier transform of the line spread function in x. Let us now define

$$h^{(o)}(f_x - b\xi; \xi) \triangleq H_x(f_x; \xi) \exp(-j2\pi\xi f_x) \qquad (3\text{-}58)$$

where the constant b retains dimensional consistancy between f_x and ξ. Substituting into Eq. 3-57 gives a

linear integral relation akin to the superposition integral:

$$G(f_x) = \int_{-\infty}^{\infty} f(\xi)h^{(o)}(f_x - b\xi;\ \xi)d\xi. \qquad (3\text{-}59)$$

Thus, we can interpret the OSD processor operation as one that 1) directly computes the output spectrum of the linear operation corresponding to $h(x - \xi;\ \xi)$ or 2) computes the output of the linear operation corresponding to $h^{(o)}(f_x - b\xi;\ \xi)$. In the latter case, we can compute the required mask transmittance from Eq. 3-58 for a desired linear operation corresponding to $h^{(o)}(\cdot,\cdot)$:

$$\begin{aligned} h(x;\ \xi) &= \int_{-\infty}^{\infty} H_x(f_x;\ \xi)e^{j2\pi f_x x}df_x \\ &= \int_{-\infty}^{\infty} h^{(o)}(f_x - b\xi;\ \xi) \\ &\quad \exp[j2\pi(x + \xi)f_x]df_x. \end{aligned} \qquad (3\text{-}60)$$

The mask $h(x;\ \xi)$, is the one which is actually utilized in the OSD processor.

As with the OSD processor, an alternate interpretation can be ascribed to the FOSD processor. Here, we let

$$k^{(o)}(f_x - \nu;\ \nu) = K_x(f_x;\ \nu)\exp(-j2\pi c\nu f_x) \qquad (3\text{-}61)$$

where, as defined in Eq. 2-106, $K_x(\cdot,\cdot)$ is the Fourier transform of the frequency response with respect to x.

We now can rewrite Eq. 3-53 as

$$G(f_x) = \int_{-\infty}^{\infty} F(\nu)k^{(o)}(f_x - \nu;\ \nu)d\nu. \qquad (3\text{-}62)$$

This integral relationship is akin to the frequency response characterization in Eq. 3-49. Thus, we can alternately interpret the output of the FOSD processor as corresponding to a frequency response characterization of a linear system with frequency response $k^{(o)}(\cdot,\cdot)$. Note that $k^{(o)}(\cdot,\cdot)$ and $h^{(o)}(\cdot,\cdot)$ are Fourier transform pairs:

$$k^{(o)}(f_x - \nu;\ \nu) = \int_{-\infty}^{\infty} h^{(o)}(f_x - b\xi;\ \xi)\exp(j2\pi\nu\xi)d\xi. \qquad (3\text{-}63)$$

This relationship follows from Eqs. 3-59 and 3-62 and Parseval's theorem.[24]

An obvious question now arises. Can the DOD and FDOD processors be alternately interpreted as displaying the output spectrum corresponding to some linear operation? The answer is yes. The derivation of the alternate system line spread function in both cases is straightforwardly derived in the above indicated spirit. Due to the fact that we are primarily concerned with the output rather than the output spectrum, we will not further dwell on these alternate interpretations.

3.6. Lensless Processing

When initially presented, it was noted that if one is interested only in the OSD processor output intensity, it was possible to place the 1-D input and line spread function mask directly adjacent the spherical lens. Besides illiminating vingnetting, this scheme also allows the lens transmittance to also be included in the mask transmittance. With the alternate interpretation of the OSD processor presented in the previous section, we arrive at the rather amazing conclusion that a 1-D space-variant system's output magnitude can be displayed utilizing only an input, a mask, and a few centimeters of free space. Such physical characteristics are desireable, of course, when one is primarily concerned with processor weight, physical stability, and real space compactness. It is difficult, in fact, to imagine a processor in a more compact form. In this section, we present some example applications and experimental results for two such 1-D lensless processors.[46]

3.6.1. Unit Magnifier

Even though it is doubtful that the lensless unit magnifier will find wide spread use, its analysis reveals some rather fascinating aspects of lensless 1-D processing. The input-output relationship for our system is defined as

$$G(f_x) = (\lambda f) f[\lambda f f_x] \tag{3-64}$$

where λf corresponds to the familiar wave length-focal length product. The line spread function corresponding to this operation is

$$h^{(o)}(f_x - b\xi;\ \xi) = \delta[f_x - \xi/\lambda f]. \tag{3-65}$$

From Eq. 3-58, it follows that

$$H_x(f_x;\ \xi) = \delta[f_x - \tfrac{\xi}{\lambda f}]\exp[j2\pi\xi f_x]. \tag{3-66}$$

Thus

$$h(x;\ \xi) = \exp[j2\pi\xi x/\lambda f]\exp[j2\pi\xi^2/\lambda f]. \tag{3-67}$$

Therefore, we can write:

$$h(x - \xi;\ \xi) = \exp[j2\pi\xi x/\lambda f]. \tag{3-68}$$

The mask transmittance, $t(x;\ \xi)$, required for lensless processing is the product of Eq. 3-68 with the transmittance of a spherical lens. Choosing the lens' focal length to be f, we have

$$\begin{aligned} t(x;\ \xi) &= h(x - \xi;\ \xi)\exp[\tfrac{-j\pi}{\lambda f}(x^2 + \xi^2)] \\ &= \exp[\tfrac{-j\pi}{\lambda f}(x - \xi)^2]. \end{aligned} \tag{3-69}$$

Remarkably, this expression is recognized as the transmittance of a cylindrical lens with focal length $f_c = f/2$

rotated 45° in the (x; ξ) plane. The mask required for unit magnification consists of a cylindrical lens, or equivalently, a cylindrical "hololens." A hololens is simply a hologram of a lens transmittance.[47-48]

In the implementation of this processor, the cylindrical hololens was recorded as shown in Fig. 3-20(a). The cylindrical lens has focal length f_c = 10cm and is illuminated from the left by a coherent plane wave. The photosensitive medium, as shown, is placed a distance $2f_c$ from the cylindrical lens and is illuminated with a coherent plane wave reference beam R. The reference beam's propagation direction is perpendicular to the x axis and is incident at an angle of $\theta = 30°$.

The lensless 1-D unit magnifier is shown in Fig. 3-20(b). For an input, we use the double pulse shown in Fig. 3-21(a). This transmittance is placed directly in front of the cylindrical hololens and is illuminated from the left by a coherent plane wave propagating in the conjugate direction to that of the reference wave used in the recording geometry. In Fig. 3-21, we show the resulting field amplitude square modulus perpendicular to the z axis at various values of z. Figure 3-21(a) is for z = 0 and is thus the double pulse input. Figure 3-21(b) is the field amplitude square modulus for a point between z = 0 and f_c. Note that a rotation of sorts is beginning

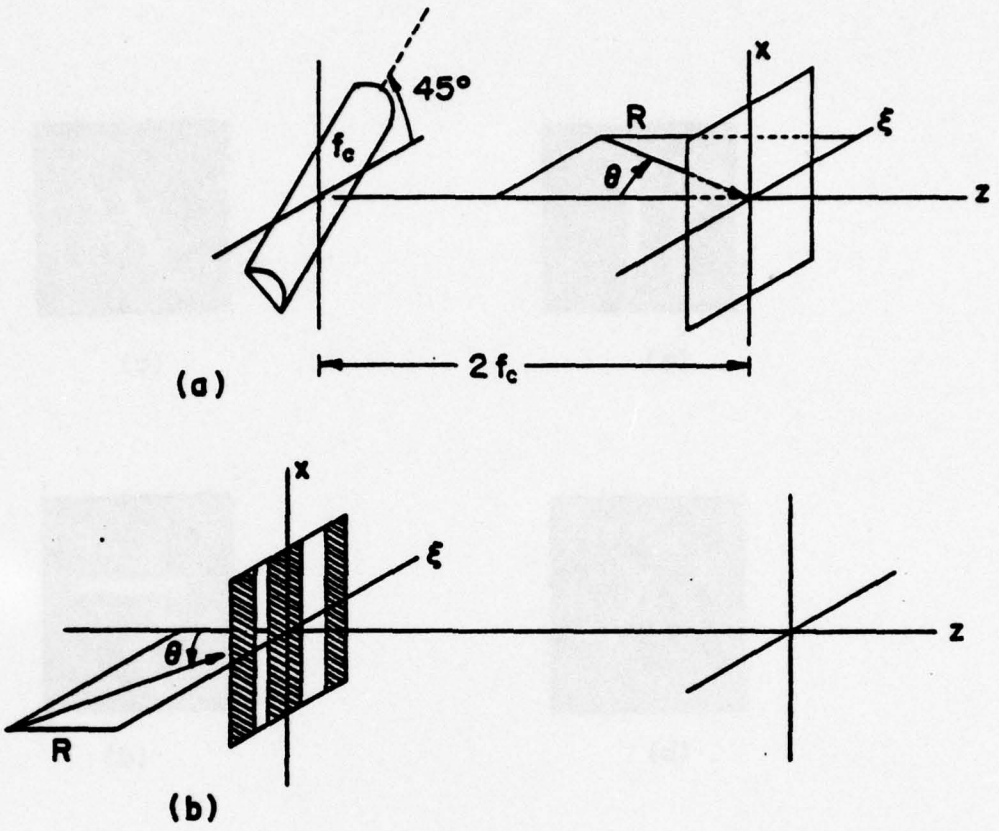

Figure 3.20 Lensless processor for unit magnification
a) Recording the cylindrical hololens
b) The lensless processor.

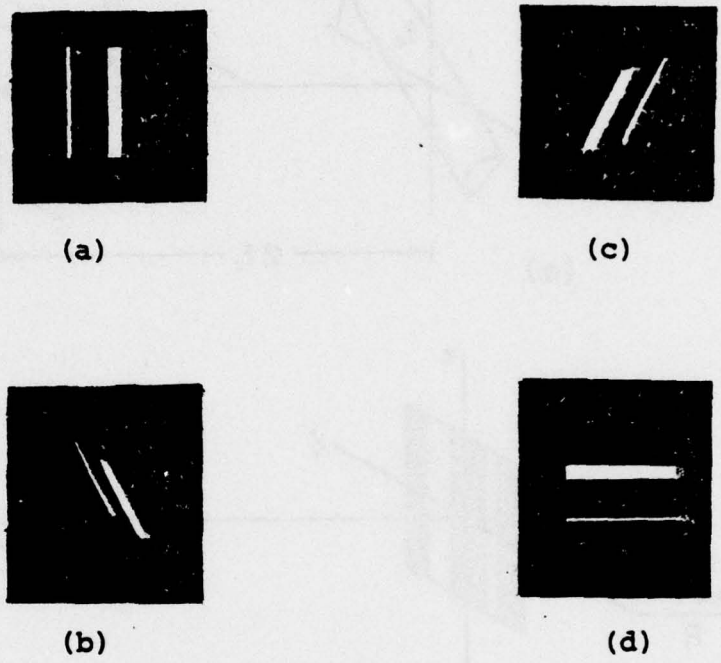

Figure 3.21 Output of the lensless processor in Figure 3.20b, for a) z = 0 b) z between 0 and f_c c) z between f_c and $2f_c$ and d) z = $2f_c$.

to take place. The field amplitude square modulus at a point between $z = f_c$ and $2f_c$ is shown in Fig. 3-21(c). Lastly, our desired processor output appears at $z = 2f_c$ as is shown in Fig. 3-21(d). The 1-D output, taken along the vertical axis, as predicted, is a unit magnified version of our 1-D input.

3.6.2. Lensless Convolution

For this example, we rewrite the convolution integral of Eq. 3-15 as

$$G(f_x) = \int_{-\infty}^{\infty} f(\xi) h^{(o)}(f_x - \xi/\lambda f) d\xi. \qquad (3\text{-}70)$$

Note that the unit magnifier discussed in the previous example is a special case of this relation for $h^{(o)}(f_x - \xi/\lambda f) = \delta(f_x - \xi/\lambda f)$.

To determine the required mask for this processor, we write from Eq. 3-58

$$H_x(f_x; \xi) = h^{(o)}(f_x - \xi/\lambda f) \exp(j2\pi\xi f_x). \qquad (3\text{-}71)$$

From this relation, we can easily show that

$$h(x - \xi; \xi) = H^{(o)}(x) \exp[\tfrac{j2\pi}{\lambda f} x\xi] \qquad (3\text{-}72)$$

where

$$H^{(o)}(x) = \int_{-\infty}^{\infty} h^{(o)}(f_x) \exp(j2\pi f_x x) df_x . \qquad (3\text{-}73)$$

To find the transmittance of the desired mask for our lensless processor, it remains to multiply Eq. 3-72 by the transmittance of a spherical lens whose focal length we shall choose to be f. The result is

$$t(x;\ \xi) = h(x - \xi;\ \xi)\exp[\frac{-j\pi}{\lambda f}(x^2 + \xi^2)]$$

$$= H^{(o)}(x)\exp[\frac{-j\pi}{\lambda f}(x - \xi)^2]. \qquad (3\text{-}74)$$

The complex exponential term is again recognized as a cylindrical lens of focal length $f_c = f/2$ rotated 45° on the (x, ξ) plane. Thus, 1-D convolution can be performed by placing the 1-D transmittances, $H^{(o)}(x)$ and $f(\xi)$ back to back adjacent a rotated cylindrical lens. The desired processor output appears at a distance $2f_c$ from this optical sandwich.

For an experimental implementation, two pairs of double pulses [Fig. 3-22(a)] were convolved [Fig. 3-22(b)]. A hologram was made of the 1-D Fourier transform of the one-dimensional transmittance corresponding to $h^{(o)}(\xi)$ using a single cylindrical lens with a focal length of 20 cm. This hologram served as the transmittance $H^{(o)}(f_x)$ shown in the processor in Fig. 3-23. The input transmittance $f(\xi)$ was placed as shown adjacent $H^{(o)}(f_x)$ and a rotated cylindrical lens. Since a 20 cm cylindrical lens was used to transform $h^{(o)}(\xi)$, we require that the

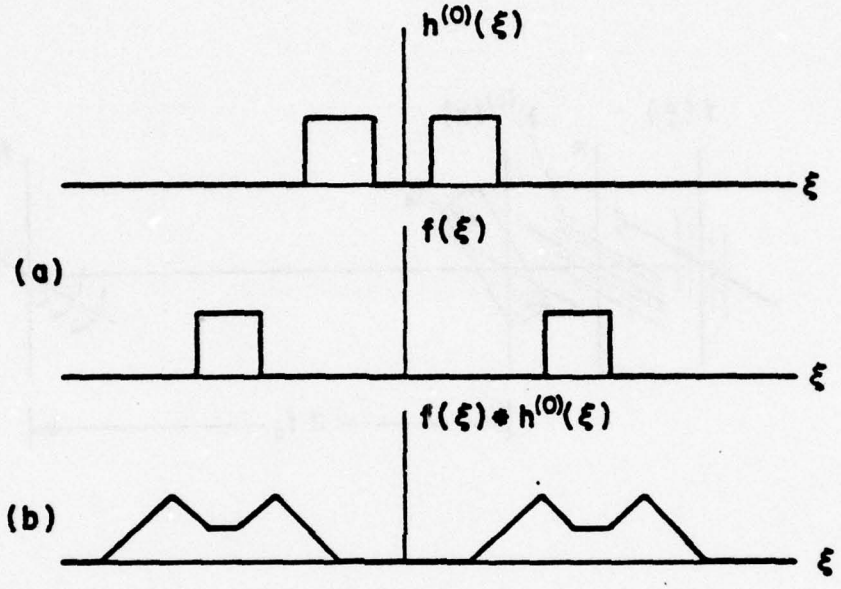

Figure 3.22 a) A pair of double pulses and
b) their convolution.

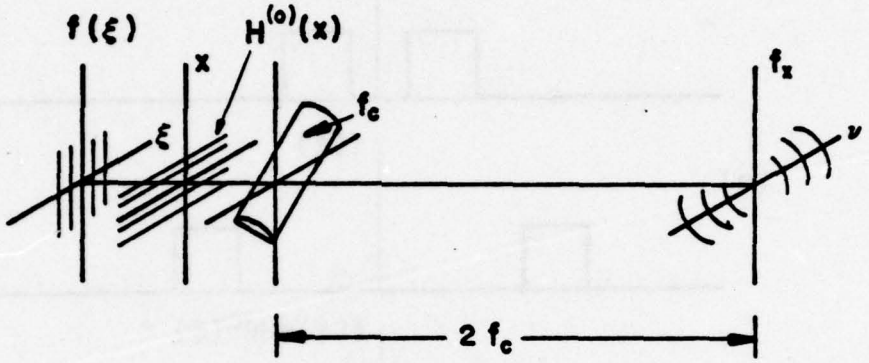

Figure 3.23 A 1-D processor for convolution.

rotated cylindrical lens have half that focal length. That is,

$$f_c = f/2 = 10\text{cm}. \qquad (3\text{-}75)$$

The processor was illuminated from the left with a coherent plane wave with wavelength 5145Å. The processor output appearing a distance $2f_c = 20\text{cm}$ to the right of the rotated lens is shown in Fig. 3-24. (The processor output was magnified by conventional means for this picture.) Although the structure of the vertical axis component of this picture is not readily apparent, the overlapping portions compare quite favorably with the convolution result in Fig. 3-22(b).

3.7. Design Considerations

We have presented four basic schemes for 1-D signal processing: DOD, OSD, FDOD, and FOSD. In this section, we address two basic questions: 1) for a given space-variant operation, which scheme is most easily implementable and 2) if a linear operation cannot be implemented in its obvious form, can we massage it into an alternate implementable form? We will illustrate these design challenges respectively with the one-dimensional linear operations of magnification and inverse Abel transformation.

Figure 3.24 The output of the processor in Fig. 3.23.

3.7.1. Magnifier Design Considerations

The DOD processor for one-dimensional magnification was previously presented and is pictured in Fig. 3-3. The line spread function

$$h(x - \xi;\ \xi) = \delta(x - M\xi) \tag{3-76}$$

is generated by focusing an incident plane wave to a line source which in turn is incident on the 1-D input. Let us now consider three possible alternate one-dimensional magnifier processor designs.

Consider, first, the FDOD processor for the magnifier. From Eq. 2-22, our required frequency response mask must have the transmittance

$$k(x - c\nu;\ \nu) = \int_{-\infty}^{\infty} \delta(x - M\xi)\exp(j2\pi\xi\nu)d\xi$$

$$= \frac{1}{M}\exp(j2\pi x\nu/M). \tag{3-77}$$

Implementation of this mask is possible by holographic means. Compared with the DOD processor, however, this scheme is obviously suboptimal in terms of ease of implementation.

Next, we inspect the OSD and FOSD magnifier processor for which we must restate our input-output relationship as

$$G(f_x) = \frac{1}{M}\, f\ (\frac{f_x}{M}). \tag{3-78}$$

Thus*

$$h^{(o)}(f_x - \xi;\ \xi) = \delta(f_x - M\xi). \qquad (3\text{-}79)$$

From Eq. 3-58, it follows that

$$H_x(f_x;\ \xi) = \delta(f_x - M\xi)\exp(j2\pi\xi f_x)$$

$$= \delta(f_x - M\xi)\exp(j2\pi M\xi^2). \qquad (3\text{-}80)$$

The line spread function mask which is required in the OSD processor is then

$$h(x;\ \xi) = \exp(j2\pi M\xi^2)\int_{-\infty}^{\infty}\delta(f_x - M\xi)e^{j2\pi f_x x}df_x$$

$$= e^{j2\pi M\xi(\xi+x)}. \qquad (3\text{-}81)$$

Again, our mask is a complex sinusoid and, again, the DOD processor scheme is superior as far as ease of implementation.

Lastly, we consider the FOSD magnification processor. From Eqs. 3-63 and 3-79:

$$k^{(o)}(x \tilde{-} c\nu;\ \nu) = \int_{-\infty}^{\infty}\delta(f_x - M\xi)\exp(j2\pi\nu\xi)d\xi$$

$$= \frac{1}{M}\exp(j2\pi f_x\nu/M). \qquad (3\text{-}82)$$

From Eq. 3-61:

*Here, b = 1 [see Eq. 3-58]

$$K_x(f_x;\ \nu) = \frac{1}{M} \exp[j2\pi f_x \nu(c + \frac{1}{M})]. \qquad (3\text{-}83)$$

Inverse transforming gives the required mask transmittance:

$$k(x;\ \nu) = \int_{-\infty}^{\infty} K_x(f_x;\ \nu)\exp(j2\pi f_x x)df_x$$

$$= \frac{1}{M}\delta[x + (c + \frac{1}{M})]. \qquad (3\text{-}84)$$

Here, as in the DOD processor, our "mask" is a Dirac delta sheet. In the FOSD processor, however, we cannot use a cylindrical lens to generate the Dirac delta sheet unless we use the input spectrum $F(\nu)$, rather than $f(\xi)$, as the processor input. Under the assumption that we do, in fact, favor $f(\xi)$ as our processor input, the DOD scheme is again superior.

The magnifier, as we have seen, is a relatively easy linear system to evaluate. In general, processor analysis in the manner just presented becomes rather analytically intractable. The potential use of such an approach, however, is obvious.

3.7.2. Inverse Abel Transform

As has been shown, the Laplace and Fourier transform can both be relatively straightforwardly evaluated by coherent optical means. The Mellin transform can also be thus evaluated.[49-50] All integral transforms are, in fact, special cases of the superposition integral. The kernels

(line spread functions) corresponding to many such transforms, however, lie outside the unit circle on the complex plane and thus cannot be directly represented by a hologram. An example of such a transform is the inverse Abel transform defined by:[14,28]

$$g(x) = \frac{-1}{\pi} \int_{|x|}^{\infty} (\xi^2 - x^2)^{-1/2} \frac{d}{d\xi} f(\xi) d\xi$$

$$= \frac{-1}{\pi} \int_{-\infty}^{\infty} \frac{\mu[\xi - |x|]}{\sqrt{\xi^2 - x^2}} \frac{d}{d\xi} f(\xi) d\xi \qquad (3\text{-}85)$$

where $\mu(\cdot)$ is the unit step function. The transform kernel is

$$h(x - \xi; \xi) = \frac{-1}{\pi} \frac{\mu(\xi - |x|)}{\sqrt{\xi^2 - x^2}} \frac{d}{d\xi}(\cdot). \qquad (3\text{-}86)$$

The kernel's dynamic range extends from zero to infinity. This, and the fact that the kernel contains a derivative operator, precludes holographic representation. Thus, the DOD processor cannot be directly utilized.

Let us then investigate the required transmittance for the FDOD processor. We utilize Parseval's theorem[28] and rewrite Eq. 3-86 as

$$g(x) = \int_{-\infty}^{\infty} \left[\frac{-1}{\pi} \int_{|x|}^{\infty} \frac{\exp(j2\pi\nu\xi)}{\sqrt{\xi^2 - x^2}} d\xi\right]$$

$$\times [-j2\pi\nu F(\nu)] d\nu \qquad (3\text{-}87)$$

where we have recognized that

$$F_\xi[\frac{d}{d\xi}f(\xi)] = -j2\pi\nu F(\nu). \qquad (3\text{-}88)$$

Our frequency response here is thus given by

$$k(x - c\nu;\ \nu) = j2 \int_{|x|}^{\infty} \frac{\exp(j2\pi\nu\xi)d\xi}{\sqrt{\xi^2 - x^2}} . \qquad (3\text{-}89)$$

where the derivative operation is here included in the multiplicative ν term. From Gradshteyn and Ryzhik[51] [Eqs. 3-771-7 and 3-771-9], this integral reduces to

$$k(x - c\nu;\ \nu) = j\pi\nu[J_o(2\pi\nu x) - jN_o(2\pi\nu x)] \qquad (3\text{-}90)$$

where $J_o(\cdot)$ and $N_o(\cdot)$ are zeroth order Bessel functions of the first and second kind respectively. Although $\nu N_o(\nu)$ is well behaved about the origin, ($N_o(\cdot)$ is not[52]), we would prefer a mask that is strictly real. Equation 3-90 obviously does not conform to this preference.

It is possible to utilize a variation of the DOD processor to compute the inverse Abel transform where the required mask transmittance is purely real. This processor, pictured in Fig. 3-25, has a transmittance of $J_o(2\pi\nu x)$ placed in plane P1. The three cylindrical lenses, L1, L2 and L3, then perform a one-dimensional Fourier transform with respect to ν. Thus the field amplitude

$$\int_{-\infty}^{\infty} J_o(2\pi x\nu)\exp(-j2\pi\xi\nu)d\nu \qquad (3\text{-}91)$$

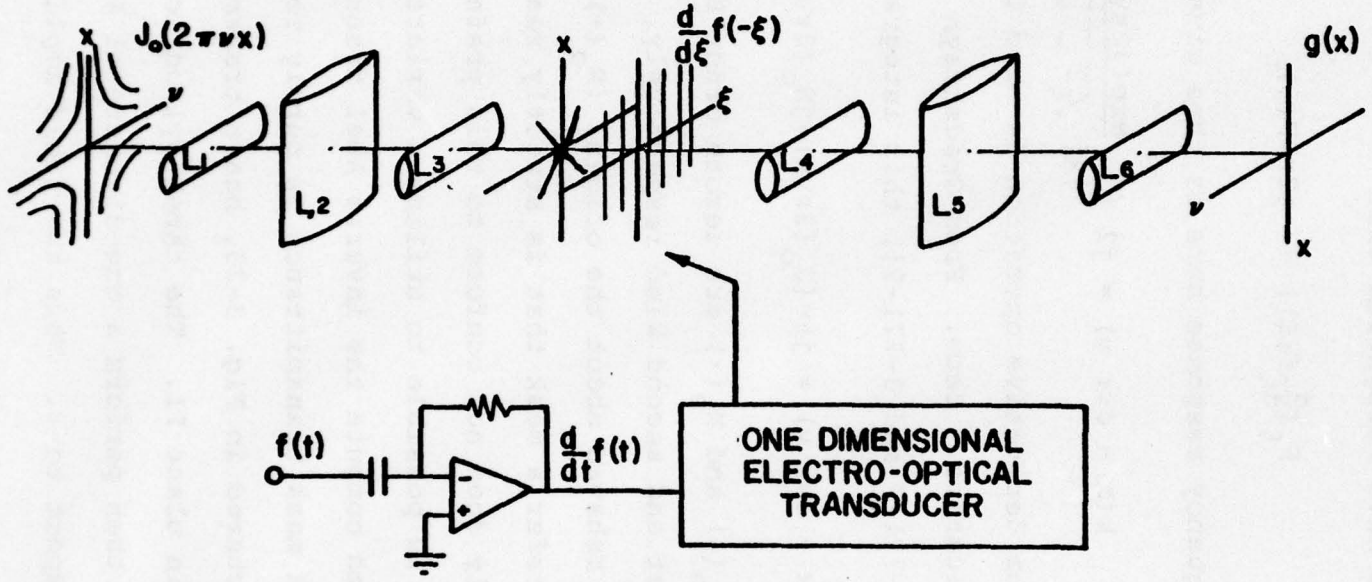

Figure 3.25 Hybrid coherent processor for inverse Abel transformation.

is incident on plane P2. Since $J_o(\cdot)$ is an even function, we can rewrite Eq. 3-91 as

$$\begin{aligned}
&\int_{-\infty}^{\infty} J_o(2\pi x\nu)\cos(2\pi\xi\nu)\,d\nu \\
&\quad = 2\int_{o}^{\infty} J_o(2\pi|x|\nu)\cos(2\pi\xi\nu)\,d\nu \\
&\quad = \begin{cases} \dfrac{1}{\sqrt{x^2-\xi^2}} & ;\ \xi < |x| \\ 0 & ;\ \xi > |x| \end{cases}
\end{aligned} \tag{3-92}$$

where we have used Eq. 6.671.2 of Gradsteyn and Ryzhik.[51] The values of the function $J_o(\cdot)$ lie within the unit circle on the complex plane and thus, in principle, can be represented holographically. The form of the relation in Eq. 3-92 looks similar to that in Eq. 3-86 except that the polarities are opposite. That is, Eq. 3-84 requires that $\xi > |x|$ while Eq. 3-92 is nonzero only for $\xi < |x|$. We can, however, rectify this situation by performing the variable substitution $\hat{\xi} = -\xi$ in Eq. 3-85 to give:

$$g(x) = \frac{1}{\pi}\int_{-\infty}^{\infty} \frac{\mu[-\xi-|x|]}{\sqrt{x^2-\xi^2}}\,\frac{d}{d\xi}\,f(-\xi)\,d\xi\,. \tag{3-93}$$

Here, our integration interval covers the desired range of $\xi < |x|$.

Returning now to our processor, we generate $\frac{d}{d\xi}f(-\xi)$ electronically with the op-amp differentiator shown. This is fed into a one-dimensional electro-optical transducer

whose output transmittance multiplies Eq. 3-92. The field amplitude immediately to the right of plane P2 is thus

$$\frac{1}{\pi\sqrt{x^2-\xi^2}}\,\mu(-\xi-|x|)\,\frac{d}{d\xi}\,f(-\xi). \qquad (3\text{-}94)$$

This product is Fourier transformed with respect to ξ by lenses L4, L5 and L6 so that incident on plane P3 is the field amplitude:

$$g_o(x,\nu) = \int_{-\infty}^{\infty} \frac{\mu[-\xi-|x|]}{\pi\sqrt{x^2-\xi^2}}\,[\frac{d}{d\xi}\,f(-\xi)]e^{-j2\pi\nu\xi}d\xi\,. \qquad (3\text{-}95)$$

For $\nu = 0$, this relation reduces to that in Eq. 3-93. Our desired inverse Abel transform corresponding to an input, $f(\xi)$, thus appears in plane P3 along the x axis.

The inverse Abel transform processor cannot be classified into any of the processor classes thusfar considered. The ideas leading to its design, however, parallel closely those considered previously. We thus conclude that, given a space-variant operation, attention should not be restricted only to the DOD, OSD, FDOD, and FOSD processors, since augmentation and perturbations of fundamental underlying concepts can be utilized to yield a design which is more highly implementable.

3.8. Conclusion

In this chapter, we have presented numerous coherent optical processors that are capable of performing a wide

class of one-dimensional operations. All of the processors require a mask, possibly holographic if the kernel is bipolar or complex, and a one-dimensional input transmittance. The DOD and OSD processors utilize a line spread function mask and respectively display the output and output spectrum. The FDOD and FOSD processors do likewise, but utilize a frequency response mask. In all of these processors, the 1-D system output is viewed along a line in the processor output plane. The Laplace transform and ambiguity function operations were shown to be two special cases where the entire output plane could be utilized.

The OSD and FOSD processors were shown to be able to be interpreted as displaying the output (instead of output spectrum) corresponding to a linear operation that could be deduced from the system line spread function. Along with the DOD and FDOD processors, there are thus four general schemes for direct one-dimensional processing each of which require different masks. For a given linear operation, we can thus, in principle, derive four separate expressions for possible masks for use in an appropriate 1-D processor. This allows for a degree of flexibility in processor design. Using these alternative schemes in design considerations was exemplified in the case of the 1-D magnifier. As was shown for the case of the inverse Abel transformer, however, attention should not be re-

stricted to the four basic processors, but rather to the fundamental concepts by which they were conceived.

CHAPTER IV

4. TWO-DIMENSIONAL SPACE-VARIANT PROCESSORS

In the previous chapter, the two-dimensional nature of coherent optical processors was utilized to perform one-dimensional operations. This chapter, on the other hand, describes various possible schemes for performing general two-dimensional operations with coherent optical processors.

There are a number of specific 2-D linear space-variant operations that can be performed by coherent processors. The thin lens, for example, performs a 2-D Fourier transformation which is a linear space-variant operation. The astigmatic processors encountered in the previous chapter, wherein orthogonal Fourier transformation and imaging are performed, are also space-variant. The operations of Laplace transform and ambiguity function display can be considered as special cases of two-dimensional space-variant astigmatic processing. The elementary act of non-unity magnification imaging, also, must rigorously be considered space-variant.[53] Besides an input transmittance, the Fourier transform, astigmatic, and imaging processors consist only of two basic elements: lenses and free space. Positioning of lenses in various other locations will of course result in other space-variant operations. The class of possible operations, however, is

somewhat limited. Rather general treatment of such multiplane optical processors is given by Carlson.[54]

An alternate treatment of generalized 2-D space-variant processing has been developed by Bryndahl et.al.[55-57] Inherent in his development is the assumption of a "slowly varying" input. Both Bryndahl's and Carlson's methods, as well as other space-variant processing schemes, are discussed by Goodman.[58]

Our treatment of the design of space-variant processors, on the other hand, will be considered from the systems viewpoint. In 1-D processor design, the continuum orthonormal basis set response characterization of linear systems was used. In 2-D processor design, we will use the characterizations developed in Chapter II where limiting assumptions or approximations were made concerning the system and/or the class of allowable inputs. These include the piecewise isoplanatic approximation (PIA), discrete orthonormal basis set response (DBR), and sampling theorem characterizations.

In the treatment of 2-D processors, two views are possible. The first is that we have an actual physical coherent processor which, for reasons of real space compactness and stability, we wish to characterize holographically. For this case, we need to physically probe the system with an appropriate set of signals. The cor-

responding system responses must then somehow be holographically cataloged in a straightforwardly accessable manner. The volume hologram approach to be discussed is a scheme based on this view.

The second manner in which 2-D space-variant design can be viewed is similar to the 1-D processor concept. That is, instead of optically recording a required mask, the mask transmittance is generated by alternate means such as computer generated holograms.[59] All schemes in this chapter, except the volume hologram treatment, can be implemented, in principle, by either the direct recording method or the computer generated mask methods.

Three basic schemes for general two-dimensional space-variant processing will be considered. The first scheme involves composite holograms and is a direct application of a space-variant system sampling theorem developed in Chapter II. The constraints on system input and line spread here impose severe limitations on allowable operations. The second scheme utilizes the volume hologram in which system responses are angle multiplexed within a thick medium. This scheme was first suggested by Burton, et.al.[19] Application of the PIA characterization to the volume hologram was investigated by Marks.[6] The sampling theorem approach was similarly applied by Deen et.al.[20-21] Other results have been reported by Walkup and Hagler[60] and Marks et.al.[8]

The third method of two-dimensional space-variant processing, proposed by Krile et.al.,[22] makes use of phase coded reference beams. An effect inherent in this method is the smearing of unwanted crosstalk terms into diffuse background noise.

Since this chapter deals with two-dimensional space-variant processing, all previous linear system characterizations, which had a 1-D favor, must be generalized to two dimensions. For example, the 2-D superposition integral is written as

$$g(x,y) = \int_{-\infty}^{\infty} \int_{-\infty}^{\infty} f(\xi,\eta)h(x-\xi,y-\eta;\xi,\eta)d\xi d\eta . \tag{4-1}$$

The kernel, $h(\cdot,\cdot;\cdot,\cdot)$, for obvious reasons, is now referred to as the system point spread function. As will become clear in the development to follow, mathematical and conceptual generalization from one to two-dimensional treatment is trivally straightforward.

We should point out that the line spread function does have meaning in the context of 2-D system characterization.[61-62] In this chapter, however, we will concern ourselves only with the 2-D system's point spread function.

4.1. System Response Generation

In the system characterizations developed in Chapter II, it was necessary to catalog the system responses to a

class of inputs which were specified by a limiting assumption placed on the allowable input class and/or system. Both the piecewise isoplanatic approximation (PIA) and the sampling theorem characterizations require knowledge of the system response to Dirac deltas placed at certain points at the system input. An alternate sampling theorem required sampling be performed at the system output. The Fourier duals of the sampling theorems require that the frequency response be sampled in either the input or output domain. For the discrete orthonormal basis set response (DBR) characterization, we need to catalog the system response to inputs consisting of each element in the basis set.

In this section, we explore physically generating these responses. That is, given an actual linear coherent optical system with input and output planes, how do we physically generate the required catalog of system responses? Once the desired responses are generated, it remains only to find a method by which to optically catalog the response (on a hologram for example) in such a manner as to be retrievable for system representation. These methods include the volume hologram and phase coded reference beam schemes which will be presented shortly. We present the response generation techniques in a separate section for the simple reason that certain cataloging methods

can, in principle, utilize more than one of the response characterizations in their implementation. We should also keep in mind that, except for the volume hologram approach, the required system response masks can either be computer generated or optically recorded.

4.1.1. Impulse Response

In the sampling theorem and PIA system characterizations, we require generation of the system point spread function. For an arbitrary coherent optical system, this can be performed as shown in Fig. 4-1. An incident coherent plane wave is focused to the point (ξ,η) on the system input plane. Since the spherical lens is circular with radius A, this "point" is better described by the Fourier transform of a circle function:[23]

$$F\left[\text{circ}\left(\frac{\sqrt{x^2 + y^2}}{A}\right)\right] = \frac{A}{\rho} J_1(2\pi A\rho) \tag{4-2}$$

where

$$\rho = \frac{\sqrt{x_i^2 + y_i^2}}{\lambda f} , \tag{4-3}$$

$$\text{circ } r \triangleq \begin{cases} 1 & ; \ |r| \leq 1 \\ 0 & ; \ |r| > 1 . \end{cases} \tag{4-4}$$

and $J_1(\cdot)$ is the first order Bessel function of the first kind. One possible expression for 2-D Dirac delta is[23]

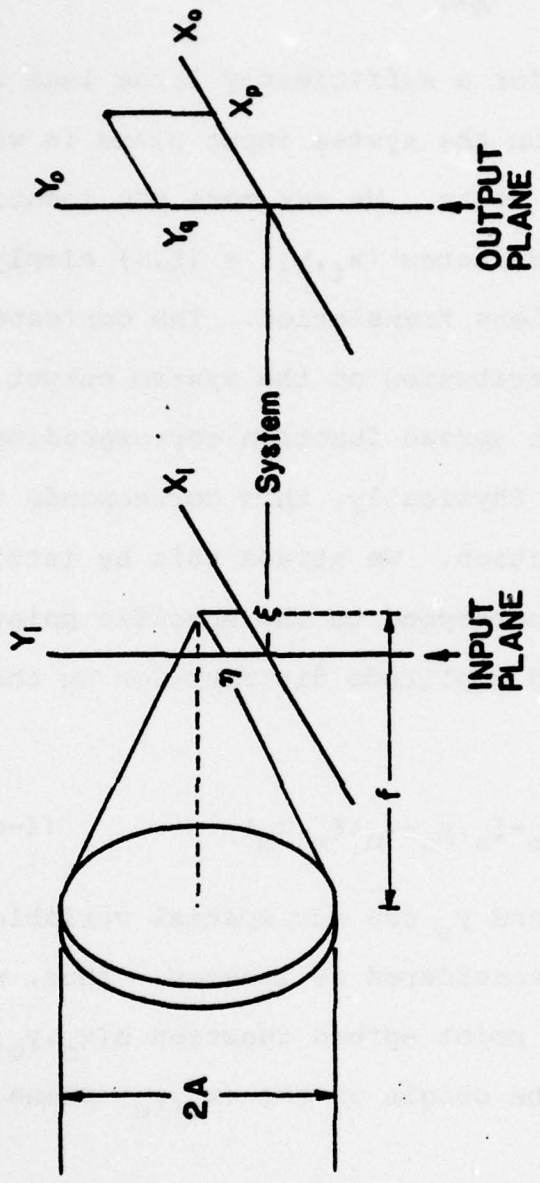

Figure 4.1 Generation of the impulse response for a coherent optical system.

$$\delta(x_i, y_i) = \lim_{A\to\infty} \frac{A}{\rho} J_1(2\pi A\rho). \qquad (4\text{-}5)$$

Thus, we conclude that for a sufficiently large lens radius, A, our field amplitude on the system input plane is well approximated by a Dirac delta. We can move the location of the delta to the coordinates $(x_i,y_i) = (\xi,\eta)$ simply through an appropriate lens translation. The corresponding field amplitude distribution on the system output plane is then the system point spread function corresponding to the input point (ξ,η). Physically, this corresponds to a sample point spread function. We stress this by letting the coordinates (ξ,η) correspond to the specific point (ξ_n,η_m). Then the field amplitude distribution on the system output plane is

$$h(x_o-\xi_n, y_o-\eta_m; \xi_n, \eta_m). \qquad (4\text{-}6)$$

In this expression, x_o and y_o are our spatial variables while ξ_n and η_m can be considered as indexes. Thus, we can generate the sample point spread function $h(x_o,y_o;\xi_n,\eta_m)$ by simply translating the origin of the (x_o,y_o) plane to the point (ξ_n,η_m).

Suppose, now, we wish to generate forms of the system point spread function sampled in x and y rather than in ξ and η. Consider, again, Fig. 4-1 with attention restricted

this time to the point $(x_o,y_o) = (x_p,y_q)$ on the output plane. As the input point source explores various values of (ξ,η), the corresponding field amplitude at the output point (x_p,y_q) is $h(x_p-\xi,y_q-\eta;\xi,\eta)$.

To holographically record a transmittance of the output sampled point spread function, we must translate a photosensitive medium placed in the (x_o,y_o) plane. Imagine first, a point source input at $(\xi,\eta) = (0,0)$ and the photosensitive medium in the (x_o,y_o) plane. Immediately in front of the medium we place an opaque mask that passes light only at the point $(x_o,y_o) = (x_p,y_q)$. Then, as though rigidly connected, the input point source and photosensitive medium translate through all values of (ξ,η). During this translation, the opaque mask remains stationary. Some reflection on the reader's part reveals that the transmittance recorded utilizing this procedure is $h(x_p, y_q;\xi,\eta)$.

4.1.2. Frequency Response Sampling

As with the impulse response, we wish to formulate methods by which the sample frequency responses of a coherent processor can be directly recorded both in the input and output domains. In two dimensions, the frequency response is defined as

$$k[x_o-c_x\nu_\xi, y_o-c_y\nu_\eta] = S[\exp\{j2\pi(\nu_\xi x_i + \nu_\eta y_i)] \tag{4-7}$$

where the constants c_x and c_y retain dimensional consistency. In coherent optics, the complex exponential required for our system input is interpreted as a tilted plane wave. This can probably be most easily seen from the geometry of Fig. 4-2.

A Dirac delta (point source) is placed in the $(\alpha.\beta)$ plane at the coordinates (a,b). The thin lens performs a Fourier transform so that the field amplitude incident on the (x_i,y_i) plane is

$$\exp[\frac{-j2\pi}{\lambda f}(x_i a + y_i b)]. \qquad (4\text{-}8)$$

From geometrical optics, we see that Eq. 4-8 describes a tilted plane wave incident on the (x_i,y_i) plane.[63] Comparing with the argument of the system operator in Eq. 4-7, we have

$$\nu_\xi = \frac{-a}{\lambda f} \quad ; \quad \nu_\eta = \frac{-b}{\lambda f} . \qquad (4\text{-}9)$$

In an actual laboratory situation, generating tilted plane waves in the manner shown in Fig. 4-2 would probably not be used. Rather, we would generate the plane waves in accordance with the direction cosines, $\cos\theta_x$ and $\cos\theta_y$. From the geometry in Fig. 4-2, these are given by

$$\cos\theta_x = -a/r \quad ; \cos\theta_y = -b/r \quad (4\text{-}10)$$

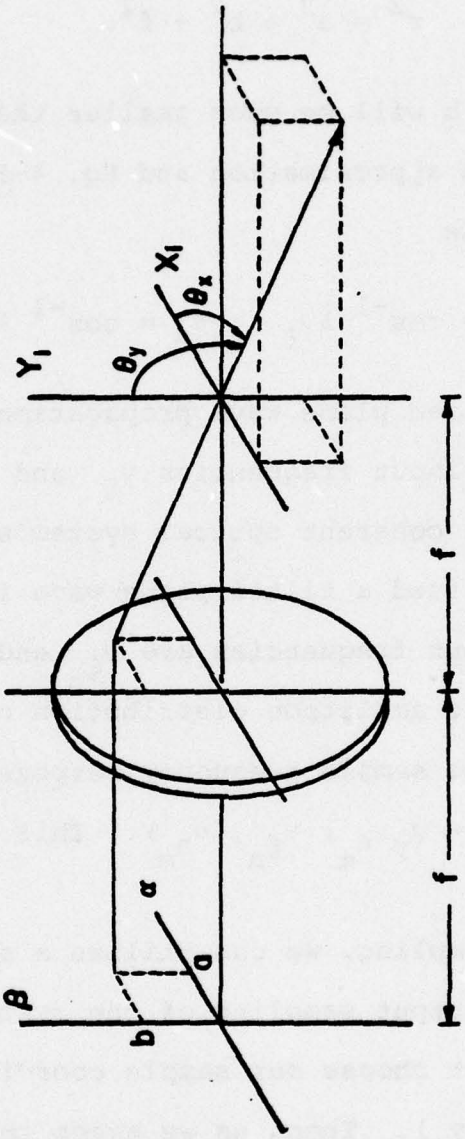

Figure 4.2 Generation of the input for the frequency response characterization of a coherent optical system.

where

$$r^2 = a^2 + b^2 + f^2. \qquad (4\text{-}11)$$

In general, a and b will be much smaller than f so that $r \simeq f$. Using this approximation and Eq. 4-9, we can then rewrite Eq. 4-10 as

$$\theta_x = \cos^{-1} \lambda\nu_\xi \quad ; \quad \theta_y = \cos^{-1} \lambda\nu_\eta \, . \qquad (4\text{-}12)$$

These are the desired plane wave propagation angles corresponding to the input frequencies ν_ξ and ν_η.

To generate a coherent optical system's frequency response, we simply feed a tilted plane wave into the system input. If the input frequencies are ν_{ξ_n} and ν_{η_m} then the corresponding field amplitude distribution on the system output plane is the sample frequency response given by $k(x_o - c_x \nu_{\xi_n}, y_o - c_y \nu_{\eta_m}; \nu_{\xi_n}, \nu_{\eta_m})$. This corresponds to input sampling.

For output sampling, we can utilize a scheme similar to that used for output sampling of the system point spread function. We first choose our sample coordinate in the output plane, (x_p, y_q). Then, as we sweep the various frequencies at the system input, our output photosensitive medium translates accordingly. For input frequencies of ν_ξ and ν_η our photosensitive mediums origin is located, in the output plane at coordinates $(c_x \nu_{\xi_n}, c_y \nu_{\eta_m})$. In this

manner, we generated the sample frequency response $k(x_p, y_q; \nu_\xi, \nu_\eta)$.

4.1.3. Sinc and Rect Response Generation

In the development of the discrete orthonormal element basis set response (DBR) characterization of linear systems in Chapter II, we investigated specifically the sinc and rect orthonormal basis sets. Here, we explore the generation of these responses in coherent optical systems.

First consider the two-dimensional $(n,m)^{th}$ element of the rect basis set here generalized from Eq. 2-62:

$$\psi_{nm}(x,y) = \frac{1}{2\sqrt{T_x T_y}} \exp[j2\pi(\nu_{\xi_n} x_i + \nu_{\eta_m} y_i)]$$

$$\times \text{rect}\left(\frac{x_i}{2T_x}\right)\text{rect}\left(\frac{y_i}{2T_y}\right) \qquad (4\text{-}13)$$

where $\nu_{\xi_n} = n/2T_x$, $\nu_{\eta_m} = m/2T_y$, and where we have restricted our input to be identically zero for $|x_i| > T_x$ and $|y_i| > T_y$. The form of Eq. 4-13 is identical to that of the input sampled frequency response except for the rect terms. Thus, we can generate the system rect response in the same manner as we generated the system frequency response: by probing the system input with tilted plane waves. The rect terms can be included by simply making the input plane opaque outside of the rectangular region $|x_i| \leq T_x$ and $|y_i| \leq T_y$. From Eq. 4-12, the angular propagation direc-

tions for the $(n,m)^{th}$ input plane wave are

$$\theta_{x_n} = \cos^{-1} \lambda\nu_{\xi_n} = \cos^{-1} \frac{n\lambda}{2T_x}$$

$$\theta_{y_m} = \cos^{-1} \lambda\nu_{\eta_m} = \cos^{-1} \frac{m\lambda}{2T_y} . \qquad (4\text{-}14)$$

The system sinc response is also straightforwardly generated. The two-dimensional $(n,m)^{th}$ element of the sinc basis set is generalized from Eq. 2-57 as

$$\psi_{nm}(x_i,y_i) = 2\sqrt{W_x W_y}$$

$$\text{sinc } 2W_x(x_i-x_n)\,\text{sinc } 2W_y(y_i-y_m) \qquad (4\text{-}15)$$

where $2W_x$ and $2W_y$ are the allowable bandwidths of the input in x_i and y_i respectively and $x_n = n/2W_x$ and $y_m = m/2W_y$.

The sinc basis set elements can be generated as shown in Fig. 4-3. A rectangular pupil is placed on the (α,β) plane and is described by

$$\text{rect}\left(\frac{\alpha}{2\lambda f W_x}\right)\text{rect}\left(\frac{\beta}{2\lambda f W_y}\right) \qquad (4\text{-}16)$$

where f is the focal length of the lens. On the (x_i,y_i) plane appears the Fourier transform of this pupil evaluated at the frequency components $(x_i/\lambda f,\ y_i/\lambda f)$ and translated to the coordinates (x_n,y_m). Outside of the proportionality terms, this field amplitude is identical to Eq. 4-15. We can generate other elements in the sinc basis set simply by translating the rectangular pupil and thin

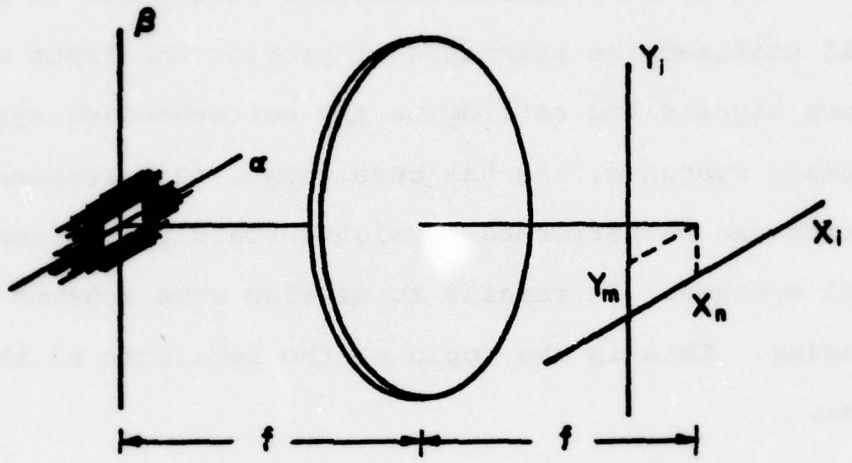

Figure 4.3 Generation of the input for the sinc response characterization of a linear system.

lens while leaving the (x_i,y_i) plane stationary. These elements serves as the input to our system and the corresponding field amplitude at the system output is the desired system sinc response.

4.1.4. Discussion

The system characterizations considered in Chapter II all utilized the principle of probing the input with various signals and cataloging the corresponding system frequency response. As has been shown, this response generation can be performed straightforwardly in coherent optical systems. It remains to develop some schemes for cataloging. This is the topic of the remainder of this chapter.

4.2. A Composite Hologram Approach

In Chapter II, we developed a sampling theorem for space-variant systems whose line spread function was bandlimited in x. From Eq. 2-73, the two-dimensional generalization of this expansion is

$$g(x,y) = \sum_n \sum_m [f(x,y)h(x_n,y_m;x,y)] * [\text{sinc}2W_x(x-x_n)\,\text{sinc}\,2W_y(y-y_m)] \qquad (4\text{-}17)$$

where $x_n = n/2W_x, y_m = m/2W_y$, and $2W_x$ and $2W_y$ are the (low-pass) bandwidths of $h(x,y;\xi,\eta)$ respectively in the x and y directions. This relationship can alternately be written as

$$g(x,y) = \sum_n \sum_m [f(x-x_n, y-y_m) h(x_n, y_m; x-x_n, y-y_m)]$$

$$* [\text{sinc}\ (2W_x x) \text{sinc}(2W_y y)]\ . \qquad (4\text{-}18)$$

We can interpret Eq. 4-18 as follows: The input, $f(x,y)$ is shifted to the coordinates (x_n, y_m) on the (x,y) plane whereupon it is multiplied by a corresponding sample point spread function. This process is repeated for all sample coordinate pairs, (x_n, y_m). All resulting products are then summed and passed through an appropriate 2-D low pass filter which gives rise to the required convolving sincs in Eq. 4-18. Note that no assumptions concerning the input have yet been made.

Suppose, now, we wish to simultaneously perform all shifted sample-input point spread function multiplication on a single plane. In order to assure that no overlapping of terms occurs, (i.e., no crosstalk), we must require for each n and m that the product, $f(x-x_n, y-y_m)\ h(x_n, y_m; x-x_n, y-y_m)$, is identically zero outside the rectangle defined by

$$|x - x_n| \leq 1/4\ W_x$$
$$|y - y_m| \leq 1/4\ W_y \qquad (4\text{-}19)$$

or, equivalently

$$\frac{2n-1}{4W_x} < x < \frac{2n+1}{4W_x}$$

$$\frac{2m-1}{4W_y} < y < \frac{2m+1}{4W_y} . \qquad (4\text{-}20)$$

This can occur in two ways: 1) Our input is identically zero for $|\xi| \leq 1/4\ W_x$ and $|\eta| \leq 1/4\ W_y$ or 2) the point spread function $h(x,y;\xi,\eta)$ is identically zero outside the interval $|\xi| \leq 1/4\ W_x$ and $|\eta| \leq 1/4\ W_y$. Thus, in order to perform all required multiplication on a single plane, severe compact support constraints must either be placed on either input or point spread function. This is in addition to the constraint that $h(x,y;\xi,\eta)$ be band-limited in both x and y.

A coherent processor capable of carrying out the sampling theorem in Eq. 4-3 under the discussed constraints is pictured in Fig. 4-4. In plane P1, we place our input, $f(\xi,\eta)$. If the compact support constraint falls on the line spread function rather than the input, it is necessary to mask that region of plane P_1 lying outside the rectangle $|\xi| \leq 1/4\ W_x$, $|\eta| \leq 1/4\ W_y$. This is without loss of information since the system we are characterizing sees the input only over these intervals.

Spherical lens, L1, performs a two-dimensional Fourier transformation on the input. The field amplitude incident on plane P2 is thus

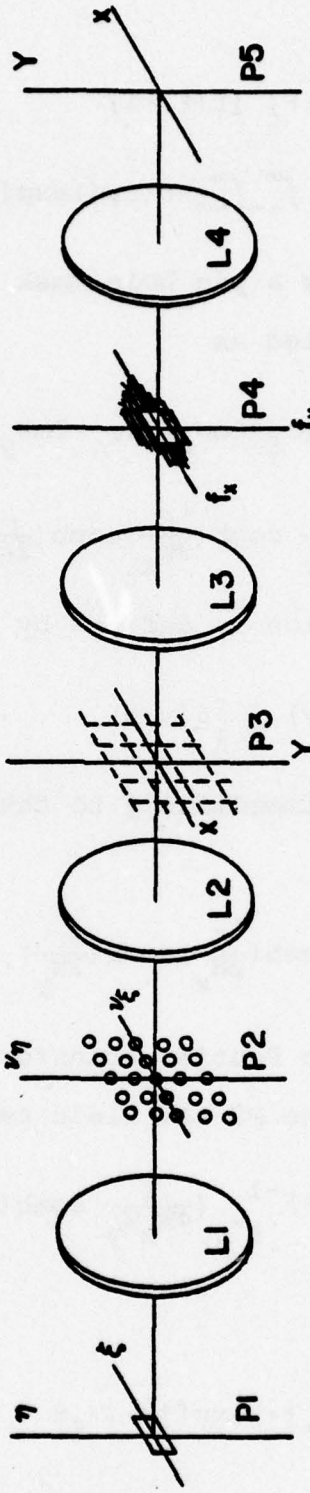

Figure 4.4 A coherent processor for implementing a sampling theorem characterization of a linear space-variant system.

$$F(\nu_\xi,\nu_\eta) = \mathcal{F}_\xi\,[f(\xi,\eta)]$$
$$= \int_{-\infty}^{\infty}\int_{-\infty}^{\infty} f(\xi,\eta)\exp[-j2\pi(\nu_\xi\xi+\nu_\eta\eta)]\,d\xi d\eta\,. \tag{4-21}$$

Placed in plane P2 is a pin hole mask the transmittance of which can be modeled as

$$t(\nu_\xi,\nu_\eta) = \sum_n\sum_m \delta(\nu_\xi-2nW_x)\,\delta(\nu_\eta-2mW_y)$$
$$= \frac{1}{4W_xW_y}\,\mathrm{comb}\left(\frac{\nu_\xi}{2W_x}\right)\mathrm{comb}\left(\frac{\nu_\eta}{2W_y}\right) \tag{4-22}$$

where the comb function is defined by

$$\mathrm{comb}(\nu) \triangleq \sum_n \delta(\nu-n)\,. \tag{4-23}$$

The field amplitude immediately to the right of P2 is then given by

$$\frac{1}{4W_xW_y}\,F(\nu_\xi,\nu_\eta)\,\mathrm{comb}\left(\frac{\nu_\xi}{2W_x}\right)\mathrm{comb}\left(\frac{\nu_\eta}{2W_y}\right). \tag{4-24}$$

This product is again Fourier transformed by lens L2 to give incident on plane P3 the field amplitude

$$\mathcal{F}^{-1}_{\nu_\xi\nu_\eta}\,[F(\nu_\xi,\nu_\eta)]*\mathcal{F}^{-1}_{\nu_\xi\nu_\eta}\left[\frac{1}{4W_xW_y}\,\mathrm{comb}\left(\frac{\nu_\xi}{2W_x}\right)\mathrm{comb}\left(\frac{\nu_\eta}{2W_y}\right)\right] \tag{4-25}$$

where

$$\mathcal{F}^{-1}_{\nu_\xi\nu_\eta}(\cdot) = \int_{-\infty}^{\infty}\int_{-\infty}^{\infty}(\cdot)\exp[j2\pi(\nu_\xi x + \nu_\eta y)]\,d\nu_\xi d\nu_\eta\,. \tag{4-26}$$

Using the scaling theorem and the fact that[23]

$$F_{\xi}[\mathrm{comb}(\xi)] = \mathrm{comb}(\nu) \tag{4-27}$$

reduces Eq. 4-25 to

$$f(x,y) * [\mathrm{comb}(2W_x x)\,\mathrm{comb}(2W_y y)]$$

$$= \frac{1}{4W_x W_y} \sum_n \sum_m f(x-x_n, y-y_m). \tag{4-28}$$

where $x_n = n/2W_x$ and $y_m = m/2W_y$. Our input is thus replicated over plane P3. Due to the compact support of the input and our choice of spacing in the pin hole mask, these replications do not overlap. We stress this by rewriting Eq. 4-28 as

$$\frac{1}{4W_x W_y} \sum_n \sum_m f(x-x_n, y-y_m)$$

$$\mathrm{rect}[2W_x(x-x_n)]\,\mathrm{rect}[2W_y(y-y_m)]. \tag{4-29}$$

Placed in plane P3 is a mask of sample point spread functions. The transmittance of this mask is

$$\sum_n \sum_n h(x_n, y_m; x-x_n, y-y_m)$$

$$\mathrm{rect}[2W_x(x-x_n)]\,\mathrm{rect}[2W_y(y-y_m)]. \tag{4-30}$$

If the transmittance is not non-negative real, we require a holographic mask. The placement of a number of holo-

grams side by side on a plane results in what is termed a composite hologram.[64] The mask can either be directly recorded or a computer generated transmittance. The mask is multiplied by Eq. 4-29 to give immediately to the right of plane P3 the field amplitude

$$\frac{1}{4W_xW_y} \sum_n \sum_m f(x-x_n, y-y_m) h(x_n, y_m; x-x_n, y-y_m) \qquad (4\text{-}31)$$

where we have now suppressed the rect terms. Comparing this with Eq. 4-18, we see that now only low pass filtering is required. This is performed by lenses L4 and L5 and the rectangular pupil on plane P4. Our desired output then appears on plane P5 and our space-variant operation has been performed.

Again, the class of space-variant operations that can be performed using this "composite hologram approach" is somewhat limited. Our constraint is that either the point spread function in ξ and η and/or the input have compact support not exceeding the reciprical bandwidths of $h(x,y;\xi,\eta)$ in x and y respectively.

To illustrate application of this processor to a specific operation, we will now consider a Fourier transform operation defined by

$$g(x,y) = \int_{-a}^{a} \int_{-b}^{b} f(\xi,\eta) \exp[-j2\pi r(x\xi + y\eta)] d\xi d\eta \qquad (4\text{-}32)$$

where a and b are positive spatial constants and r, with dimension of frequency squared, retains the required dimensionless nature of the exponent. The point spread function corresponding to this operation is

$$h(x-\xi,y-\eta;\xi,\eta) = \exp[-j2\pi r(x\xi + y\eta)]$$
$$\text{rect}(\frac{\xi}{2a})\,\text{rect}(\frac{\eta}{2b}). \qquad (4\text{-}33)$$

It follows that

$$h(x,y;\xi,\eta) = \exp[-j2\pi r\{(x\xi + y\eta) + (\xi^2 + \eta^2)\}]$$
$$\text{rect}(\frac{\xi}{2a})\,\text{rect}(\frac{\eta}{2b}). \qquad (4\text{-}34)$$

The two-dimensional transfer function for this system is then

$$H_{xy}(f_x,f_y;\xi,\eta) = \mathcal{F}_{xy}[h(x,y;\xi,\eta)]$$
$$= \delta(f_x-r\xi)\,\delta(f_y-r\eta)$$
$$\exp[-j2\pi r(\xi^2 + \eta^2)]$$
$$\text{rect}(\frac{\xi}{2a})\,\text{rect}(\frac{\eta}{2b}). \qquad (4\text{-}35)$$

Due to the multiplicative Dirac delta terms, we can make the substitutions $\xi = f_x/r$ and $\eta = f_y/r$. This gives

$$H_{xy}(f_x,f_y;\xi,\eta) = \delta(f_x-r\xi)\,\delta(f_y-r\eta)$$
$$\exp[-\frac{j2\pi}{r}(f_x^2 + f_y^2)]\,\text{rect}(\frac{f_x}{2ra})\,\text{rect}(\frac{f_y}{2rb}). \qquad (4\text{-}36)$$

Clearly, the point spread function is bandlimited in both x and y with

$$W_x = ra$$
$$W_y = rb. \tag{4-37}$$

Note also from Eq. 4-34, that $h(x,y;\xi,\eta)$ is zero outside of the interval $|\xi| \leq 1/4\ W_x$, $|\eta| \leq 1/4\ W_h$ if we impose the inequalities

$$|\xi| \leq a \leq \frac{1}{4ra}$$
$$|\eta| \leq b \leq \frac{1}{4rb} \tag{4-38}$$

or, equivalently, since $r > 0$,

$$a \leq \frac{1}{2\sqrt{r}} \quad ; \quad b \leq \frac{1}{2\sqrt{r}}\ . \tag{4-39}$$

If these inequalities are assumed, no compact support assumptions for the input need be made.

To this point, we have only established that the sampling theorem in Eq. 4-33 can be applied. The next step is to compute the required transmittance of the sample point spread function mask. From Eq. 4-34, we can write

$$h(x_n,y_m;x,y) = \exp[-j2\pi r\{x(x + x_n) + y(y + y_m)\}]$$
$$\operatorname{rect}(\frac{x}{2a})\operatorname{rect}(\frac{y}{2b}). \tag{4-40}$$

It follows that

$$h(x_n, y_m; x-x_n, y-y_m)$$

$$= \exp[-j2\pi r\{(x-x_n)x + (y-y_m)y\}]$$

$$\text{rect}\left(\frac{x-x_n}{2a}\right)\text{rect}\left(\frac{y-y_m}{2b}\right)$$

$$= \exp[-j2\pi r(x^2 + y^2)]\,\text{rect}\left(\frac{x-x_n}{2a}\right)\text{rect}\left(\frac{y-y_m}{2b}\right)$$

$$\times \exp[j2\pi r(xx_n + yy_m)]. \qquad (4\text{-}41)$$

This is our composite hologram mask transmittance. Note that the $\exp[-j2\pi r(x^2 + y^2)]$ term can be interpreted as the transmittance of a thin convex lens with focal length f determined by the relation[23]

$$r = 1/\lambda f \qquad (4\text{-}42)$$

where λ is the wavelength of the spatially coherent illumination. From the inequalities in Eq. 4-39, the focal length must satisfy

$$f \geq \frac{4}{\lambda}\,[\max(a,b)]^2. \qquad (4\text{-}43)$$

For visible light, $\lambda << \max[a,b]$.

The composite hologram approach just presented obviously has a Fourier dual. The 2-D system frequency response is used instead of the point spread function characterization. The system constraints have, for the most part, different physical interpretations. A con-

straint which is identical in both schemes is the bandlimiting assumption on the first variables of the frequency response. That is, if the point spread function is bandlimited in x and y, then so is the system frequency response. The different interpretations appear in the constraints on the system input and last two variables of the frequency response. For the point spread function characterization, we required the input to have a compact support not exceeding the reciprocal bandwidths of the point spread function in its first two variables. In the frequency response characterization, we require the input spectrum have finite support. That is, the input must be bandlimited. A similar constraint applies to the frequency response with respect to its second variable.

The coherent processor capable of performing the frequency response sampling theorem is identical in form so that in Fig. 4-4 except that plane P1 and lens L1 are omitted. The bandlimited input is placed directly on plane P2 directly adjacent to the pin hole mask. Plane P3 contains the appropriate frequency response mask. Lenses L3 and L4 and the rectangular pupil in plane P4 perform the required low pass filtering. Our output appears on plane P5.

4.3. Volume Hologram Approach

The composite hologram scheme just presented catalogs sample point spread functions side by side on a holographic transmittance. It requires, however, rather stringent compact support constraints on the system input and point spread function. An alternate cataloging scheme, not requiring these constraints, makes use of the angular sensitivity of the volume hologram. Here, the system responses are angle multiplexed within a thick medium. As we will see, however, the scheme does not straightforwardly generalize to two dimensions. It is presented here with the thought of possible utilization in a hybrid processing scheme. This topic is in need of further investigation.

4.3.1. Diffraction Efficiency of the Volume Hologram

The diffraction efficiency performance of the volume hologram has been treated admirably with the coupled wave theory of Kogelnik.[65] Kogelnik's general theory can be found in many optics texts[64,66] and is presented via an alternate derivation by Alferness.[67] Kogelnik's theory has also been applied to specific media.[68-70]

In our treatment of volume hologram diffraction efficiency, however, we shall use the one-dimensional scalar optics model of Smith[66] which follows from the pioneering work of van Heerden.[71] We use the scalar optics model

primarily due to its relative analytic simplicity in comparison with coupled wave theory. The scalar optics treatment also remains consistant with the other scalar optics models used in this thesis.

An understanding of the basic diffraction efficiency phenomena of the volume hologram can best be qualitatively understood by inspection of Fig. 4-5. In Fig. 4-5a, a thick photosensitive recording medium of width t and refractive index n is illuninated with two coherent plane waves of wavelength λ. The plane waves are incident at angles θ_r and θ_o where the subscripts respectively denote reference and object waves. The thick media is exposed and processed to form a volume hologram. We illuminate the hologram, as shown in Fig. 4-5b, with a plane wave incident at an angle of θ_p. In general, three plane waves will exit the hologram. The beam b_t is the zeroth order non-diffracted component and b_c is the conjugate or "twin image" beam. The plane wave of interest is b_o, since, if $\theta_p = \theta_r$, then b_o will propagate in the same direction as our original object beam. The diffraction efficiency with respect to b_o is the ratio of the energy of the field amplitude of b_o to the energy of the field amplitude of the incident playback beam. Heuristically and in fact, the diffraction efficiency is maximum when the playback beam is in the same direction as

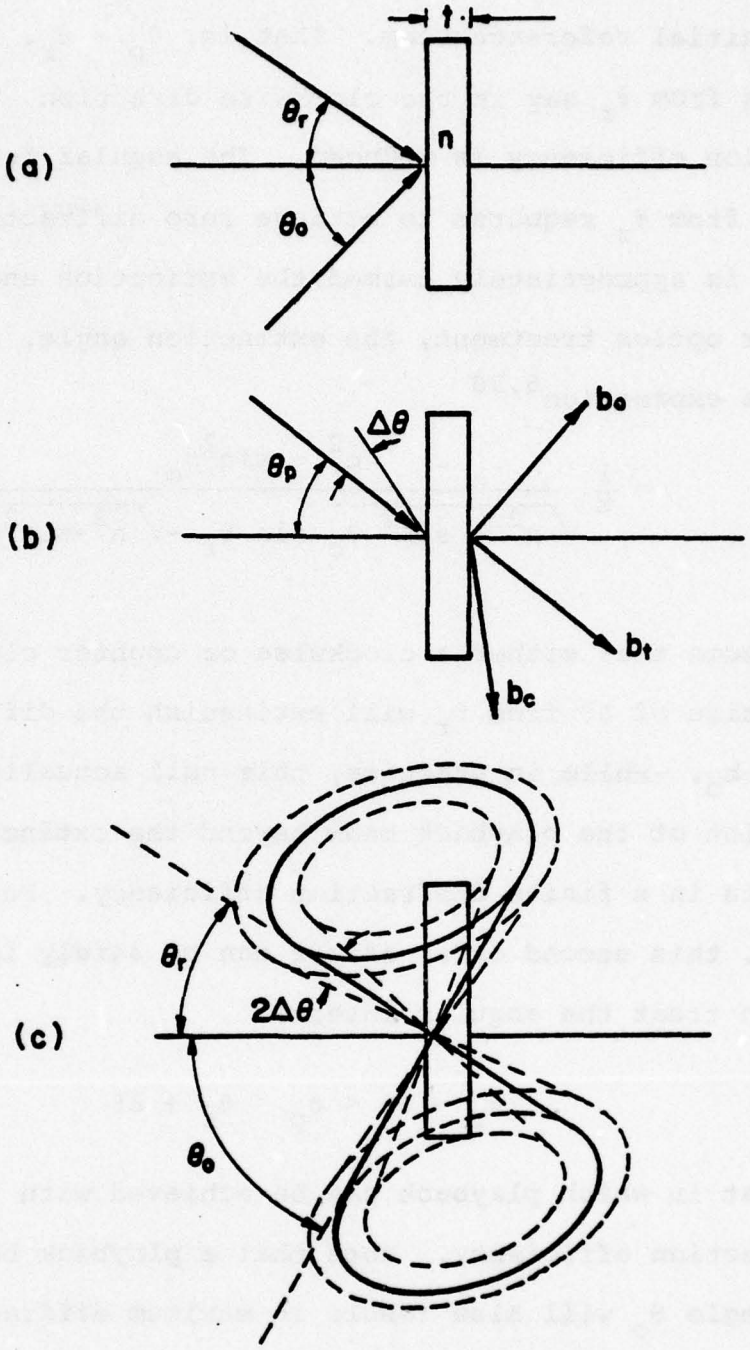

Figure 4.5 Recording two incident plane waves in a volume medium (a) The recording geometry (b) Playback geometry (c) The resulting Bragg and extinction cones.

our initial reference beam. That is, $\theta_p = \theta_r$. As θ_p deviates from θ_r say in the clockwise direction, the diffraction efficiency is reduced. The angular deviation of θ_p from θ_r required to achieve zero diffraction efficiency is appropriately termed the extinction angle. Through scalar optics treatment, the extinction angle, $\Delta\theta$, is given by the expression[6,20]

$$= \frac{\lambda}{t} \frac{n^2 - \sin^2\theta_o}{\sqrt{n^2 - \sin^2\theta_o}\sin\theta_r - \sqrt{n^2 - \sin^2\theta_r}\sin\theta_o} . \qquad (4\text{-}44)$$

We assume that either a clockwise or counter clockwise deviation of $\Delta\theta$ from θ_r will extinguish the diffracted beam, b_o. While in practice, this null actually occurs, rotation of the playback beam beyond the extinction angle results in a finite diffraction efficiency. For our purposes, this second order effect can be safely ignored and we can treat the angular interval

$$\theta_r - \Delta\theta < \theta_p < \theta_r + \Delta\theta \qquad (4\text{-}45)$$

as that in which playback can be achieved with finite diffraction efficiency. Note that a playback beam at the angle θ_o will also result in maximum diffraction efficiency. In future treatment however, we will avoid this angular playback region so that additional unwanted diffracted terms will not be generated.

Note that the analysis to this point has been one-dimensional. An obvious question arises: What if the playback beam in Fig. 4-5b was incident on the volume hologram in a direction not lying in the plane defined by two recorded beams? The diffraction mechanism in this more general case can be best understood with the geometry of Fig. 4-5c. Using the recording beam directions indicated in Fig. 4-5a, we form the "Bragg cone" shown.[64] Next, visualize any plane passing through that line corresponding to the intersection of the volume hologram plane and the plane defined by the two recording beams. For all possible illuminating plane waves with propagation directions lying on this plane, the relative maximum diffraction efficiency occurs for those two propagation directions on the Bragg cone. Still on this plane, we can extinguish the diffracted beam by rotating the incident beam an angular interval corresponding in concept to the extinction angle. Thus, in a first order analysis, we can speak of "extinction cones" which, as shown by the dotted lines in Fig. 4-5c, lie within and without the Bragg cone. As we shall see, this generalized view of the extinction angle concept is the very mechanism that prohibits two-dimensional generalization of the space-variant processing schemes to be presented.

4.3.2. Space-Variant System Representation

We can utilize the extinction angle phenomenon inherent in volume holography to implement space-variant systems. Representation of space-variant systems with volume holograms using the piecewise isoplanatic approximation (PIA) was earlier investigated by Marks.[6] Here, we will outline the implementation of a sampling theorem characterization presented in Chapter II.[20-21] Implementation of a discrete orthonormal basis set response (DBR) characterization using the system sinc response is also presented.

The sampling theorem for variation limited systems with bandlimited input is repeated here from Eq. 2-84:

$$g(x) = \sum_n f(\xi_n) h(x-\xi_n;\xi_n) * \text{sinc } 2W_s x. \quad (4\text{-}46)$$

A scheme for implementing this sampling theorem is pictured in Fig. 4-6. We excite our variation limited system with a Dirac delta placed at input coordinate $\xi = \xi_n$. The corresponding field amplitude on the system output plane is thus $h(x-\xi_n;\xi_n)$. Also placed on the system output plane is a Dirac delta placed at $x = \xi_n + a$. The desired value of a, as we shall see, is determined by the spatial extent of the sample line spread function.

The field amplitude on the x axis in Fig. 4-6 is

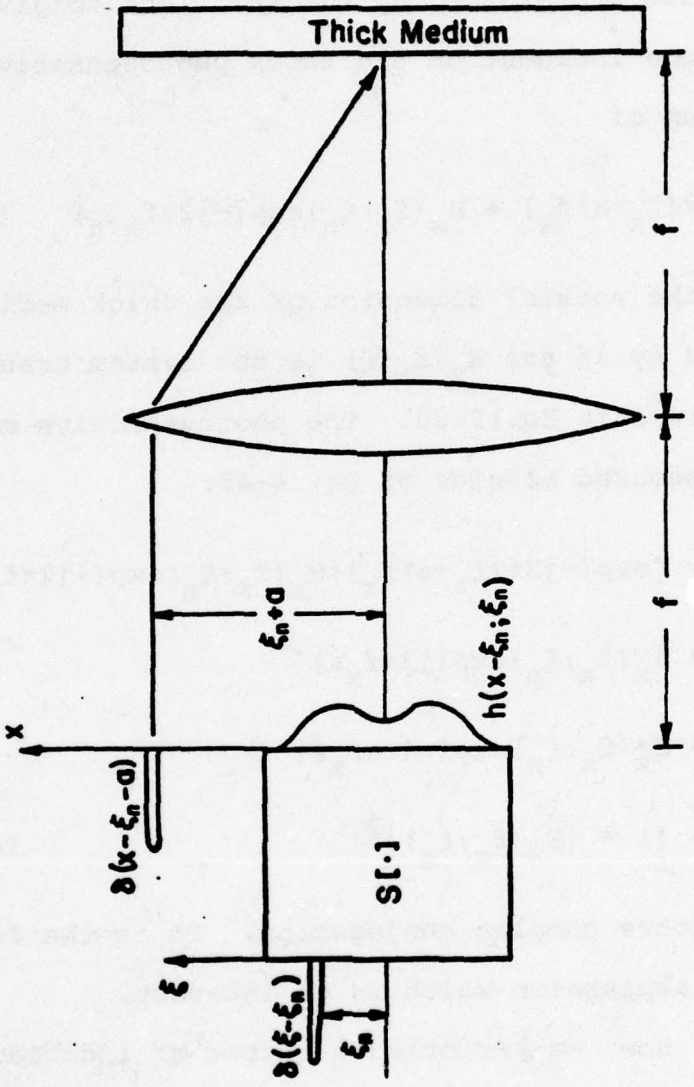

Figure 4.6 Recording geometry for the volume hologram approach.

given by

$$\delta(x-\xi_n-a) + h(x-\xi_n;\xi_n). \qquad (4\text{-}47)$$

This is Fourier transformed by the thin lens to give a field amplitude incident on the thick photosensitive recording medium of

$$\exp[-j2\pi(\xi_n+a)f_x] + H_x(f_x;\xi_n)\exp[-j2\pi f_x\xi_n] \qquad (4\text{-}48)$$

where f_x is the spatial dimension of the thick media's plane divided by λf and $H_x(f_x;\xi)$ is the system transfer function defined in Eq. 2-26. The photosensitive medium records the squared modulus of Eq. 4-48:

$$\begin{aligned} I_n(f_x) &= |\exp[-j2\pi(\xi_n+a)f_x]+H_x(f_x;\xi_n)\exp(-j2\pi f_x\xi_n)|^2 \\ &= H_x(f_x;\xi_n)\exp[j2\pi f_x a] \\ &+ H_x^*(f_x;\xi_n)\exp[-j2\pi f_x a] \\ &+ [1 + |H_x(f_x;\xi_n)|^2] \end{aligned} \qquad (4\text{-}49)$$

where "*" denotes complex conjugation. It is the first term in this expression which is of interest.

Suppose, now, we performed a number of individual sequential exposures of this kind for various values of n. The resulting volume hologram would then have a transmittance of

$$I(f_x) = \sum_n I_n(f_x)$$

$$= \sum_n H_x(f_x;\xi_n)\exp(j2\pi f_x a)$$

$$+ \sum_n H_x^*(f_x;\xi_n)\exp(-j2\pi f_x a)$$

$$+ \sum_n [1 + |H_x(f_x;\xi_n)|^2]. \qquad (4\text{-}50)$$

Rigorously, a scale factor should be included in this expression so that $I(f_x)$ is less than or equal to unity for all f_x. We omit it here with no loss in generality.

With the volume hologram transmittance in Eq. 4-50, we can implement the sampling theorem with the processor pictured in Fig. 4-7. Our (bandlimited) input, $f(\xi)$, is placed in plane P1. Also placed in this plane is a pin hole mask calibrated in accordance with the positioning of the reference Dirac deltas used in the system recording scheme. If we illuminate plane P1 from the left with a normally incident plane wave, the field amplitude immediately to the right of plane P1 can be modeled by

$$\sum_n f(\xi_n)\delta(\xi-\xi_n-a). \qquad (4\text{-}51)$$

This is Fourier transformed by lens L2 to give incident on the volume hologram the field amplitude

$$\sum_n f(\xi_n)\exp[-j2\pi f_x(\xi_n+a)]. \qquad (4\text{-}52)$$

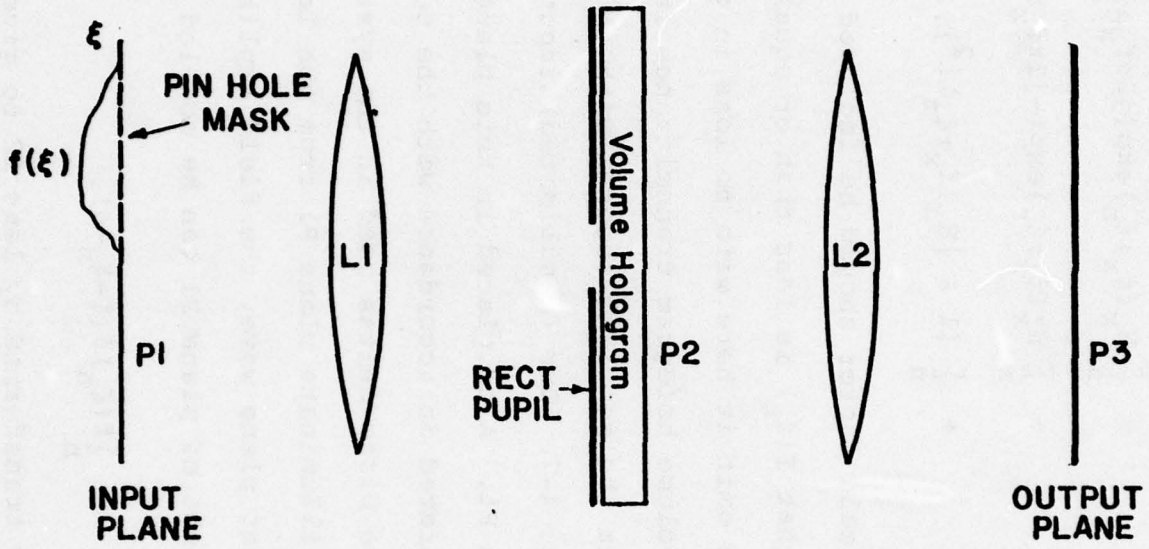

(b)

Figure 4.7 Playback geometry for the volume hologram approach.

Now, if the hologram in plane P2 were <u>not</u> volume, the field amplitude immediately to the right of plane P2 would be given by the product of Eqs. 4-52 and 4-50. Since the hologram is thick, however, angularly sensitive diffraction efficiency effects take place. Comparing the recording and playback geometries in Figs. 4-6 and 4-7 we see that only the n^{th} reference Dirac delta and the n^{th} input sample result in plane waves that are incident on the volume medium at identical angles. If we require that the angular incidence corresponding to adjacent samples lie outside the equivalent extinction angle, it then follows that the only diffracted term corresponding to $f(\xi_n)\exp[-j2\pi f_x(\xi_n + a)]$ is $H_x(f_x;\xi_n)\exp(j2\pi f_x a)$. Thus, we have angle multiplexed our sample transfer functions within the emulsion of the volume hologram in such a manner that they will be accessed only by appropriately incident plane waves. It follows, then, that the field amplitude exiting the volume hologram is

$$\sum_n [f(\xi_n)\exp\{-j2\pi f_x(\xi_n+a)\}][H_x(f_x;\xi_n)\exp(j2\pi f_x a)]$$

$$= \sum_n f(\xi_n)H_x(f_x;\xi_n)\exp(-j2\pi f_x \xi_n). \quad (4\text{-}53)$$

Also in plane P2, we place a rectangular pupil, $\mathrm{rect}(f_x/2W_s)$. The field amplitude immediately to the right of plane P2 is then recognized as the Fourier transform of the sampling

theorem expression in Eq. 4-46:

$$G(f_x) = \sum_n f(\xi_n) H_x(f_x;\xi_n) \exp(-j2\pi f_x \xi_n) \times \text{rect}\left(\frac{f_x}{2W_x}\right). \quad (4\text{-}54)$$

Lens L2 performs a Fourier transform on this expression. Equation 4-46 then describes the field amplitude on plane P3 and our space-variant operation has been performed.

There are a number of fundamental limitations to this scheme that should be pointed out. First of all, with reference again to Fig. 4-6, note that there can be no overlapping of the Dirac delta reference region and the sample line spread function regions for all n. This must be assured to avoid unwanted crosstalk on playback. Thus, the system line spread function must be "single sided" for all ξ. The system input must likewise be single sided. But we have assumed the input to be bandlimited and no single sided signal can be rigorously bandlimited. This seeming inconsistancy can be overcome by appealing to the concept of the "essentially" bandlimited signal,[72] a term coined by those applying sampling theorem concepts to causal (temporal single sided) signals. A second fundamental limitation of this scheme is its inherent one-dimensional nature. That is, the scheme cannot be directly extended into two dimensions since the required diffrac-

tion efficiency mechanism does not generalize to two dimensions. Instead, we are confronted by the previously discussed Bragg cones.

Another disadvantage, in a mathematical sense, is oversampling. In accordance with our treatment in Chapter II, we are sampling the input at a rate $2W_s = 2W_\nu + 2W_f$ where $2W_\nu$ is the system variation bandwidth and $2W_f$ is the bandwidth of the input. The actual minimum sampling rate for the input is $2W_f$. We can, however, utilize the minimum allowable (Nyquist) rate for the input if we angle multiplex the system's sinc response instead of its sample line spread function. Recall, from Eq. 2-59, that a linear system can be characterized by

$$g(x) = \sum_n f(\xi_n) S[\text{sinc } 2W_f(\xi-\xi_n)] \qquad (4\text{-}55)$$

where, now, $\xi_n = n/2W_f$. This relation is computationally similar to the sampling theorem expression in Eq. 4-46 except for the fact that the interpolation functions here are sinc responses instead of low-passed sample line spread functions. In fact, the recording and playback schemes in Figs. 4-6 and 4-7 can be used to implement the sinc response characterization with only two minor modifications. First, we need to excite the system with $\text{sinc}2W_f(\xi-\xi_n)$ instead of $\delta(\xi-\xi_n)$. The sincs can easily be generated in the

manner previously discussed. The second modification is removal of the rectangular pupil on the hologram plane in the playback geometry.

Implementation of the sinc response characterization has the same fundamental limitations as the sampling theorem characterization implementation. There are, however, certain distinct advantages. First of all, the class of representable systems is increased. That is, the sampling theorem requires a variation limited system while the DBR characterization, of which the sinc response characterization is a special case, is essentially independent of the system's parameters. Secondly, since sampling is performed at a lower rate in the sinc response characterization, we would expect to require fewer hologram exposures for a given degree of output accuracy.

The primary disadvantage of the volume hologram implementation of both the sinc response and sampling theorem characterizations is the resulting one-dimensional resolution capability. It is possible, however, that they could be used as an element in either a hybrid or more elaborate processing scheme.

4.4. Phase Coded Reference Beam Approach

Phase-coded reference beams have been used for color holography[64,73] and for multiplexing point source objects

for digital storage.[74] Krile et.al.[22,75] have applied the phase coded reference beam idea to two-dimensional space-variant system characterization. The result is the smearing out of unwanted crosstalk terms into diffuse background noise. This is in contrast to the volume hologram approach where unwanted crosstalk terms were filtered by the volume hologram's angular bandpass. An overwhelming advantage of the phase-coded reference beam approach over the volume hologram approach, however, is its capability of two-dimensional system representation.

We will here illustrate utilization of phase coded reference beams in implementing the sampling theorem of Eq. 2-84. As we shall see, mathematical relations describing its operation became quite lengthy. For this reason, analysis will be performed in one dimension although the results are straightforwardly extended into two dimensions.

The recording geometry for this scheme is pictured in Fig. 4-8 and closely resembles the structure of the volume hologram recording scheme of Fig. 4-6. The system is excited with a displaced Dirac delta. The sample line spread function, $h(x-\xi_n;\xi_n)$, appears at the system output. Placed on this same plane is a random diffuser with transmittance $d(x)$ which is displaced clear of the system output plane. We illuminate the diffuser from the left with a coherent plane wave over the interval $\xi_n+a-T<x<\xi_n+a+T$

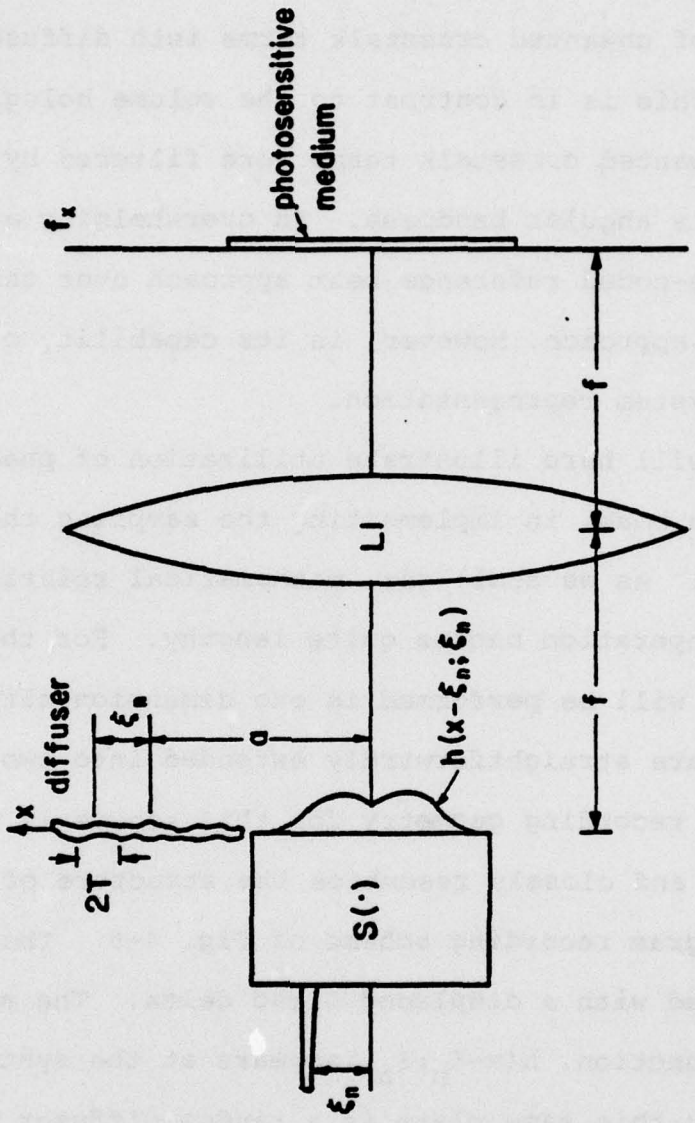

Figure 4.8 Recording geometry for the phase coded reference beam approach.

where a denotes the displacement of the diffuser and 2T is the interval width. The field amplitude in the front focal plane of lens L1 is thus

$$h(x-\xi_n;\xi_n) + d_n(x) \tag{4-56}$$

where

$$d_n(x) = d(x)\,\mathrm{rect}\left[\frac{x-\xi_n-a}{2T}\right]. \tag{4-57}$$

This is Fourier transformed by the thin lens to give incident on the photosensitive media the field amplitude

$$H_x(f_x;\xi_n)e^{-j2\pi f_x\xi_n} + D_n(f_x) \tag{4-58}$$

where $D_n(f_x) = \mathcal{F}_x[d_n(x)]$. The transmittance of the resulting hologram is the squared modulus of this expression:

$$\begin{aligned} I_n(f_x) &= H_x(f_x;\xi_n)D_n^*(f_x)e^{-j2\pi f_x\xi_n} \\ &\quad + H_x^*(f_x;\xi_n)D_n(f_x)e^{j2\pi f_x\xi_n} \\ &\quad + |H_x(f_x;\xi_n)|^2 + |D_n(f_x)|^2. \end{aligned} \tag{4-59}$$

It is the first term in this expression, of course, which is of interest.

Suppose, then, that a number of such exposures were recorded on the same media for various values of n. The resulting hologram transmittance is then

$$I(f_x) = \sum_n I_n(f_x). \qquad (4\text{-}60)$$

Note that, in order for the same portion of the diffuser not to be used in more than one of these exposures, that we must require $\xi_{n+1}-\xi_n \leq 2T$. Let us assume adjoined patches so that $\xi_{n+1}-\xi_n = 2T$ for all n.

Consider next the playback geometry in Fig. 4-9. The diffuser, lens L1, and the hologram are left in the same position as in Fig. 4-8. To the left of the diffuser an input transmittance, $f(\xi)$, is sandwiched between two flys eye lens arrays. Each lenslet is assumed to have width 2T. The left most lenslet is illuminated from the left by a coherent plane wave. Thus, incident on our input transmittance is the field amplitude.

$$\sum_m \delta(\xi-\xi_m-a). \qquad (4\text{-}61)$$

That is, each of the lenslets in the left most array is assumed to focus the plane wave incident on its pupil to a point source. Equation 4-61 then follows as a result of the discussion on Dirac delta generation discussed previously in this chapter.

Equation 4-61 now multiplies the input transparency to give

$$\sum_m f(\xi_m)\delta(\xi-\xi_m-a). \qquad (4\text{-}62)$$

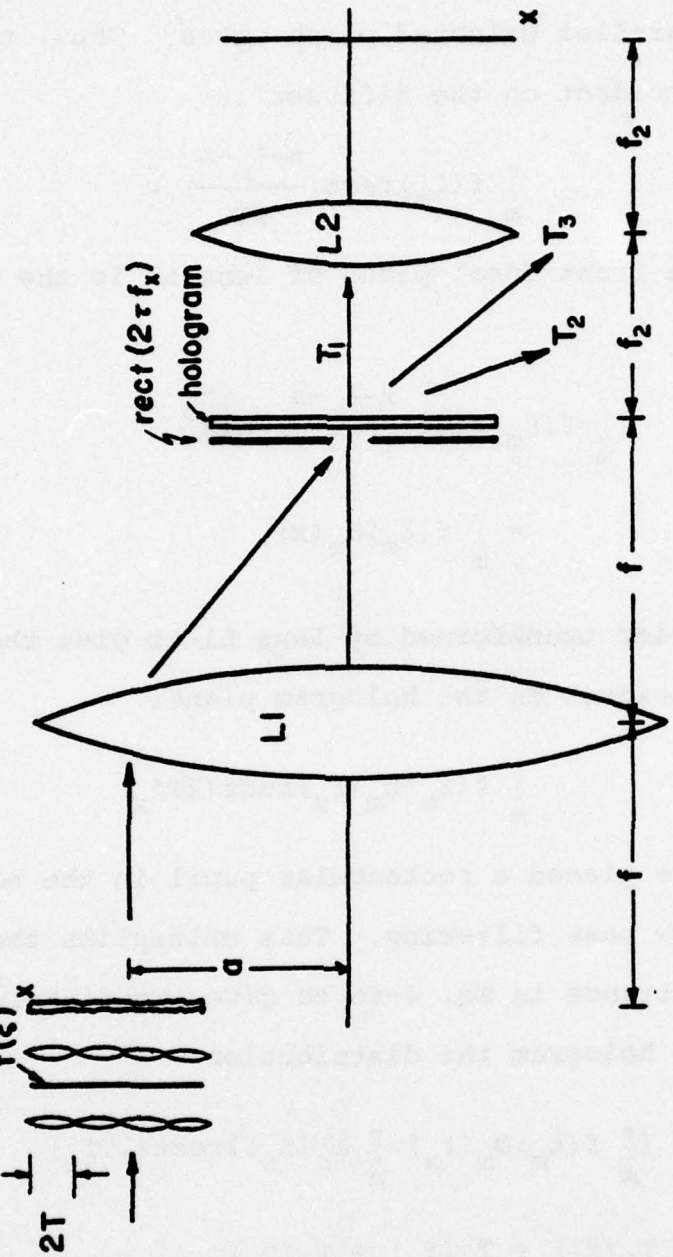

Figure 4.9 Playback geometry for the phase coded reference beam approach.

Each weighted Dirac delta in this sum is then laterally transformed by the right most flys eye array to yield a series of parallel weighted plane waves. Thus, the field amplitude incident on the diffuser is

$$\sum_m f(\xi_m)\,\mathrm{rect}\left(\frac{x-\xi_m-a}{2T}\right). \tag{4-63}$$

Thus, in the front focal plane of lens L1 is the distribution

$$\sum_m f(\xi_m)\,\mathrm{rect}\left(\frac{x-\xi_m-a}{2T}\right)\, d(x)$$

$$= \sum_m f(\xi_m)\, d_m(x). \tag{4-64}$$

This is Fourier transformed by lens L1 to give the field amplitude incident on the hologram plane:

$$\sum_m f(\xi_m)\, D_m(f_x)\,\mathrm{rect}(2Tf_x) \tag{4-65}$$

where we have placed a rectangular pupil in the hologram plane for low pass filtering. This multiplies the hologram transmittance in Eq. 4-60 to give immediately to the right of the hologram the distribution

$$D(f_x) = \left[\sum_m f(\xi_m)\, D_m(f_x) \sum_n I_n(f_x)\right]\mathrm{rect}(2Tf_x)$$

$$= T_1(f_x) + T_2(f_x) + T_3(f_x) \tag{4-66}$$

where

$$T_3(f_x) = \sum_m \sum_n f(\xi_m) D_m(f_x) [|H_x(f_x;\xi_n)|^2 + |D_n(f_x)|^2] \text{rect}(2Tf_x)$$

$$T_2(f_x) = \sum_m \sum_n f(\xi_m) D_m(f_x) H_x^*(f_x;\xi_n) D_n(f_x) \exp[j2\pi f_x \xi_n] \text{rect}(2Tf_x) \qquad (4\text{-}67)$$

$$T_1(f_x) = \sum_m \sum_n f(\xi_m) D_m(f_x) H_x(f_x;\xi_n) D_n^*(f_x) \exp[-j2\pi f_x \xi_n] \text{rect}(2Tf_x).$$

Lets interpret each of these sums individually. $T_3(\cdot)$ is the zero order "through" term which results from the incident beam propagating unaltered in direction through the hologram transmittance. Term $T_2(\cdot)$ is the amplitude of the so called conjugate or "twin image" diffracted term. As is shown in Fig. 4-9, this term will be general exit the hologram at a rather steep angle for the chosen recording geometry. It is $T_1(\cdot)$ that we are interested in. As shown, the general propagation direction of the wave with amplitude $T_1(\cdot)$ is down the system axis. Let us then, suppose (more or less realistically) that we can either suppress the effects of $T_2(\cdot)$ and $T_3(\cdot)$ by filtering, or that their appearance on the processor output plane does not overlap with the $T_1(\cdot)$ term. With this assumption, we can restrict attention to $T_1(\cdot)$.

Consider, then, the effect of lens L2 which performs a Fourier transform on $T_1(f_x)$ to give the amplitude $t_1(x)$ on the processor output plane.

$$t_1(x) = \sum_n \sum_m f(\xi_m) h(x-\xi_n;\xi_n) * \text{sinc}\, \frac{x}{2T} * [d_n(x) \star d_m(x)]. \qquad (4\text{-}68)$$

Here we have made use of the convolution and autocorrelation theorems of Fourier transform theory.[28]

To this point, we have made no comment concerning the character of the diffuser. Comparison of Eq. 4-68 with the sampling theorem expansion in Eq. 2-84, however, makes clear the desired property of diffuser. Specifically, with $1/2T = 2W_s$, we would like

$$d_n(x) \star d_m(x) = \delta(x)\delta_{nm} \qquad (4\text{-}69)$$

where δ_{nm} is the Kronecker delta. That is, for $n = m$, the autocorrelation of a single patch of the diffuser should be peaked like a Dirac delta. Otherwise, for $n \neq m$, the crosscorrelation of two diffuser patches should ideally be zero. If this condition could be met, then Eq. 4-68 would reduce to

$$t_1(x) = \sum_n f(\xi_n) h(x-\xi_n;\xi_n) * \text{sinc}\, \frac{x}{2T}. \qquad (4\text{-}70)$$

Outside of a proportionality constant, this is the ex-

AD-A050 973 TEXAS TECH UNIV LUBBOCK OPTICAL SYSTEMS LAB F/G 20/6
SPACE-VARIANT COHERENT OPTICAL PROCESSING.(U)
DEC 77 R J MARKS AFOSR-75-2855
UNCLASSIFIED SCIENTIFIC-1 AFOSR-TR-78-0212 NL

3 OF 3
AD
A050973

END
DATE
FILMED
4-78
DDC

pression for the sampling theorem in Eq. 2-84 for $2W_x=1/2T$. Thus, our space-variant operation has been performed and $t_1(x) = g(x)$.

Unfortunately, implementing a diffuser which has the property of Eq. 4-69 is obviously not rigorously possible. Thus, we must settle for a diffuser which exhibits this property to a good approximation. Such a diffuser would exhibit peaked autocorrelation for all patches and a broad low level crosscorrelation for each unequal patch pair. A direct consequence of a latter characteristic is the occurence of cross talk terms in Eq. 4-68. These terms, however, will be smeared out into diffuse background noise. An investigation into various diffusers for use in the phase coded reference beam scheme is presently being undertaken by Krile et.al.[76]

As a final note in this section, we again stress that, unlike the volume hologram scheme, the phase coded reference beam approach can be implemented in two dimensions and thus, in this regard, is much more powerful.

4.5. Discussion

In this chapter, we have discussed system response generation and two-dimensional space-variant system representation. Certain types of system responses were shown to be straightforwardly performed. These include the

system sinc and rect responses. The system point spread function was also shown to be easily generated for both input and output sampling cases.

Three methods of 2-D system representation were presented. Let us briefly contrast the advantages and disadvantages of each.

The composite hologram implementation for systems whose point spread functions are bandlimited in their output variables is probably the most straightforwardly implementable of the three schemes. The required mask can, in principle, either be obtained through direct optical recording or from computer generated hologram. The primary drawback of this scheme, however, is the extremely narrow allowable class of systems and inputs to which the scheme can be applied.

The volume hologram approach, although containing a two-dimensional flavor, permits straightforward representation only of one-dimensional systems. In this regard, the one-dimensional processors in Chapter III would seem to be superior. Another fundamental drawback is the necessity of direct optical recording. That is, no scheme for computer generated volume holograms has been formulated to date. The beauty of the volume hologram approach, however, is the clean manner in which it filters out unwanted crosstalk terms. Utilization of the volume holo-

gram in future hybrid two-dimensional space-variant processors is a distinct possibility. Its use in supressing part of the crosstalk in the phase coded reference beam approach has also been suggested.[22]

In terms of application to the widest class of 2-D systems, the phase coded reference beam approach seems to be the best of the three schemes. The required holographic mask can be either directly recorded or obtained from a computer generated hologram. The primary disadvantage of the scheme is the appearance of crosstalk terms in the form of diffuse background noise. This problem, however, can be minimized by construction of more optimal diffusers.

CHAPTER V

5. CONCLUSIONS

In this report we have introduced new views on linear system characterization theory and have proposed various schemes for coherent linear space-variant processing. A recap of these results and reflections on possible future work are in order.

The continuum orthonormal response system characterization introduced in Chapter II offers a generalized view of linear system description. The familiar line spread function and frequency response characterizations were shown to be special cases. Of more practical interest are the three system characterizations wherein constraints are placed on the system and/or input. The piecewise isoplanatic approximation (PIA) is such a case. The constraint here is that the system line spread function change "slowly" in shape over an isoplanatically modeled interval.

Additional investigation of the PIA could be performed in several areas. One as of yet unsolved problems is the convergence of the PIA to the true system output as each patch grows arbitrarily small and the patch density becomes arbitrarily large. Interestingly, the energy (integral of the modulus squared) of the PIA and true outputs, for certain systems even in the limit is not

equal.[7] More drastically, the PIA of a finite energy output might have an infinite energy.[7] It is this author's conjecture that only very loose constraints can be placed on the convergence of the PIA for the most general case. Possibly tighter bounds can be placed on a specific system or system class. A similar area of investigation would be the study of filtering the PIA output to improve convergence.

A second interesting yet unsolved area of investigation concerning the PIA is definition of the isoplanatic patch. Lohman and Paris[26] have offered such a definition which, unfortunately, seems limited in application to imaging systems. Arsenault and Brousseau[77] have also noted deficiencies in the Lohman-Paris definition. We can conclude from Lohman and Paris, however, that a definition of the isoplanatic patch need be only system dependent (and thus input independent). Possibly the concept of the variation spectrum introduced in this thesis offers the basis for a new more universal definition of the isoplanatic patch.

A second constrained system characterization presented in Chapter II was the discrete orthonormal basis element response (DBR) characterization. Here, the system is completely defined for an input class by cataloging the system response to each element in an orthonormal basis set. The inputs are limited to that class spanned by

the basis set. The sinc and rect responses were shown to be particularly straightforwardly implementable in coherent processor applications respectively for band- and space-limited inputs. Due to vignetting and finite pupil effects, only bandlimited and space-limited signals are present within any space-variant processor[78] (within the treatment of scalar optics[79]).

As with the PIA, an interesting study of the DBR characterization is convergence. A given input convergence does not necessitate a given output convergence. For example, as our system, consider a Fourier transformer with bandlimited input. Using the sinc basis set, our input is reconstructed via the conventional Whittaker-Shannon sampling theorem which displays uniform convergence.[36] The system output, which will be reconstructed via a Fourier series, displays Gibbs phenomena[24] and thus does <u>not</u> uniformly converge (convergence is in the mean). Thus the input and output display different convergence properties. The converse holds for a Fourier transformer with space-limited input using the rect basis elements. It would seem that for "physically realizable systems" with finite energy inputs that, if our input space were spanned, then so would our output space. We could then expect, it seems, at least mean square convergence.

Another possible area of investigation of the DBR is the best choice of a basis set. A criteria on which the basis set could be chosen is output convergence. That is, for a given allowable output error, we would want to choose that basis set whose expansion converged quickest on the output with fewest terms. Fabrication and use of orthonormal element masks for characterization of coherent processors would also be an interesting undertaking.

The final constrained system characterizations presented in Chapter II were the sampling theorems. The sampling theorems, in principle, seem to be the most directly applicable to coherent processor implementation. The system sinc response, herein denoted as a DBR characterization, could also be argued to belong to the sampling theorem class.

Besides direct application to coherent processing, the sampling theorems are also useful in other areas. In circuit theory, they give rise to methods of time-variant filter synthesis.[10] Also, in treatment of linear systems on the digital computer, the sampling theorem results give an idea of the sampling rate required for good approximation. Although such sampling rates have been discussed elsewhere in a somewhat more limited scope,[80] no analytic expressions for the resulting system characterization have been previously presented.

A curious question arises concerning utilization of the proposed sampling rates. As is discussed in the main text, sampling is performed on all members at a rate above the minimum allowable sampling rate for each member individually. Seemingly, we gain by this oversampling a simple computational form that is a direct discrete case of the superposition integral. If sampling of each member is performed at its corresponding minimum sampling rate, the resulting expressions are vastly more complex. However, in actual digital implementation, this manner of sampling would seem to require less memory for a given degree of allowable error. Thus, a tradeoff between the two sampling schemes seems to be simplicity vs. required computer memory. A more definitive study of this tradeoff in term of space-bandlimited products would be an interesting undertaking.

There are also other possible avenues of investigation. One is effects of trunctation. It would seem that this would be a straightforward extension of work already performed on truncation effects in the conventional Whittker-Shannon sampling theorem.[81-82] Another interesting topic would be a study of the effects of jitter[83] (irregularly spaced sample points).

All of the constrained system characterizations in Chapter II are deterministic and, in principle, should

hold relatively true in the presence of low level noise. One can, however, envision cases where an intermediate noise level would give rise to non-negligible error. The allowance of this occurance uncovers an entire new area of possible study. For space-variant systems that are essentially deterministic, however, the system characterizations as presented in Chapter II offer a new wealth of both analytic and practical treatment.

Let us now move on to Chapter III in which numerous schemes for one-dimensional space-variant processing were presented. All processors considered make use of either an astigmatic or Fourier transform type processor. The class of space-variant operations that can be performed by these processors is extremely broad being fundamentally limited only by mask implementability. Even in this regard, we have a degree of flexibility. That is, if a mask for a given operation is not implementable for a given processor, it might be implementable for an alternate processor. As was shown, the one-dimensional space-variant processors have a variety of applications including coordinate distortion, integral transform display, convolution, correlation, and cross-spectral density display. There were also two serendipities of the processor schemes wherein the entire processor output plane was utilized. These were the Laplace transform and ambiguity

function display schemes. The simplicity of the ambiguity function processor has allowed for its inclusion in a collection of projects designed to introduce the undergraduate Electrical Engineer to coherent optical processing.[84-85]

A major result of 1-D processor study is the lensless processor. Here, the space-variant operation is performed by a single mask directly adjacent to which we place our 1-D input. It is hard to imagine a coherent processor in a less compact form.

Despite the diversity already demonstrated for the 1-D processors group, a number of fundamental investigations remain. At best, our treatment of the processors was only first order. We completely neglected such fundamental parameters such as finite pupil size and vignetting which in certain instances can cause significant degradation in processor performance. Mueller and Carlson[39] for example have shown that bandlimiting effects of the astigmatic processor impose fundamental limitations on the performance of the Laplace transform processor. As such, it would be instructive to perform a general investigation on the first order degrative effects of the various 1-D processors.

Mask fabrication is another fundamental area in need of further research. Three possibilities are 1) optically

holographically recorded masks, 2) masks generated by CRT display[39] and 3) computer generated holograms. A combination of these methods might also be employed.

One of the possible potential uses of the 1-D processors is in filtering of temporal signals. For example, 1-D processors have distinct advantages over the conventional 2-D convolution/correlation coherent processors where movement or Fourier encoding is required. Utilizing one-dimensional electro-optical transducers to provide the 1-D processor input, such operations could be performed in near real time.

Of more fundamental importance in temporal signal processing is the concept of "time-variant filtering." Through discussions with colleques and inspection of the literature, it is this author's opinion that this topic has not yet even begun to be investigated. There are even recent publications in which rather elementary time-variant filters are being analysed let alone applied in signal processing. As such, it would seem that application of the 1-D processor to temporal signal processing can be applied to time-variant filtering only when the advantages and applications of such filters are known. We should here stress that these comments apply only to use of the term "time-variant filtering" as a generalization of the concept of time-<u>invariant</u> filtering by electric circuits.

Lastly, let us reflect on Chapter IV wherein various possible schemes for general two-dimensional space-variant processing were presented. The first scheme (the composite hologram approach) was a straightforward implementation of a sampling theorem applicable when the system point spread function is bandlimited in its output variables. The method, however, places severe constraints on the support of the input and is thus applicable in only a small number of cases.

The volume hologram scheme was discussed next and was shown to be fundamentally one-dimensional in its application to space-variant processing. The ability of the volume hologram to store a number of wavefronts with angular accessibility, however, still leaves the possibility for its use in a hybrid two-dimensional processor. Its use in partial supression of diffuse background noise in the phase-coded reference beam scheme is also a distinct possibility.

Utilization of phase-coded reference beams is, to date, the most promising method for two-dimensional coherent space-variant processing. The fundamental drawback to this scheme is the smearing of unwanted crosstalks terms into diffuse background noise. Although this effect cannot be totally eliminated, it can be minimized by the use of codes which display peaked Dirac delta type autocorrelation and nearly zero crosscorrelation. An investiga-

tion into optimizing the diffusers in this fashion is presently underway.[75]

REFERENCES

1. L. J. Cutrona, E. N. Leith, C. J. Palermo and L. J. Porcello, "Optical Data Processing and Filtering Systems," IRE Trans. Inf. Theory IT-6, 386 (1960).

2. K. Preston, Coherent Optical Computers, (McGraw-Hill, New York, 1972).

3. T. Kailath, "Channel Characterizations: Time-Variant Dispersive Channels," In Lectures on Communications Systems Theory, edited by E. J. Baghdady (McGraw-Hill, New York, 1960).

4. H. J. Butterweck, "General Theory of Linear, Coherent Optical Data-Processing Systems," J. Opt. Soc. Am. 67, 1(1977).

5. R. J. Marks II, J. F. Walkup and M. O. Hagler, "Line Spread Function Notation," Appl. Opt. 15, 2289 (1976).

6. R. J. Marks II, "Holographic Recording of Optical Space-Variant Systems," MS thesis, Rose-Hulman Institute of Technology, Terre Haute, Indiana, (August, 1973).

7. R. J. Marks II and T. F. Krile, "Holographic Representation of Space-Variant Systems: System Theory," Appl. Opt. 15, 2241 (1976).

8. R. J. Marks II, J. F. Walkup and M. O. Hagler, "Volume Hologram Representation of Space-Variant Systems," in Applications of Holography and Optical Data Processing, edited by E. Marom, A. A. Friesem and E. Wiener-Aunear, (Pergamon, Oxford, 1977).

9. R. J. Marks II, J. F. Walkup and M. O. Hagler, "A Sampling Theorem for Space-Variant Systems," J. Opt. Soc. Am. 66, 918 (1976).

10. R. J. Marks II, J. F. Walkup and M. O. Hagler, "Sampling Theorems for Linear Shift-Variant Systems," Proc. of the 20th Midwest Symposium on Circuits and Systems, Texas Tech University, Lubbock, Texas (August, 1977).

11. R. J. Marks II and S. V. Bell, "Astigmatic Coherent Processor Analysis," Opt. Eng. (March-April 1978).

12. L. J. Cutrona, "Recent Developments in Coherent Optical Technology," in Optical and Electro-Optical Information Processing, J. T. Tippet et al., Eds. (MIT Press, Cambridge, 1965).

13. J. W. Goodman, P. Kellman and E. W. Hansen, "Linear Space-Variant Processing of One-Dimensional Signals," Appl. Opt. 16, 733 (1977).

14. R. J. Marks II, J. F. Walkup, M. O. Hagler and T. F. Krile, "Space-Variant Processing of 1-D Signals," Appl. Opt. 16, 739 (1977).

15. R.A.K. Said and D. C. Cooper, Proc. Inst. Elec. Eng. 120, 423 (1973).

16. R. J. Marks II, J. F. Walkup and T. F. Krile, "Ambiguity Function Display: An Improved Coherent Processor," Appl. Opt. 16, 746 (1977); addendum 16, 1777 (1977).

17. R. J. Marks II, J. F. Walkup and T. F. Krile, "An Improved Coherent Processor for Ambiguity Function Display," Proc. of the International Computing Conference, Capri, Italy (Sept. 1976).

18. R. J. Marks II and J. F. Walkup, "Coherent Optical Processors for Ambiguity Function Display and One-Dimensional Correlation/Convolution Operations," Proc. of the SPIE Symposium/Workshop on the Effective Utilization of Optics in Radar Systems, Huntsville, Alabama (Sept. 1977).

19. L. C. Burton, M. O. Hagler and T. F. Krile, "Holographic Representation of Multi-Element Optical Systems," IEEE J. Quantum Elec., QE-9, 633A (1973).

20. L. M. Deen, "Holographic Representations of Optical Systems," M.S. Thesis (Department of Electrical Engineering, Texas Tech University, Lubbock, Tex., 1975).

21. L. M. Deen, J. F. Walkup and M. O. Hagler, "Representations of Space-Variant Optical Systems Using Volume Holograms," Appl. Opt. 14, 2438 (1975).

22. T. F. Krile, R. J. Marks II, J. F. Walkup and M. O. Hagler, "Holographic Representations of Space-Variant Systems Using Phase-Coded Reference Beams," Appl. Opt. (Dec. 1977).

23. J. W. Goodman, Introduction to Fourier Optics, (McGraw Hill, New York, 1968).

24. J. B. Thomas, An Introduction to Statistical Communication Theory, (Wiley, New York, 1969).

25. T. Kailath, "Channel Characterization: Time-Variant Dispersive Channels," in Lectures on Communications Systems Theory, edited by E. J. Baghdady, (McGraw-Hill, New York, 1960).

26. A. W. Lohmann and D. P. Paris, "Space-Variant Image Formation," J. Opt. Soc. Am., 55, 1007 (1965).

27. N. Liskov, "Analytical Techniques for Linear Time-Varying Systems," Ph.D. dissertation (Electrical Engineering Research Laboratory, Cornell University, Ithaca, N.Y. 1964).

28. R. N. Bracewell, The Fourier Transform and its Applications, (McGraw-Hill, New York, 1965).

29. G. R. Cooper and C. D. McGillem, Method of Signal and System Analysis, (Holt, Rinehart and Winston, New York, 1967).

30. A. S. Davydov, Quantum Mechanics (NEO, Maine, 1966).

31. P. Elias, D. S. Grey and D. Z. Robinson, "Fourier Treatment of Optical Processes," J. Opt. Soc. Am., 42, 127 (1952).

32. P. B. Fellgett and E. H. Linfoot, "On the Assessment of Optical Images," Philos. Trans. R. Soc. London, A247, 369 (1955).

33. D. Slepian, "On Bandwidth," Proc. IEEE 64, 292 (1976).

34. E. T. Whittaker, "On the Functions Which Are Represented by the Expansions of the Interpolation Theory," Proc. Roy. Soc. Edinburgh 35, 181 (1915).

35. C. E. Shannon, "A Mathematical Theory of Communication," Bell Sys. Tech. J. 27, 379 and 623 (1948).

36. N. C. Gallagher Jr. and G. L. Wise, "A Representation for Bandlimited Functions," Proc. IEEE 63, 1624 (1975).

37. W. T. Rhodes, "Log-Frequency Variable Resolution Optical Spectrum Analysis Using Holographic Mapping Techniques," to appear in Opt. Comm. (1978).

38. W. T. Rhodes and J. Florence, "Frequency Variant Optical Signal Analysis," Appl. Opt. 15, 3073 (1976).

39. M. R. Mueller and F. P. Carlson, "Bandlimiting Effects in an Optical Laplace Transform Computer," Appl. Opt. 14, 2207 (1975).

40. P. W. Woodward, Probability and Information Theory, With Applications to Radar, (Pergamon, Oxford, 1963).

41. A. Papoulis, "Ambiguity Function in Fourier Optics," J. Opt. Soc. Am. 64, 779 (1974).

42. D. Casasent and F. Casasayas, "Optical Processing of Pulsed Doppler and FM Stepped Radar," Appl. Opt. 14, 1364 (1975).

43. M. C. Bartlett, L. W. Couch and R. C. Johnson, "Ambiguity Function Simulator," Proc. IEEE 63, 1625 (1975).

44. A. W. Rihaczek, Principles of High Resolution Radar, (McGraw-Hill, New York, 1969).

45. W. T. Rhodes, private correspondance (October 8, 1976).

46. R. J. Marks II, J. F. Walkup and C. A. Irby, "Techniques in One-Dimensional Space-Variant Processing," J. Opt. Soc. Am. 76, 1423A (1977).

47. D. G. McCauley, C. E. Simpson and W. J. Murbach, "Holographic Optical Element for Visual Display Applications," Appl. Opt. 12, 232 (1973).

48. J. N. Latta, "Computer-Based Analysis of Hologram Imagry and Aberrations," Appl. Opt. 12, 599 (1971).

49. D. Casasent and D. Psaltis, "New Optical Transforms for Pattern Recognition," Proc. IEEE 65, 77 (1977).

50. P. Kellman and J. W. Goodman, "Coherent Optical Implementation of 1-D Mellin Transforms," Appl. Opt. 16, 2609 (1977).

51. Gradskteyn and Ryzhik, "Tables of Integrals, Products, and Series, 4th Ed., (Academic Press, New York, 1965).

52. M. Abranowitz and I. A. Stegun, Handbook of Mathematical Functions, (Dover, New York, 1964).

53. A. A. Sawchuk, "Space-Variant Image Restoration by Coordinate Transformation," J. Opt. Soc. Am. 64, 138 (1974).

54. F. P. Carlson, "Generalized Linear Processors for Coherent Optical Computers," Proc. IEEE 65, 10 (1977).

55. O. Bryndahl, "Geometrical Transformations in Optics," J. Opt. Soc. Am. 64, 1092 (1974).

56. Wai-Hon Lee and O. Bryndahl, "Imaging on Curves Surfaces," Opt. Comm. 12, 382 (1974).

57. O. Bryndahl, "Optical Map Transformations," Opt. Comm. 10, 164 (1974).

58. J. W. Goodman, "Operations Achievable with Coherent Optical Information Processing Systems," Proc. IEEE 65, 29 (1977).

59. T. S. Huang, "Digital Holography," Proc. IEEE 59, 1335 (1971).

60. J. F. Walkup and M. O. Hagler, "Volume Hologram Representations of Space-Variant Optical Signals," Proc. 1975 Electro-Optical Syst. Design Conf., (Industrial and Scientific Conf. Management, Chicago, 1975).

61. E. W. Marchand, "Derivation of the Point Spread Function from the Line Spread Function," J. Opt. Soc. Am. 54, 915 (1964).

62. E. W. Marchand, "From Line to Point Spread Function: The General Case," J. Opt. Soc. Am. 55 352 (1965).

63. M. V. Klein, Optics, (Wiley, New York, 1970).

64. R. J. Collier, C. B. Burckhardt and L. H. Lin, Optical Holography, (Academic Press, New York, 1971).

65. H. Kogelnik, "Coupled Wave Theory for Thick Hologram Gratings," Bell Syst. Tech. Jour. 48, 2909 (1969).

66. H. M. Smith, Principles of Holography, 2nd edition, (Wiley-Interscience, New York, 1975).

67. R. Alferness, "Analysis of Optical Propagation in Thick Holographic Gratings," Appl. Phys 7, 29-33 (1975).

68. R. A. Bartolini, A. Bloom and H. A. Weakliem, "Volume Holographic Recording Characteristics of an Organic Medium," Appl. Opt. 15, 1261 (1976).

69. W. J. Tomlison, E. A. Chandross, H. P. Weber and G. D. Aumiller, "Multicomponent Photopolymer Systems for Volume Phase Holograms and Grating Devices," Appl. Opt. 15, 534 (1976).

70. R. Magnusson and T. K. Gaylord, "Laser Scattering Induced Holograms in Lithium Niobate," Appl. Opt. 13, 1545 (1974).

71. P. J. van Heerden," Theory of Optical Information Storage in Solids," Appl. Opt. 2, 393 (1963).

72. G. C. Temes, V. Barcilon and F. C. Marshall III, "The Optimization of Bandlimited Systems," Proc. IEEE 61, 196 (1973).

73. R. J. Collier and K. S. Pennington, "Multicolor Imaging from Holograms Formed on Two-Dimensional Media," Appl. Opt. 6, 1091 (1967).

74. J. T. LaMacchia and D. L. White, "Coded Multiple Exposure Holograms," Appl. Opt. 7, 91 (1968).

75. T. F. Krile, R. J. Marks II, J. F. Walkup and M. O. Hagler, "Space-Variant Holographic Optical Systems Using Phase-Coded Reference Beams," Proc. of the International Optical Computing Conference, San Diego (August, 1977).

76. T. F. Krile, M. O. Hagler, W. D. Redus and M. I. Jones, "Families of 2-D Phase Coded Diffusers for Multiplex Holography," J. Opt. Soc. Am. 67, 1435A (1977).

77. H. H. Arsenault and N. Brousseau, "Space Variance in Quasi-Linear Coherent Optical Processors," J. Opt. Soc. Am., 63, 555 (1973).

78. G. Toraldo di Francia, "Degrees of Freedom of an Image," J. Opt. Soc. Am. 59, 799 (1969).

79. Y. I. Khurgin and V. P. Yakovlev, "Progress in the Soviet Union on the Theory and Applications of Band-limited Functions," Proc. IEEE 65, 1005 (1977).

80. T. S. Huang, "Digital Computer Analysis of Linear Shift-Variant Systems," Proc. NASA/ERA Seminar (December 1969).

81. K. Yao and J. B. Thomas, "On Truncation Error Bounds for Sampling Representations of Bandlimited Signals," IEEE Trans. Aerospace Electron. Syst. 2, 640 (1966).

82. F. J. Beutler, "On the Truncation Error of the Cardinal Sampling Expansion," IEEE Trans. Inform. Theory IT-22, 568 (1976).

83. J. R. Higgins, "A Sampling Theorem for Irregularly Spaced Sample Points," IEEE Trans. Inform. Theory IT-22, 621 (1976).

84. G. K. Froehlich, "Optical Information Processing Experiments for Undergraduate Engineers," M.S. Thesis, Dept. of Electrical Engineering, Texas Tech University, Lubbock, Texas (January 1977).

85. G. K. Froehlich, J. F. Walkup and M. O. Hagler, "A Set of Optical Information Processing Experiments," IEEE Trans. Ed. (Feb., 1978).

APPENDIX A

SPATIAL AND FREQUENCY INVARIANCE

The concept of space-invariant[23] and time-invariant[24] systems is well established. For linear space-invariant systems, the system line spread function takes on the form

$$h(x-\xi;\xi) \rightarrow h(x-\xi). \qquad \text{(A-1)}$$

As discussed in Chapter I, 2-D linear space-invariant systems can be easily implemented with coherent optical processors. Furthermore, linear space-invariant systems can be straightforwardly analyzed through application of conventional Fourier transform theory.

There are some linear systems whose classification as variant or invariant is not clear. Arsenault and Brousseau[77] have discussed a class of linear systems which are invariant for a certain input class. An example of a line spread function for such a system is

$$h(x-\xi;\xi) = h_i(x-\xi)\,\mathrm{rect}\left(\frac{\xi}{2T}\right). \qquad \text{(A-2)}$$

Due to the rect term, this line spread function does not rigorously conform to the invariance criterion in Eq. A-1. If, however, we limit our input signal class to those functions identically zero outside the interval $|\xi| \leq T$, then the rect term is superfluous. Arsenault and Brous-

seau have termed such systems "quasi-linear" although "quasi-invariant" might be more appropriate.

A second system class which has a vague classification contains those linear systems with line spread functions of the form

$$h(x-\xi;\xi) \rightarrow h(x-M\xi) \qquad \text{(A-3)}$$

where M is a fixed constant. Although similar in form, this line spread function does not rigorously conform to the invariance criterion in Eq. A-1. A system considered elsewhere in this thesis which is contained in this system class is the non-unity magnification imaging system [See Eq. 3-8]. Goodman[23] classifies the magnifier as space-invariant while Sawchuk[53] calls it "rigorously" space-variant.

Alternate linear system classification categories are frequency-variant and frequency-invariant systems. A linear system is said to be frequency-invariant if

$$k(x-c\nu;\nu) \rightarrow k(x-c\nu) \qquad \text{(A-4)}$$

where c is a constant and $k(\cdot,\cdot)$ is the system frequency response defined in Eq. 2-19. If the frequency response does not conform to Eq. A-4, the system is said to be frequency-variant. The term "frequency" can here apply to either spatial or temporal frequency.

An example of a temporal frequency-invariant system

is a delay line whose delay time, x, is proportional to the applied frequency (ν). An example of a spatial frequency-invariant system is the familiar thin lens Fourier transformer. Using Eq. 2-22, the frequency response of the Fourier transformer is

$$k(x-c\nu;\nu) = \int_{-\infty}^{\infty} \exp\left[\frac{-j2\pi}{\lambda f} x\xi\right] e^{j2\pi\nu\xi} d\xi$$

$$= \lambda f \delta[x-\lambda f\nu]. \qquad \text{(A-5)}$$

Note that the constant c is here determined by system parameters

$$c = \lambda f. \qquad \text{(A-6)}$$

We can easily show that a space-invariant system can never be frequency-invariant. Using Eq. 2-22 as applied to a space-invariant system, we have

$$k(x-c\nu;\nu) = \int_{-\infty}^{\infty} h(x-\xi) e^{j2\pi\xi\nu} d\xi$$

$$= H_x(\nu) e^{-j2\pi x\nu} \qquad \text{(A-7)}$$

where $H_x(f_x) = F_x[h(x)]$. Clearly, this relation can never confrom to the frequency invariance criterion by Eq. A-4. (Note that the constant c is here <u>not</u> specified by any system parameters.) We can similarly show that a frequency-invariant system can never be space-invariant.

In two-dimensional coherent processors, a space-invariant system can be straightforwardly be made into a frequency-invariant system (or visa-versa) simply by placing a thin spherical lens a focal length's distance f in front of the system's input plane. The input plane is redefined to be the lens' front focal plane. Then, for an input $\exp(j2\pi\xi\nu)$, the system output is

$$k(x-c\nu;\nu) = \lambda f h(x-\lambda f\nu) \qquad \text{(A-8)}$$

where $h(\cdot)$ is the original space-invariant system's impulse response. Clearly, the augmented system is frequency-invariant with $c = \lambda f$.

In the definition of frequency-invariance in Eq. A-4, the constant c is assumed to have dimension of inverse frequency squared. This retains dimensional consistancy between the spatial frequency ν and the spatial variable x. Inclusion of such a constant in the spatial invariance definition in Eq. A-1 was not required since x and ξ are dimensionaly consistant. Note, however, that if we had included an arbitrary constant in the spatial invariance criterion, then we would arrive at Fq. A-3. Thus, we might logically adopt Eq. A-3 as a generalized definition of spatial invariance.

We have here considered space-(time-) and frequency-invariant systems. A term used in the literature which

can be applied collectively to all such linear systems is "shift-invariant."[10,80]

APPENDIX B

UTILIZING MINIMUM SAMPLING RATES IN A SPACE-VARIANT SAMPLING THEOREM

The sampling theorem expressions in Eqs. 2-83 and 2-84 are not optimum in the sense of utilizing maximum allowable sampling intervals. That is, we are sampling both the input and line spread function at a rate of 2W, while the minimum required sampling rates are $2W_f$ and $2W_\nu$, respectively. As will be shown, however, the resulting expression employing these minimum sampling rates is rather unattractive for computation and implementation purposes.

Consider, then, the following sampling theorem expansion of a space-variant system's line spread function:

$$h(x;\xi) = \sum_q h(x;\xi_q)\,\mathrm{sinc}2W_\nu(\xi-\xi_q), \qquad \text{(B-1)}$$

where $2W_\nu$ is the variation bandwidth and $\xi_q = q/2W_\nu$. One may similarly apply the sampling theorem to the system input to give

$$f(\xi) = \sum_p f(\xi_p)\,\mathrm{sinc}2W_f(\xi-\xi_p), \qquad \text{(B-2)}$$

where $\xi_p = p/2W_f$ and $2W_f$ is the input's bandwidth. Substituting Eqs. B-1 and B-2 into Eq. 2-25 gives

$$G(f_x) = \frac{1}{4W_f W_\nu} \sum_p \{f(\xi_p) \sum_q H_x(f_x;\xi_q)[\text{rect}(\frac{f_x}{2W_\nu}) \times \exp(-j2\pi f_x \xi_q)] * [\text{rect}(\frac{f_x}{2W_f})\exp(-j2\pi f_x \xi_p)]\}. \quad \text{(B-3)}$$

where "*" denotes convolution. Equation B-3 is identical to Eq. 2-84 yet employs larger sampling intervals. The above relationship, however, has the disadvatage of not assigning each sample input value to a single corresponding sampled line spread function. Note that the two convolving rects in Eq. B-3 give an upper bound of $2W_s=2W_f + 2W_\nu$ on the output spectrum's bandwidth. This is the same constraint contained in Eq. 2-83.

Inverse transforming Eq. B-3 gives

$$g(x) = \sum_p \sum_q f(\xi_q)h(x;\xi_q) * [\text{sinc } 2W_\nu(x-\xi_p)\text{sinc } 2W_f(x-\xi_q)]. \quad \text{(B-4)}$$

This is the spatial domain sampling theorem expansion for minimum sampling rates.

We now consider the version of Eq. B-4 which arises when the line spread function is bandlimited in x with low pass bandwidth of $2W_x$. In this case, we can write

$$h(x;\xi_q) = \sum_r h(x_r;\xi_q)\text{sinc } 2W_x(x-x_r) \quad \text{(B-5)}$$

where $x_r = r/2W_x$. Substituting into Eq. B-4 gives

$$g(x) = \sum_p \sum_q \sum_r f(\xi_q) h(x_r; \xi_q) I_{pqr}(x) \qquad \text{(B-6)}$$

where our interpolation function is

$$I_{pqr}(x) = \text{sinc } 2W_x(x-x_r) \qquad \text{(B-7)}$$
$$*[\text{sinc } 2W_\nu(x-\xi_p)\,\text{sinc } 2W_f(x-\xi_q)].$$

This relationship is obviously less computationally attractive than that in Eq. 2-83. Note that evaluation of Eqs. B-6 and B-7 at $x_m = m/2W$ gives Eqs. 2-101 and 2-102.